

Dynamics of the preprotein translocase of the mitochondrial outer membrane

Von der Fakultät für Geo- und Biowissenschaften der Universität Stuttgart
zur Erlangung der Würde eines Doktors der Naturwissenschaften (Dr. rer. nat)
genehmigte Abhandlung

vorgelegt von

Melissa Ann Poynor

aus Emmeloord, NL

Hauptberichter:	Prof. Dr. S. Nußberger
Nebenberichter:	PD. Dr. R. Eckert
Tag der mündlichen Prüfung:	28.01.2008

Biologisches Institut, Abteilung Biophysik
Dezember 2007

Ich erkläre hiermit, dass ich die vorliegende Arbeit selbstständig verfasst habe und keine anderen als die angegebenen Quellen und Hilfsmittel benutzt habe.

Stuttgart, den 17.12.2007

For Ethel Poynor

Contents

1 Zusammenfassung	5
2 Summary	7
3 Introduction	9
3.1 Mitochondria – a specialized compartment surrounded by a barrier	9
3.2 Protein translocation into mitochondria	11
3.3 The TOM complex	15
3.3.1 Components of the TOM complex	16
3.3.2 Structural and electrophysiological properties of the pore formed by the TOM machinery	19
3.3.3 Translocation mechanism of the TOM machinery	20
3.4 Aim of this study	21
4 Material and Methods	23
4.1 General equipment	23
4.2 <i>Neurospora crassa</i> culture	23
4.2.1 <i>N.crassa</i> strains and growth media	24
4.2.2 <i>N. crassa</i> cultivation	25
4.3 <i>Escherichia coli</i> culture	25
4.4 Biochemical methods	27
4.4.1 Isolation of mitochondria from <i>N. crassa</i>	27
4.4.2 Isolation of mitochondrial outer membrane vesicles	27
4.4.3 Purification of His-tagged TOM core complex from mitochon- dria	29
4.4.4 Purification of Tom40 from mitochondria	31
4.4.5 Purification of TOM core complex from OMVs	31

4.4.6	Purification of recombinant Su9 ₁₋₆₉ DHFR from <i>E.coli</i>	32
4.4.7	Size exclusion chromatography	33
4.4.8	Precipitation of proteins with methanol	34
4.4.9	Determination of protein concentration with the Bradford Method	34
4.4.10	Gel electrophoresis	35
4.4.11	Documentation of polyacrylamide gels	38
4.4.12	Elution of proteins separated by SDS-PAGE	39
4.4.13	Blue-native polyacrylamide gel electrophoresis (BNGE)	40
4.4.14	Elution of proteins separated by BNGE	41
4.4.15	Transfer of proteins to nitrocellulose or PVDF membranes	42
4.4.16	Immunodecoration	43
4.5	Structural biological methods	45
4.5.1	Reconstitution of membrane proteins for 2-D crystallization	45
4.5.2	3-D crystallization	47
4.6	Spectroscopical methods	49
4.7	Electrophysiological Methods	53
4.7.1	Setup	53
4.7.2	Painted bilayer membranes	54
4.7.3	Single channel measurements	55
4.7.4	Data analysis	55
4.7.5	Determination of the ion selectivity	58
5	Results	59
5.1	Biochemical characterization	60
5.1.1	Isolation of TOM core complex from mitochondria	60
5.1.2	Isolation of TOM core complex from OMVs	64
5.1.3	Isolation of TOM core complex lacking one of the small Tom proteins from outer membrane vesicles	66
5.1.4	Isolation of monomeric Tom40 from mitochondria	68
5.1.5	Isolation of VDAC	70
5.2	Crystallization of the TOM machinery	71
5.2.1	Reconstitution of TOM core complex into lipid membranes for 2-D crystallization	71
5.2.2	3-D crystallization	75

5.3	Binding studies of precursor protein with TOM core complex	76
5.3.1	Labeling of Su9 ₁₋₆₉ DHFR	78
5.3.2	Labeling of TOM core complex	83
5.3.3	FCS Measurements	86
5.4	Electrophysiological measurements	92
5.4.1	Electrophysiological characterization of VDAC	92
5.4.2	Electrophysiological characterization of the channel properties of TOM core complex	93
5.4.3	Electrophysiological characterization of the kinetic properties of TOM core complex channels	105
5.4.4	Electrophysiological characterization of the channel properties of Tom40	108
5.4.5	The influence of higher voltages on the channel properties of Tom40	113
5.4.6	Electrophysiological characterization of the channel properties of TOM core complex lacking one of the small Tom proteins	117
6	Theory	120
6.1	I-V relationships in ion channels	120
6.2	Voltage dependency	123
6.3	Characteristics of a double-barreled pores	127
7	Discussion	130
7.1	TOM core complex	130
7.1.1	Biochemical and biophysical characterization of TOM core complex	131
7.1.2	Electrophysiological properties of TOM core complex	133
7.2	TOM core complex lacking one of the small Tom proteins	139
7.2.1	Biochemical characterization of TOM core complex lacking one of the small Tom proteins	140
7.2.2	Electrophysiological properties of TOM core complex lacking one of the small Tom proteins	140
7.3	Tom40	141
7.3.1	Biochemical characterization of Tom40	141
7.3.2	Electrophysiological properties of Tom40	142
7.4	Conclusions	145

7.5	Future prospects	148
8	Abbreviations	149
9	Curriculum Vitae	164
10	Acknowledgements	165

1 Zusammenfassung

Die Evolution der eukaryotischen Zellen ist vor allem durch die Aneignung von umfangreichen internen Membranen, die subzelluläre Organellen umgeben, geprägt. Diese dynamischen Kompartimente tragen zum Wachstum und Stoffwechsel der Zelle bei. Die Mitochondrien gehören zu den Organellen, die von zwei Phospholipidmembranen umgeben sind. Die meisten mitochondrialen Proteine sind im Kern kodiert, werden im Zytosol synthetisiert und anschließend in die Mitochondrien importiert. Der TOM-Komplex, die Translokase der mitochondrialen Außenmembran, spielt dabei eine entscheidende Rolle. Alle mitochondrialen Proteine, die im Kern kodiert sind, müssen hier vorbei und werden entweder in die Außenmembran eingebaut oder in den Intermembranraum transferiert. Die letzteren werden daraufhin zu den anderen Komponenten der Import- und Sortierungsmaschinerie geleitet. Für diese unterschiedlichen Aufgaben besitzt der TOM-Komplex eine dynamische Struktur und wechselt zwischen mehreren Konformationszuständen. Ziel dieser Arbeit war es, diese Dynamik genauer zu untersuchen und zu charakterisieren.

Im Rahmen der vorliegenden Arbeit wurden dafür bestehende Protokolle optimiert und neue etabliert, die zur Isolierung der TOM Maschinerie aus verschiedenen Mutanten des filamentösen Pilzes *Neurospora crassa* dienten. Mit dem aufgereinigten Material wurden anschließend verschiedene biophysikalische Studien durchgeführt. Zu diesen zählten 2-D und 3-D Kristallisation, Fluoreszenzkorrelationspektroskopie, sowie elektrophysiologische Studien. Vor allem mit der letzten Methode ist es gelungen, weitere Einblicke in die Dynamik von TOM zu gewinnen.

Es lagen mindestens sechs unterschiedliche Konformationszustände vor, die der TOM Kanal einnehmen konnte. Interessanterweise konnten diese Konformationszustände in zwei Populationen eingeteilt werden. Bei zwei Zuständen verhielt sich der Protein leitende Kanal wie eine zylindrische Pore. Die Porenöffnung

war so groß, dass die passierenden Ionen die Einflüsse der Porenwand nicht spüren. Solche Kanäle weisen eine lineare Strom-Spannungskennlinie auf. Die Strom-Spannungskennlinie der anderen Population von Konformationszuständen deutete jedoch auf eine andere Situation hin. In diesen Konformationszuständen wurden die passierenden Ionen von der Porenwand beeinflusst. Sie mußten daher zuerst eine Energiebarriere überschreiten, um durch den Kanal zu gelangen.

Des Weiteren konnte gezeigt werden, dass das essentielle Protein Tom22 eine entscheidende Rolle bei dem Schalten zwischen diesen Konformationszuständen spielte. Mit den erzielten Ergebnissen konnten so zwei Modelle aufgestellt werden, die die hochkomplexe Dynamik der TOM Maschinerie beschreiben.

Diese Studie liefert die Grundlage für zukünftige Untersuchungen, bei denen die Dynamik der TOM Maschinerie in der Gegenwart von Präproteinen untersucht werden kann. Ein Vergleich mit der hier im Detail aufgeklärten Dynamik der Translokase ohne Präprotein wird es ermöglichen die Translokation von Proteinen über die mitochondriale Außenmembran auf einer biophysikalischen Ebene zu verstehen.

2 Summary

The evolution of eukaryotic cells was accompanied by the acquisition of extensive internal membranes that enclose subcellular organelles. These dynamic membrane-bounded compartments contribute to growth and metabolism of the cell all in a unique manner. The mitochondria are organelles enclosed by two phospholipid membranes. Almost all mitochondrial proteins are encoded in the nucleus, synthesized in the cytosol, and are posttranslationally imported into the mitochondria. A key component of the mitochondrial import machinery is the TOM complex (translocase of the mitochondrial outer membrane).

The aim of this study was to gain more information on the dynamics displayed by this translocase that enables the translocation of a variety of preproteins either into or across the mitochondrial outer membrane.

In this study, I have optimized and developed protocols for the isolation of the TOM machinery from various mutants of the filamentous fungus *Neurospora crassa*. I have subjected the purified protein to various biophysical experiments such as 2-D and 3-D crystallization, fluorescence correlation spectroscopy, and electrophysiological measurements. Especially with the latter method, I was able to shed more light on the highly dynamic behavior of the TOM machinery. At least six distinct conductance levels existed between which the complex switched. Interestingly, these conductance states could be divided into two different classes. Two conductance levels existed that are consistent with the model of a cylindrical pore through which ions pass via diffusion. The I-V characteristics found with the other conductance levels, however, were more consistent with a diffusion over an energy barrier due to interactions of the ions with the pore wall. Furthermore, I gained evidence that Tom22 plays an important role for the transition between these different conformational states probably by reducing the energy required for this process. Finally, I present two models to explain the observed kinetic properties of the TOM machinery.

These results may serve as the basis for future studies in which the dynamics of the TOM machinery in the *absence* of preprotein, as presented here, can be compared with similar studies conducted in the *presence* of preprotein. The information gained from such experiments will allow us to understand the mechanism underlying the translocation of preproteins across the mitochondrial outer membrane at the biophysical level.

3 Introduction

In this thesis I have studied the protein translocase of the mitochondrial outer membrane – the TOM complex. This translocase serves as the main entry site for virtually all mitochondrial proteins that are encoded in the nucleus. Although, previous studies have elucidated the functions of the TOM machinery at a cellular level, little is still known about the exact mechanism of the translocation of the proteins through this complex. The aim of my study was to gain further insights into this process by applying biochemical and biophysical approaches. This chapter is meant as an overview to understand the importance and the necessity of this complex.

3.1 Mitochondria – a specialized compartment surrounded by a barrier

Membranes consisting of phospholipids play an important role in all organisms. They act as semi-permeable barriers to ions and macromolecules (Davson and Danielli, 1938). These membranes enabled the development of single cells, as well as the compartmentalization within the cells. The latter, the development of membrane-embedded organelles, was a milestone during the evolution of the eukaryotic cell. Through their spatial separation, these new dynamic compartments were able to contribute to growth and metabolism of the cell in a unique manner. The following organelles are located within eukaryotic cells:

- **The nucleus** accommodates the vast majority of the genetic material, the DNA.
- **The endoplasmic reticulum (ER)** is the site where a majority of proteins are folded into their native conformation and are post-translationally modified.
- **The Golgi apparatus** is primarily responsible for the packaging and processing of macromolecules such as newly synthesized proteins and lipids.

- The very acidic **lysosomes** harbor digestive enzymes like ribonucleases, phosphatases, and deoxyribonucleases.
- **The peroxisomes** contain enzymes for the degradation of fatty acids and amino acids.
- **Chloroplasts** are organelles in plant cells and eukaryotic algae that conduct photosynthesis.
- **Mitochondria** are multifunctional organelles. As they are the focus of this study they are described in more detail below.

As most of the cell's supply of ATP (Adenosine 5'-triphosphate), the main energy source of a cell, is synthesized in mitochondria, they are often referred to as the "cellular power plants". Further metabolic tasks such as the Krebs cycle, β -oxidation, urea cycle, and amino acid metabolism are localized in these organelles. Furthermore, mitochondria are central to many forms of cell death (Kuwana and Newmeyer, 2003). Recently, it has been shown that they are also involved in the maturation of cellular Fe-S proteins (Lill and Kispal, 2000).

The importance of the mitochondria is demonstrated through a number of neurodegenerative disorders such as Parkinson and Huntington disease that arise from failures of the mitochondrial respiratory-chain (DiMauro and Schon, 2003; Orth and Schapira, 2001).

Mitochondria are organelles that come in many different shapes. Depending on the tissue from which they originate, they can be small and spheroid or more tubular. The mitochondria are a dynamic network resulting from many processes of fission and fusion (Bereiter-Hahn and Vöth, 1994).

Mitochondria are organelles that consist of a smooth outer membrane surrounding an inner membrane, dividing two aqueous compartments – the matrix and the inter-membrane space. The inner membrane surface is increased through invagination (Palade, 1952). Recent studies indicate that the topology of the mitochondrial inner membrane correlates with mitochondrial functions (Manella, 2006). Therefore, changes in inner membrane morphology might represent a novel form of metabolic regulation.

In contrast to most other membranes, the outer membrane of mitochondria appears to be freely permeable to various small molecules due to VDAC (voltage dependent anion channel) located in this membrane (Colombini, 1979). In contrast, the mitochondrial inner membrane is tightly sealed. ATP synthesis, for

example, is powered by the protons moving down the electrochemical gradient across the inner membrane.

Mitochondria contain their own DNA and Ribosomes. The existence of this DNA can be explained with the eubacterial origin of these organelles. The endosymbiotic theory explains the acquisition of mitochondria during the evolution of the eukaryotic cell (Dyall et al., 2004; Gray, 1999). Originally, these organelles must have possessed a complete genome, but during evolution some of the genes were either no longer required and were lost, or were transferred from the organelle to the nucleus, reducing the mitochondrial DNA to a genome that only encodes 5-60 proteins. All the other mitochondrial proteins are encoded in the nucleus and are synthesized in the cytosol. For the translocation of these newly synthesized proteins to their final destination, they have to be transferred across or into the lipid barrier surrounding the mitochondria. For this, an import- as well as a sorting-machinery evolved during the evolution of the mitochondria. A number of components involved in the protein translocation have been identified.

As we will see in the following section, the import- and sorting-machineries of the mitochondria are very complex due to the double membrane surrounding these organelles. A number of pathways have been described for proteins with various destinations within the mitochondria.

3.2 Protein translocation into mitochondria

Different protein import pathways exist in mitochondria that target precursor proteins to their designated compartment or membrane. In each pathway a set of molecular machines is involved. Each machine consists of a core module with additional modules (Dolezal et al., 2006; Endo et al., 2003; Milenkovic et al., 2007; Neupert and Herrmann, 2007; Wiedemann et al., 2004).

In Fig.3.1 and Table 3.2 the different pathways and major protein complexes are described.

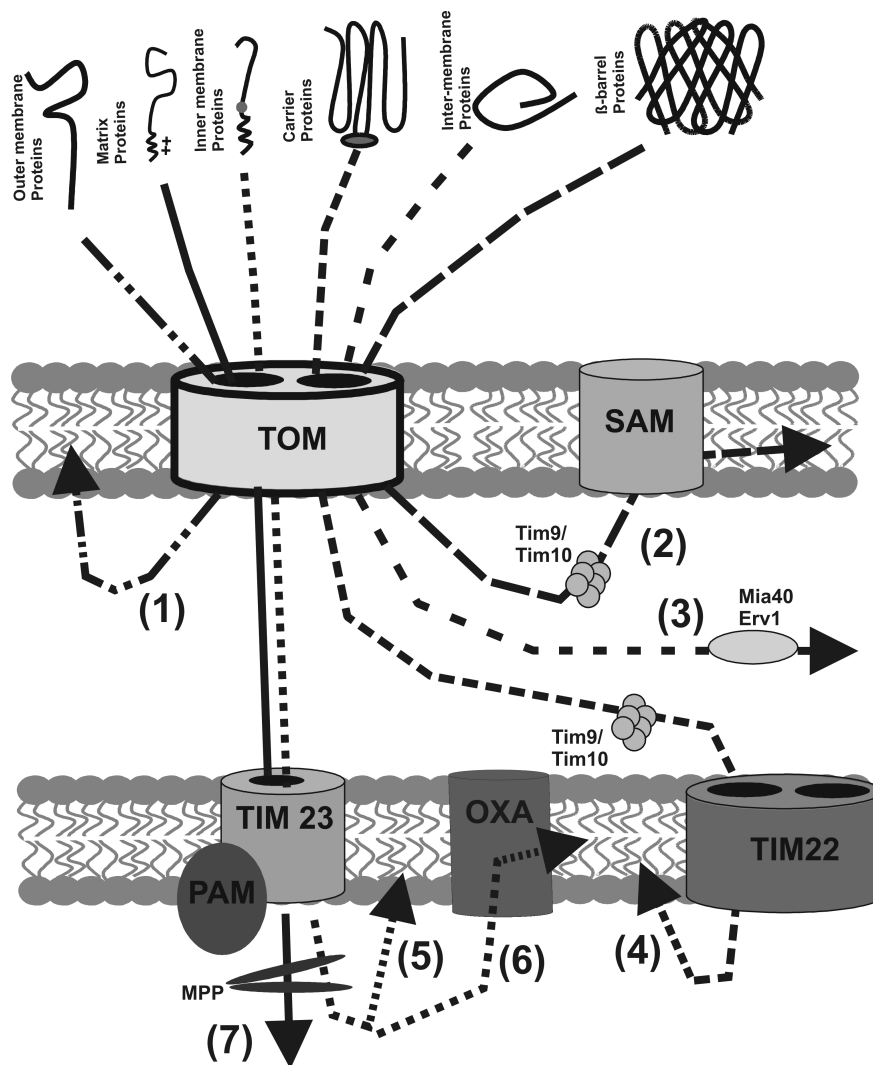


Figure 3.1: Protein translocation pathways into mitochondria

A number of oligomeric complexes are involved in the translocation of precursor proteins targeted to various compartments of the mitochondria. The TOM complex is the initial contact site for all proteins. It mediates the insertion of membrane proteins into the outer membrane (1) and is involved in the transfer of proteins into the inter-membrane space. With the aid of the small Tim proteins, Tim9 and Tim10, outer membrane proteins with a β -barrel fold, are directed from the inter-membrane space to the SAM complex and are subsequently inserted into the outer membrane (2). Proteins destined to remain in the inter-membrane space are stabilized by Mia40 and Erv1 (3). Proteins destined for the inner membrane are either directed to the TIM22 complex via Tim9 and Tim10, as it is the case for proteins with a hydrophobic internal signal sequence (4), or they are translocated through the TIM23 complex. The latter are either directly inserted into the inner membrane (5) or require the aid of the OXA complex (6). The TIM23 complex pathway is used by proteins destined to the matrix (7).

Table 3.1: Components involved in the import and sorting of nuclear encoded proteins destined for the mitochondria

	Description	Imported proteins	Subunits
TOM	translocase of the outer membrane	all nuclear-encoded mitochondrial proteins	Tom70, Tom40, Tom22, Tom20, Tom7, Tom6, Tom5
SAM	sorting and assembly machinery	β -barreled proteins of the outer membrane	Sam50, Sam37, Sam35, Mdm10
TIM23	translocase of the inner membrane	matrix proteins, inner membrane proteins	Tim50, Tim23, Tim21, Tim17
PAM	presequence translocase-associated motor	matrix proteins	Pam18, Pam16, Tim44, Mge1, mtHsp70
TIM22	translocase of the inner membrane	hydrophobic inner membrane proteins	Tim54, Tim22, Tim18, Tim12
OXA	oxidase assembly	inner membrane proteins with prokaryotic equivalents	Oxa1
MPP	mitochondrial processing peptidase	proteins with N-terminal presequence	Mas1, Mas2
Tiny TIM's	small Tim proteins in the IMS	hydrophobic inner membrane proteins	Tim13, Tim10, Tim9, Tim8
Erv1	essential for respiration and vegetative growth	proteins of the inter-membrane space	–
Mia40	mitochondrial inter-membrane space import and assembly	proteins of the inter-membrane space	–

Import of proteins destined for the outer membrane (1)

Proteins with a simple topology (e.g. proteins anchored with one transmembrane helix) only require the TOM complex for their correct insertion into the mitochondrial outer membrane. It has been suggested that these proteins do not pass the general import pore of the TOM machinery but are integrated into the outer membrane through a pathway at the protein-lipid interface (Ahting et al., 2005). The exact mechanism behind this process is, however, still not understood.

Import of β -barrel proteins into the outer membrane (2)

Proteins of the mitochondrial outer membrane with a β -barrel fold require a second complex for their insertion into the outer membrane – the SAM complex (Paschen et al., 2003; Wiedemann et al., 2003). A similar machinery has been

found in gram-negative bacteria in which Omp85 facilitates the insertion of β -barrel proteins into the bacterial outer membrane (Gentle et al., 2004; Voulhoux et al., 2003). The transfer of β -barrel precursor proteins from the TOM complex to the SAM complex is accompanied by the binding to the small Tim proteins, Tim9 and Tim10, which have a chaperone-like function (Vial et al., 2002).

Import of inter-membrane space proteins (3)

Two components, Mia40 and Erv1, have recently been identified as part of the inter-membrane space import machinery (Chacinska et al., 2004; Mesecke et al., 2005; Rissler et al., 2005; Terziyska et al., 2005). Both proteins contain characteristic cysteine motifs. They bind a specific class of soluble metal-binding inter-membrane proteins, which contain highly conserved cysteine residues, such as the copper chaperone Cox17 and the fraction of Cu/Zn-superoxiddismutase located in the inter-membrane space (Beers et al., 1997; Sturtz et al., 2001)

Import of proteins with internal targeting signals into the inner membrane (4)

Proteins destined for the inner membrane with multiple transmembrane domains, e.g. members of the ADP/ATP carrier protein family, have internal targeting signals. Tim9 and Tim10 bind to these precursor proteins after their translocation through the TOM complex. Recent studies suggest that this binding prevents aggregation of the hydrophobic precursor proteins (Vergnolle et al., 2005; Webb et al., 2006). Eventually, they deliver the precursor proteins to the TIM22 machinery. The subsequent lateral release of the precursor proteins into the inner membrane requires a membrane potential across the inner membrane.

Import of matrix targeted proteins and inner membrane proteins with a hydrophobic stop-transfer signal (5+7)

Mitochondrial proteins destined for the matrix have a positively charged N-terminal targeting signal. After translocation through the TOM complex they are transferred to the translocase of the inner membrane, the TIM23 complex, which is associated with the import motor complex PAM. The core subunit, Tim23, forms a channel that is cation selective and is activated by the inner membrane potential and presequence binding (Truscott et al., 2001). Further studies showed that the hydrophilic cis domain of another subunit – Tim50 – induces a closure of the

Tim23 channel in a presequence-regulated manner (Meinecke et al., 2006). Passage of precursor proteins through this complex is strictly dependent on the membrane potential across the inner membrane. Additionally, mtHsp70, a subunit of the PAM complex, drives the precursor across the inner membrane by ATP hydrolysis (Schneider et al., 1994). In the matrix the N-terminal targeting sequence is removed by a metalloendopeptidase, the mitochondrial processing peptidase, MPP (Taylor et al., 2001). Proteins with an additional targeting sequence – a hydrophobic stop transfer signal – are laterally released into the inner membrane after removal of the N-terminal sequence (Glaser et al., 1990; van Loon et al., 1986).

Import of proteins with prokaryotic equivalents into the inner membrane (6)

Another group of proteins located in the inner membrane have been described to be first imported into the matrix via the TIM23 complex (Hell et al., 2001; Stuart, 2002). Thereafter, they are integrated into the inner membrane with the aid of the OXA-complex, a protein import machinery which is a distant homolog to the bacterial YidC machinery (Kuhn et al., 2003; Preuss et al., 2005). So far, all proteins that have been described to undergo this process have prokaryotic equivalents. This “export-machinery” is also used by inner membrane proteins encoded by the mitochondrial DNA such as the subunits ATPase 6 and ATPase 8 of the F₁F₀-ATP synthase (Stuart, 2002).

3.3 The protein translocase of the outer mitochondrial membrane

The above description of the different import pathways in mitochondria emphasizes the importance of the TOM complex as the main entry gate of virtually all mitochondrial proteins. This protein complex has, therefore, been the subject of many studies. These were mostly performed in Baker’s yeast (*Saccharomyces cerevisiae*) and in the filamentous fungus *Neurospora crassa*. The former was the first eukaryotic organism to be completely sequenced (Goffeau et al., 1996), and genetic studies can easily be performed in this organism. The latter organism has the advantage that mitochondria thereof can be obtained in high amounts (Sebald et al., 1979). *N. crassa* was also the choice of model organism for this study. Studies performed in other organisms, however, indicated that function and structure

of the TOM complex were highly conserved during evolution (Hoogenraad et al., 2002; Macasev et al., 2004).

3.3.1 Components of the TOM complex

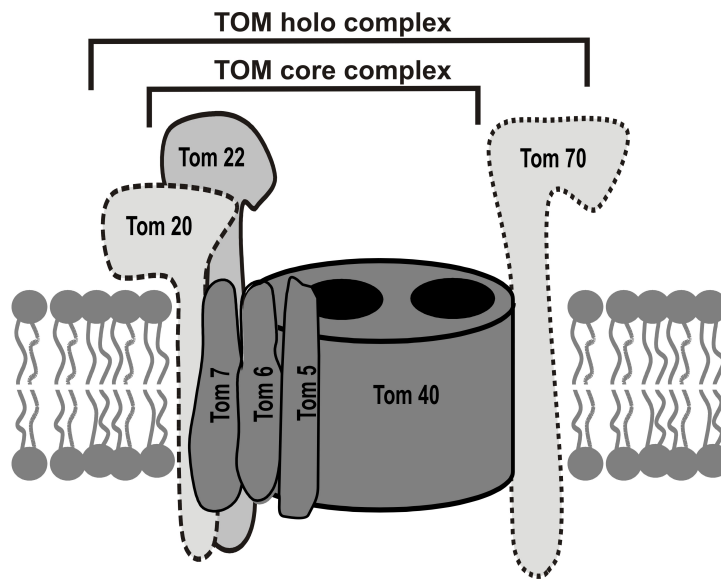


Figure 3.2: TOM complex

The components of the TOM complex in the outer membrane. The main components are Tom40, Tom22, Tom7, Tom6, and Tom5. They form the general import pore, the TOM core complex. The subunits Tom70 and Tom22 have receptor like functions.

The main tasks which the TOM complex has to accomplish are (i) the recognition of newly synthesized polypeptides in the cytosol, (ii) binding of the substrate proteins by surface components, (iii) partially unfolding of proteins, (iv) translocation of peptides across the lipid membrane, and (v) targeting these proteins to their appropriate compartment.

Studies performed on the TOM complex in *N. crassa* have revealed five components (Tom40, Tom22, Tom7, Tom6, Tom5) that form the general import pore – termed TOM core complex. Two additional proteins, Tom70 and Tom20, function as receptors. These are only loosely attached to the rest of the complex (Ahting et al., 1999). During biochemical isolation procedures they easily disassociate. The following functional properties have been assigned to the individual subunits (Neupert and Herrmann, 2007; Rehling et al., 2004; Stojanovski et al., 2006):

Tom70

Tom70 is a major surface receptor for mitochondrial protein precursors destined to the mitochondrial inner membrane, such as members of the ADP/ATP carrier family. Recently, the crystal structure of the cytosolic domain of yeast Tom70 (residues: 94-607) was determined and provided valuable insights into the role of Tom70 in the precursor transport across the mitochondrial outer membrane (Wu and Sha, 2006). The structure revealed two distinct domains: a peptide binding groove in the N-terminal domain and a large pocket in the C-terminal domain. The former most likely binds the molecular chaperone Hsp70 (heat shock protein), and the latter is involved in the binding of mitochondrial precursors. Each domain consists primarily of tetratricopeptide repeat (TPR) motifs, which are organized into right-handed superhelices. Membrane proteins with their hydrophobic regions are especially predestined for aggregation, which can be prevented by chaperone binding and, therefore, shielding of the hydrophobic patches. The binding site for Hsp70 supports the hypothesis that Tom70 cooperates with Hsp70 in targeting the precursor proteins to mitochondria (Young et al., 2003).

Tom20

Tom20 is the third cytosolic preprotein receptor, besides Tom70 and Tom22 (Brix et al., 1997). It is mainly involved in the binding of mitochondrial proteins with an N-terminal presequence which bind to its cytosolic domain. An NMR structure of the cytosolic core domain of Tom20 in combination with a peptide has been solved (Abe et al., 2000). It showed that the presequence of the peptide forms an amphiphilic helix enabling a binding to Tom20 with its hydrophobic side. Recently, this study was supplemented with crystallization studies of Tom20 with precursor protein. The analysis of the obtained crystals suggested that there is a dynamic equilibrium between multiple conformational states occupied by the bound precursor protein (Saitoh et al., 2007).

Tom7, Tom6, and Tom5

The small Tom proteins Tom7, Tom6, and Tom5 consist of 50-70 amino acids and are anchored in the mitochondrial outer membrane with one transmembrane helix. Only a few residues are exposed to the inter-membrane space. They seem to stabilize the complex, but their individual functions are still unclear (Sherman

et al., 2005). The loss of individual small Tom proteins results only in minor effects. Comparing the function of the small proteins from *N. crassa* with *S. cerevisiae* indicates that they play a more important role in yeast than in *N. crassa* (Schmitt et al., 2005). It has been suggested that they might have eventually been lost in higher organisms as only Tom7 has been identified in higher organisms so far (Sherman et al., 2005).

Tom22

As the central receptor of the TOM machinery, Tom22 is thought to bind pre-proteins through its highly negatively charged N-terminal domain in the cytosol (Kiebler et al., 1993). An additional binding site is located at the C-terminal domain of Tom22 in the inter-membrane space (Bolliger et al., 1995; Mayer et al., 1995a). One single transmembrane segment connects these two domains with each other. Furthermore, Tom22 functions as the general organizer of the pore (van Wilpe et al., 1999) and seems to be involved in the contact sites between the TOM and TIM machineries (Albrecht et al., 2006; Chacinska et al., 2005; Mokranjac et al., 2003). Analysis of crystals obtained from the binding domain of Tim21 of *S. cerevisiae*, a subunit of the TIM23 complex, suggests that the negatively charged inter-membrane space domain of Tom22 electrostatically interacts with conserved residues of Tim21 (Albrecht et al., 2006).

Tom40

Tom40 is a membrane embedded protein and is the pore-forming unit of the complex (Ahting et al., 2001; Becker et al., 2005; Hill et al., 1998). Cross-linking experiments have revealed cis and trans binding sites on Tom40 for precursor proteins (Rapaport et al., 1998). Studies examining the accessibility to antibodies have indicated that in *S. cerevisiae* and *N. crassa* the N- and C- terminal extend into the inter-membrane space (Künkele et al., 1998b). Structural predictions of the transmembrane domain of Tom40 have suggested a β -barrel structure similar to bacterial porins (Mannella et al., 1996). In contrast to porins with about 50 % β -structure, circular dichroism (CD) and Fourier transform infrared spectroscopy (FTIR) revealed a maximum of 31 % of β -barrel and about 22 % α -helix for native Tom40 (Ahting et al., 2001), and 30-40 % β -barrel was detected by Becker et al. for recombinant protein (Becker et al., 2005). Recently, a structural and functional homolog

of fungal Tom40 has been identified in rat. When refolded from inclusion bodies expressed in *E. coli* 63 % β -sheet was revealed (Suzuki et al., 2000, 2004). Taken together, the structural properties of Tom40 are still very unclear.

3.3.2 Structural and electrophysiological properties of the pore formed by the TOM machinery

Despite all knowledge gained on the TOM core complex at a cellular level, very little is known about the entire structure of the TOM machinery and the exact mechanism of protein translocation. In addition to some structural studies of the cytosolic domains of the various receptors (described above), a low resolution analysis of negatively stained TOM holo complex, TOM core complex, and Tom40 with electron tomography has been performed (Ahting et al., 1999, 2001), suggesting three-hole, two-hole, and one-hole structures, respectively. The two-pore particles were ca. 12 nm long with a width of ca. 7 nm and about ca. 7 nm in height. The population of one-hole particles in the TOM core complex preparation was 19 %. This amount was increased when treating TOM core complex with trypsin (44 %). The particles detected in the Tom40 preparation were very diverse. Several molecules with one (36 %) and two (7 %) stain-filled openings were present, as well as other undefined structures indicating an inhomogeneous isolation of Tom40 protein (Ahting et al., 2001).

A first electrophysiological characterization of the translocase of the mitochondrial outer membrane was performed by Henry et al. (Fèvre et al., 1993; Henry et al., 1996; Juin et al., 1995, 1997). They discovered a cationic channel of large conductance when analyzing yeast and mammalian outer mitochondrial membranes with three different methods – “tip-dip” bilayers, patch clamp of giant liposomes, and planar bilayers. Due to blockage of the channel by basic peptides, they termed this channel PSC (peptide-sensitive channel). Further electrophysiological measurements conducted by Künkele et al. with isolated TOM holo complex, indicated that PSC is identical with TOM (Künkele et al., 1998b). The TOM channels were described as cation-selective and voltage-gated pores with three main conductance levels. Additionally they observed slow and fast transitions to states of lower conductance. Further studies on native Tom40 (Ahting et al., 2001), as well as recombinant Tom40 (Becker et al., 2005; Hill et al., 1998), demonstrated that in yeast and fungus Tom40 is the pore forming unit of the complex. Recently, it has been shown that recombinant rat Tom40 forms presequence sensitive cation

specific channels as well (Suzuki et al., 2004). However, the roles of the other subunits concerning channel formation and gating behavior have not been further analyzed in detail yet.

3.3.3 Translocation mechanism of the TOM machinery

An unsolved question concerns the source of energy for the translocation of precursor proteins through the TOM machinery. The driving forces across the inner membrane are ATP-hydrolysis and the membrane potential across the inner membrane. The former is accomplished by the hydrolysis of ATP bound to mtHsp70, a subunit of the PAM complex, which is in tight interaction with the TIM23 complex (Geissler et al., 2001; Liu et al., 2003; Schneider et al., 1994). The latter could be responsible for an electrophoretical transfer of the presequence with its positive charges across the inner membrane (Roise and Schatz, 1988) as well as the dimerization of Tim23 (Bauer et al., 1996). Tim23 dimers act as receptors for precursor proteins. Binding of the precursors to the receptor, however, results in dimer dissociation which triggers opening of the TIM channel and insertion of the preprotein.

The translocation across the outer membrane, however, must be fueled with a different source of energy as there is neither a membrane potential across the outer mitochondrial membrane nor ATP-dependent chaperones in the inter-membrane space. One proposed mechanism is that by coupling the TOM and the TIM translocases, precursors could pass the passive TOM pore by being “pulled” by the TIM complex (Endo et al., 2003). Another explanation is the increase in binding affinity of the precursor proteins to the TOM complex (Komiya et al., 1998). Indeed, binding sites on the cytosolic side (on Tom70, Tom22, and Tom20) have been described, as well as binding sites in the inter-membrane space, so-called trans binding sites, on Tom40, Tom22, and Tom7 (Bolliger et al., 1995; Esaki et al., 2004; Mayer et al., 1995b). By binding to the trans sites, the precursors are protected against protease treatment, since they are removed from the pool of the unfolded species in the cytosol (Esaki et al., 2003; Yano et al., 2004).

Electrophysiological measurements have indicated that the TOM machinery is not a passive aqueous pore, that allows the precursor proteins to cross the outer membrane through diffusion (Ahting et al., 1999, 2001; Becker et al., 2005; Grigoriev et al., 2004; Henry et al., 1996; Hill et al., 1998; Künkele et al., 1998b; Meisinger et al., 2001; Muro et al., 2003). In these experiments it has been shown

that the TOM core complex can switch between various conformational states. Transitions between such states are accompanied by changes in the conductivity of the channel.

An explanation for these different conformational states could be the different tasks that the TOM machinery has to perform. On the one hand, some proteins are laterally released into the mitochondrial outer membrane. On the other hand, the remaining proteins translocated through the TOM complex. Such a highly dynamic structure has been described for another protein translocase, the translocon of the ER membrane (Bessonneau et al., 2002; de Keyzer et al., 2003; Johnson and van Waes, 1999). The recently solved X-ray structure of the protein-conducting channel SecYEG from bacteria indicates that the pore can open in two directions (J.Gumbart and Schulten, 2006; Van den Berg et al., 2004). This dynamical behavior allows proteins to either enter into the lumen of the ER or exit laterally into the lipid phase.

3.4 Aim of this study

The aim of this study was to gain further insights into the structure and dynamics of the TOM machinery using biophysical methods to elucidate the mechanism of protein translocation across the outer mitochondrial membrane. The experiments applied to approach this task can be divided into four classes: biochemical isolation and characterization of the TOM machinery (i), structural analysis (ii), analysis of the binding properties (iii), and electrophysiological characterization of the channels formed by the TOM machinery (iv).

(i) The basis for the following biophysical experiments was the isolation of TOM protein in large amounts. For the applied methods it is very important that the samples are virtually free of any contaminations. For this, existing isolation protocols had to be improved and new protocols had to be established.

(ii) Gaining structural information on the TOM complex would provide the basis for a better understanding of its function. Solving the structure of a large oligomeric membrane protein is, however, not an easy task. In this study, first trials were undertaken to reconstitute TOM core complex into lipid membranes which is the basis for 2-D crystallization. In another approach, purified Tom40 protein was used in 3-D crystallization trials.

(ii) Binding studies: FCS (fluorescence correlation spectroscopy) and FCCS (fluorescence cross correlation spectroscopy) are methods for the determination of diffusion constants, binding affinities, and binding as well as translocation times. A further aim of this study was to fluorescently label purified TOM core complex and a model substrate, Su9_{1–69}DHFR, to perform such measurements and analyze the binding of this precursor protein to the TOM machinery.

(iii) Electrophysiological approach: Single channel measurements provide information about the dynamic behavior of the channel and the permeability of channels for small ions. The aim of this study was to comprehensively describe the dynamics of the TOM machinery in the absence of preprotein. The information obtained with this study is the basis for further experiments in which the influence of preprotein can be examined. Such studies will shed much light onto the mechanism underlying the translocation of proteins across the mitochondrial membrane.

4 Material and Methods

4.1 General equipment

- **Chemicals**

All chemicals were purchased from Roth (Karlsruhe, Germany), Merck (Darmstadt, Germany), Sigma Aldrich (Munich, Germany), and Fluka (Buchs, Switzerland), unless stated differently.

- **Devices**

Autoclave

(Systec 3870 ELV – Systec GmbH, Wetzlar, Germany)

pH meter

(Microprocessor pH Meter – WTW, Weilheim, Germany)

Scales

(Iso9001 – Sartorius, Göttingen, Germany)

Kern770 – Kern und Sohn, Balingen, Germany)

Vacuum pump

(Vacuubrand – Wertheim, Germany)

Water purifier

(Wagner Munz, Munich, Germany)

Vortex

(Vortex Genie2 – Roth, Karlsruhe, Germany)

Magnetic stirrer

(IKA Combimag RCT – Jahnke and Kunkel GmbH, Staufen, Germany)

4.2 *Neurospora crassa* culture

For the biophysical characterization of TOM core complex, protein was isolated from the filamentous fungus *Neurospora crassa* (*N. crassa*).

4.2.1 *N. crassa* strains and growth media

N. crassa strains used:

- wild-type (74A)
- GR 107, contains a hexahistidinyI-tagged form of Tom22 (Künkele et al., 1998a; Ahting et al., 1999)
- Tom5^{RIP} (Δ Tom5), lacks Tom5 (Schmitt et al. 2005)
- Tom6^{RIP} (Δ Tom6), lacks Tom6 (Sherman et al. 2005)
- Tom7^{KO} (Δ Tom7), lacks Tom7 (Sherman et al. 2005)

N. crassa Growth media:

- **Trace elements solution**
 - 5 % (w/v) Citric acid
 - 5 % (w/v) ZnSO₄
 - 1 % (w/v) FeNH₄SO₄
 - 0.25 % (w/v) CuSO₄
 - 0.05 % (w/v) MnSO₄ x H₂O
 - 0.05 % (w/v) H₃BO₃
 - 0.05 % (w/v) Na₂MoO₄
- **Biotin solution**
 - 50 % (v/v) ethanol
 - 0.01 % (v/v) biotin
- **50x Vogel's minimal medium**
 - 15 % (w/v) Na₃-Citrate x H₂O
 - 25 % (w/v) KH₂PO₄
 - 10 % (w/v) NH₄NO₃
 - 1 % (w/v) MgSO₄
 - 0.5 % (w/v) CaCl₂
 - 0.005 % (v/v) trace elements-solution
 - 0.0025 % (w/v) biotin solution
- **Complete medium**
 - 2 % (v/v) 50x Vogel's minimal medium
 - 1 % (v/v) glycerol
 - 1.5 % (w/v) sucrose
 - 0.2 % (w/v) yeast extract
 - 0.1 % (w/v) caseinhydrolysat

for agar flasks:

2 % (w/v) agar

culture specific additives:Tom5^{RIP} – 0.0001 % (w/v) nicotinamide

0.01 % (w/v) inositol

1.5 % (w/v) glucose (instead of sucrose)

GR 107 – 1.3 M histidine

4.2.2 *N. crassa* cultivation

Silicate dried hyphae were used to inoculate complete medium supplemented with 2 % (w/v) agar in an Erlenmeyer flask. Incubation for two days at 25°C in the dark was followed by five days incubation at room temperature and daylight. The grown conidia from this primary culture (A- flask) were either used to inoculate further flasks (B- flasks) or to make silicate stocks. For the latter, conidia were resuspended in 10 ml skim milk (10 % (w/v) solution). This suspension was filtered through a sterile cotton filter, and 300 μ l of the filtrate were mixed with 1 g silicate. This solution was dried in an exicator at room temperature for three weeks and then stored at 4°C.

To obtain large amounts of *N. crassa* hyphae, conidia from 20 B- flasks were harvested in distilled water and transferred to 8 liter Vogel's minimal medium containing 2 % (w/v) sucrose. After 16 hours of growth at 25°C with aeration and light the culture was diluted to 80 liters in the same medium. This was incubated for 8 more hours with the same conditions before harvesting the hyphae with an altered washing machine that functioned as a centrifuge. The wet weight of the hyphae was determined before either storing them at - 20°C or using them instantly for isolation of mitochondria.

4.3 *Escherichia coli* culture

- *E. coli* strains used

(BL21, containing pQE40 vector with C-terminal His-tagged version of Su9₁₋₆₉DHFR and ampicillin as well as kanamycin resistance was kindly provided by Dr. Doron Rapoport (Institut für Biochemie, Universität Tübingen, Germany))

- **Buffers and reagents**

- Growth medium*

- (1 % (w/v) NaCl, 1 % (w/v) Tryptone, 0.5 % (w/v) yeast extract)

- Agar plates*

- (2 % (w/v) bacto-agar is added to growth medium and autoclaved. When the solution is chilled below 60°C, 100 µg/l ampicillin and 30 µg/l kanamycin is added and poured into a petri dish)

- Antibiotics*

- (ampicillin – Roth, Karlsruhe, Germany
kanamycin – Fluka, Buchs, Switzerland)

- IPTG*

- (PEQLAB Biotechnologie GMBH, Erlangen, Germany)

- **Devices**

- petri dish*

- (Greiner Bio-One GmbH, Frickenhausen, Germany)

- Thermoshaker*

- (Thermoshake – C. Gerhard GmbH, Königswinter, Germany)

- Spectrometer*

- (Ultrospec II, Pharmacia Biosystems, Freiburg, Germany)

- Centrifuge*

- (Evolution RC + SA-3000 rotor, Sorvall, Kendro Laboratory Products, Langensfeld, Germany)

The isolation of recombinant Su9_{1–69}DHFR was performed according to standard protocols for the isolation of protein from *E. coli* cultures (Sambrook et al., 1989). For overnight cultures 5 ml growth medium supplemented with 100 µg/l ampicillin and 30 µg/l kanamycin was inoculated with a single colony and incubated at 37°C with shaking overnight. The next morning the overnight culture was diluted 1:100. When the culture reached the late log phase (OD₆₀₀ = 0.8) protein synthesis was induced by adding 1 mM IPTG to the culture. After three hours the protein containing cells were harvested by centrifugation (17.000xg; 5 minutes; room temperature) and stored at - 20°C until use.

4.4 Biochemical methods

4.4.1 Isolation of mitochondria from *N. crassa*

- **Buffers and reagents**

SET buffer

(250 mM sucrose, 2 mM EDTA, 20 mM Tris-HCl pH 8.5, 1 mM PMSF)

ST buffer

(250 mM sucrose, 20 mM Tris-HCl pH 8.5)

- **Devices and Material**

Waring blender

(Rotor GT800 – Rotor Lips AG, Uetendorf, Switzerland)

Corundum mill

(custom-made)

Centrifuge

(Evolution RC + SA-3000 rotor – Sorvall, Kendro Laboratory Products, Langensfeld, Germany)

Sand

(neoLab Migge, Heidelberg, Germany)

About 1 kg of hyphae were mixed with 2 liter SET buffer and were homogenized in a Waring blender. The homogenized hyphae were complemented with 500 g quartz sand and the cell walls were disrupted by passing this suspension through a corundum mill. Cellular residues were pelleted and discarded with two centrifugation steps at 3.000xg for 5 minutes and 4°C. Thereafter, the mitochondria were sedimented at 17.700xg for one hour. To improve the degree of purity this step was repeated. Mitochondria were resuspended in ST buffer with a final protein concentration of 50 mg/ml, shock frozen in liquid nitrogen, and stored at -20°C.

4.4.2 Isolation of mitochondrial outer membrane vesicles

- **Buffers and reagents**

Swelling buffer

(5 mM Tris-HCl pH 8.5, 1 mM EDTA, 1 mM PMSF)

ETP buffer

(1 mM EDTA, 20 mM Tris-HCl pH 8.5, 1 mM PMSF with 0.25 M, 0.72 M, 0.9 M, and 2 M sucrose, respectively)

Resuspending buffer
(50 mM Tris-HCl pH 8.5)

- **Devices**

Ultracentrifuge
(L7-65 Ultracentrifuge with Beckmann SW28 rotor and Beckmann Ti70 rotor – Beckman Coulter, Krefeld, Germany)

Water bath
(GFL - Gesellschaft für Labortechnik, Burgwedel, Germany)

Glass- Teflon- homogenisator
(custom-made)

Mitochondria (either freshly prepared or shock frozen and stored at - 20°C) were incubated in hypotonic swelling buffer at a concentration of 2 mg/ml for 30 minutes at 4°C with stirring. Swollen mitochondria were sedimented with a centrifugation step (17.000xg, 4°C). These were then resuspended in swelling buffer and incubated for 5 minutes at 37°C. The swollen mitochondria were then homogenized for 40 minutes in an automatic Glass- Teflon- homogenizer at 4°C. This led to the separation of the outer membrane vesicles (OMVs) from mitoplasts (mitochondria with disrupted outer membranes). These two fractions were separated with a sucrose gradient. For this purpose, 20 ml homogenate was added to 10 ml 0.9 M sucrose in ETP buffer and overlaid with 9 ml 0.25 M sucrose in ETP buffer and centrifuged with a Beckmann SW28 rotor for one hour (141.000xg, 4°C). Intact mitochondria, mitoplasts, and inner membrane fragments, were sedimented. OMVs were harvested from the “intermediate density fraction” between the 0.25 M and 0.9 M sucrose layers. The sample was then loaded on the bottom and allowed to float upwards to solutions with lower density. For this centrifugation step, the sucrose concentration of the harvested fraction was adjusted to 0.9 M by adding 2 M sucrose. This solution (15 ml) was covered with 10 ml 0.72 M sucrose in ETP and 3 ml ETP. The gradient was centrifuged overnight at 141.000xg at 4°C. OMVs collected between the top two layers were diluted in 50 mM Tris-HCl pH 8.5 and centrifuged in a Beckmann Ti70 rotor at 141.000xg for 30 minutes and 4°C. The sedimented OMVs were resuspended in a small volume of 50 mM Tris-HCl pH 8.5, shock frozen in liquid nitrogen, and stored at - 20°C until use.

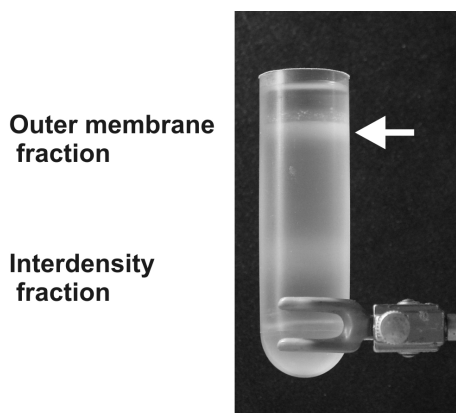


Figure 4.1: Second sucrose gradient during OMV preparation

The outer membrane vesicles are found in the top fraction at the boundary between buffers containing 0.72 M sucrose and 0 M sucrose (arrow). Proteins from the mitochondrial inner membrane are located in the intermediate density fraction.

4.4.3 Purification of His-tagged TOM core complex from mitochondria

- **Buffers and reagents**

10 % (w/v) DDM solution
(Glycon, Luckenwalde, Germany)

Solubilization buffer
(20 mM Tris-HCl pH 8.5, 300 mM NaCl, 20 % (v/v) glycerol, 1 % (w/v) DDM, 20 mM Imidazol, 1 mM PMSF)

Equilibration buffer
(20 % (v/v) glycerol, 20 mM Tris-HCl pH 8.5, 0.2 % (w/v) DDM)

NW1
(20 mM Tris-HCl pH 8.5, 10 % (v/v) glycerol, 0.1 % (w/v) DDM, 1 mM PMSF)

NW2
(50 mM potassium acetate, 10 mM MOPS pH 7.2, 10 % (v/v) glycerol, 0.1 % (w/v) DDM, 1 mM PMSF)

NB
(50 mM potassium acetate, 10 mM MOPS pH 7.2, 10 % (v/v) glycerol, 0.1 % (w/v) DDM, 300 mM imidazole, 1 mM PMSF)

ResA
(50 mM potassium acetate, 10 mM MOPS pH 7.2, 10 % (v/v) glycerol, 0.03 % (w/v) DDM)

ResB

(50 mM potassium acetate, 10 mM MOPS pH 7.2, 10 % (v/v) glycerol, 0.03 % (w/v) DDM, 1 M KCl)

- **Devices and material**

Ultracentrifuge

(L7-65 Ultracentrifuge with Beckmann Ti70 rotor – Beckman Coulter, Krefeld, Germany)

Yellow ribbon filter paper circles

(150 mm diameter; Schleicher and Schuell GmbH, Dassel, Germany)

HPLC (high pressure liquid chromatography)

(from GE Healthcare, Munich, Germany: Äkta Purifier System; Ni-NTA column (HisTrap, 1 ml); anion exchange column (ResourceQ, 1ml))

The *N. crassa* strain GR-107 contains a hexahistidinyI-tagged form of Tom22, which allows a large scale purification of TOM core complex from isolated mitochondria (Ahting et al., 1999). The detergent n-dodecyl- β -maltopyranosid (DDM) was used for solubilization of the mitochondrial membrane. The mitochondria were solubilized in solubilization buffer for 30 minutes with stirring, at 4°C and a protein concentration of 10 mg/ml. Insoluble residues were sedimented with a centrifugation step in a Beckmann Ti70 rotor at 260.000xg and were discarded. The supernatant was filtered through a yellow ribbon filter paper before being loaded to an equilibrated Ni-NTA column (15 ml of equilibration buffer). After washing the column with washing buffer NW1 the pH value of the column was switched from 8.5 to 7.2 by performing an additional washing step with buffer NW2. HexahistidinyI-tagged TOM core complex was then eluted from the column with elution buffer NB. The eluted TOM core complex was loaded onto a Resource Q column, which was equilibrated with buffer ResA in advance. After removing excessive bound proteins with buffer ResA, a linear salt gradient from 0 to 1M KCl (ResB) was applied to the column leading to the elution of TOM core complex at a salt concentration of 400 mM KCl. The collected samples were then analyzed with SDS-PAGE and their protein concentration was determined with the Bradford method before being stored at 4°C for up to three weeks at a concentration of 0.5 mg/ml.

4.4.4 Purification of Tom40 from mitochondria

- **Buffers and reagents**

Buffers from section 4.4.3

(Solubilization buffer, Equilibration buffer, NW1, NW2, NB)

OCT

(50 mM potassium acetate, 10 mM MOPS pH 7.2, 10 % (v/v) glycerol, 3 % (w/v) n-octyl β -D-glucopyranoside)

- **Devices and material**

Ultracentrifuge

(L7-65 Ultracentrifuge with Beckmann Ti70 rotor – Beckman Coulter, Krefeld, Germany)

Yellow Ribbon filter paper circles

(150 mm diameter; Schleicher and Schuell GmbH, Dassel, Germany)

HPLC (high pressure liquid chromatography)

(from GE Healthcare, Munich, Germany: Äkta Purifier System, Ni-NTA column (HisTrap, 1 ml))

A method was developed to isolate Tom40 protein directly from mitochondria. As described for the purification of TOM core complex above, mitochondria were solubilized in 1 % (w/v) DDM and loaded onto Ni-NTA column. This was followed by two washing steps with buffer NW1 and NW2. Tom40 was eluted from the column by applying buffer OCT. Due to the shorter alkyl-chain of octylglucoside compared to that of DDM, the interaction between Tom40 and Tom22 was weakened. Since Tom22 was immobilized to the column with the hexahistidinytag it remained bound, while Tom40 eluted from the column. Subsequently Tom22 and further proteins were washed from the column with buffer NB. The collected Tom40 fractions were analyzed with SDS-PAGE, and their protein concentration was determined with the Bradford method. In most cases, a size exclusion chromatography (see section 4.4.7) was performed to improve the purity of the sample and to exchange n-octyl β -D-glucopyranoside with DDM.

4.4.5 Purification of TOM core complex from OMVs

- **Buffers and reagents**

OMV-solubilization buffer

(1 % (w/v) DDM, 50 mM potassium acetate, 10 mM MOPS pH 7.2, 20 % (v/v) glycerol, and 1 mM PMSF)

ResA buffer

(50 mM potassium acetate, 10 mM MOPS pH 7.2, 10 % (v/v) glycerol, 0.03 % (w/w) DDM)

ResB buffer

(50 mM potassium acetate, 10 mM MOPS pH 7.2, 10 % (v/v) glycerol, 0.03 % (w/w) DDM, 1M KCl)

- **Devices**

Ultracentrifuge

(L7-65 Ultracentrifuge with Beckmann Ti50 rotor– Beckman Coulter, Krefeld, Germany)

HPLC (high pressure liquid chromatography)

(from GE Healthcare, Munich, Germany: Äkta Purifier System, anion exchange column (Resource Q, 1ml))

To purify TOM core complex from mutants lacking the hexahistidinyI-tagged form of Tom22 a method was developed to isolate TOM core complex directly from outer membrane vesicles (OMVs). After solubilization of the OMVs at a protein concentration of 2.5 mg/ml in OMV-solubilization buffer at 4°C for 30 minutes, insoluble material was removed by centrifugation in a Beckmann Ti50 rotor at 130.000xg for 40 minutes. Solubilized protein was bound to an anion exchange column that was equilibrated with ResA buffer in advance. After removing excessive bound proteins with excessive washing (30 ml buffer ResA), a linear salt gradient from 0 to 1M KCl (ResB) was applied to the column. TOM core complex eluted at a KCl concentration of 400 mM. The collected fractions were analyzed by gel electrophoresis, and their protein concentration was determined with the Bradford method. Size exclusion chromatography was performed to increase the purity of the samples (see section 4.4.7).

4.4.6 Purification of recombinant Su9_{1–69}DHFR from *E.coli*

- **Buffers and reagents**

SA buffer

(10 % (v/v) glycerol, 300 mM NaCl, 50 mM Na₂HPO₄ pH 8.0, 10 mM imidazole, 1 mM PMSF)

SB buffer

(10 % (v/v) glycerol, 300 mM NaCl, 50mM Na₂HPO₄ pH 8.0, 500 mM imidazole, 1 mM PMSF, 5 mM DTT)

Lysozyme

(Sigma Aldrich, Munich, Germany)

- **Devices**

- Centrifuge*

- (Evolution RC + SLA-300 rotor – Sorvall, Kendro Laboratory Products, Langensfeld, Germany)

- Sonifier 250*

- (SKAN AG, Basel, Switzerland)

- HPLC (high pressure liquid chromatography)*

- (from GE Healthcare, Munich, Germany: Äkta Purifier System, Ni-NTA column (HisTrap, 1 ml))

The harvested cells from 400 ml bacteria culture (see section 4.3) were resuspended in 10 ml SA buffer. This suspension was supplemented with 5 mg lysozyme and incubated at 4°C for 20 minutes in order to degrade the cell walls. This was followed by 3 washing steps. For this, the pellet was resuspended in 10 ml SA buffer and centrifuged with a SLA 300 Rotor at 3.000xg for 5 minutes. After the final washing step, the pellet was resuspended in 10 ml SA buffer and was sonicated 10 times for 10 sec with a Branson Sonifier (30 % pulse; output 3; 80 % duty cycle). The resulting suspension was centrifuged (39,000xg, 15 minutes) and the supernatant was loaded onto a Ni-NTA column with the Äkta Purifier System. The column had been pre-equilibrated with 20 ml SA buffer. The bound protein was then eluted with 30 ml SB buffer. The collected samples were shock frozen in liquid nitrogen and stored at - 20°C until further use.

4.4.7 Size exclusion chromatography

- **Buffers and reagents**

- SE buffer*

- (50 mM potassium acetate, 10 mM MOPS pH 7.2, 10 % (v/v) glycerol, 0.1 % (w/v) DDM)

- Protein standard*

- (Thyroglobulin (Thy), 669 kD; Apoferritin (Apo), 443 kD; Alcohol dehydrogenase (Adh), 150 kD; Bovine serum albumin (BSA), 66 kD; Ovalbumin (Ova), 43 kD; Ribonuclease A (Rib), 13.7 kD; from Sigma Aldrich (Munich, Germany) and GE Healthcare (Munich, Germany))

- **Devices**

- HPLC (high pressure liquid chromatography)*

- (from GE Healthcare, Munich, Germany: Äkta Purifier System, size exclusion column (Superose 6))

Size exclusion chromatography was used to increase the degree of purification of protein samples and for the analysis of the oligomeric state of the protein under native conditions. For this, a Superose 6 column was washed with 2 column volumes of distilled water before being equilibrated with 1.5 column volumes of SE buffer. 500 μ l sample were passed over the column, and samples of 1 ml fraction sizes were collected while the absorbance of the eluate was monitored at 280 nm. Comparison of the elution volume with those from protein standards, allowed a quantitative analysis of the molecular mass of the sample protein.

4.4.8 Precipitation of proteins with methanol

- **Buffers and reagents**

- Laemmli-loading buffer*

- (60 mM Tris-HCl pH 6.8, 2 % (w/v) SDS, 10 % (v/v) glycerol, 5 % (v/v) β -mercaptoethanol, 0.05 % (w/v) bromphenol-blue)

- **Devices**

- Tabletop centrifuge*

- (Biofuge Fresco – Kendro Laboratory Products, Langenselbold, Germany)

- Exicator*

- (Nucelite – Nalgen, Neerijse, Belgium)

To load larger amounts of protein onto a SDS gel, the samples were precipitated with methanol and resuspended in a smaller volume (Wessel and Flügge, 1984). Furthermore, a better resolution of the protein bands was obtained as interfering chemicals such as detergents and urea are removed.

For this, samples were diluted 1:4 in methanol and sedimented with a centrifugation step at 16.000xg for 5 minutes. After being dried in an exicator at room temperature for 10 minutes, the pelleted proteins were resuspended in Laemmli-loading buffer and subjected to gel electrophoresis (see section 4.4.10).

4.4.9 Determination of protein concentration with the Bradford Method

- **Buffers and reagents**

- Reaction reagent*

- (Bio Rad- Proteinassay – BioRad, Munich, Germany)

Protein standards

(Immunoglobulin G (2 mg/ml) – BioRad, Munich, Germany)

- **Devices**

Spectrometer

(Ultrospec II – Pharmacia Biosystems, Freiburg, Germany)

The method described by Bradford (1976) is based on an absorbance shift that occurs when arginine and hydrophobic amino acid residues of the protein sample bind the Coomassie dye. Measuring the absorption at a wavelength of 595 nm and comparing this with the measured values for a protein standard with a known concentration allows the quantification of the color reaction. In this study the calibration curve was established with Immunoglobulin G. Protein samples and protein standard were diluted to a final volume of 24 μ l before adding 1 ml of reaction reagent. The samples were incubated for 5 minutes at room temperature before measuring the absorption at 595 nm.

4.4.10 Gel electrophoresis

- **Buffers and reagents**

Gel buffer – Tricine-SDS-PAGE

(3 M Tris-HCl pH 8.45, 0.3 % (w/v) SDS)

“Acrylamide-mix” – Tricine-SDS-PAGE

(48 % (w/v) acrylamide, 1.5 % (w/v) bisacrylamide)

Composition of SDS-PAGE and Tricine-SDS-PAGE

(see following table)

Running buffer – SDS-PAGE

(248 mM Tris-HCl; 1.92 M glycine; 35 mM SDS)

Cathode buffer (10x) – Tricine-SDS-PAGE

(1 M Tris-HCl pH 8.25; 1 % (w/v) SDS; 1 M Tricine)

Anode buffer (10x) – Tricine-SDS-PAGE

(1 M Tris-HCl pH 8.9)

Laemmli-loading buffer

(60 mM Tris-HCl pH 6.8, 2 % (w/v) SDS, 10 % (v/v) glycerol, 5 % (v/v) β -mercaptoethanol, 0.05 % (w/v) bromphenol- blue)

Protein standard

(Roti-Mark Standard – Roth, Karlsruhe, Germany)

(Myosin (200 kD), β -Galactosidase (119 kD), Serum albumin (66 kD), Ovalbumin (43 kD), Carbonic anhydrase (29 kD), Trypsin inhibitor (20 kD), Lysozyme (14.5 kD))

- **Devices**

Glass plates, caskets, and electrophoresis tanks

(Protean III system – BioRad, Munich, Germany; glass plates: 8 x 6 cm and spacers of 0.7 mm thickness; electrophoresis conditions: 20 mA, 200 V)

(custom-made apparatus – glass plates: 16 x 14 cm and spacers of 1 mm thickness; electrophoresis conditions: 100 mA, 200 V)

Heater plate

(Thermostat 5320 – Eppendorf, Hamburg, Germany)

Power-supply

(Consort E861 – Sigma Aldrich, Munich, Germany)

The method according to Laemmli (1970) allows the separation of protein samples according to their molecular mass. By adding Laemmli-loading buffer to the samples and boiling these at 95°C for 5 minutes, disulfide bridges are reduced, and the proteins are denatured. The binding of the SDS to protein results in an almost uniform mass to charge ratio. The negative net charge allows the proteins to migrate through the gel. The resolution is dependent on the pore size of the acrylamide matrix and can also be improved by pouring a stacking gel above the actual separating gel. The pH jump between these two gels leads to a focusing of the sample resulting in a sharper band during migration. Establishing a calibration curve with samples of known molecular mass allows a quantitative analysis by comparing migration distances.

To cast the gel, the glass plates and spacers were thoroughly rinsed with 70 % ethanol and placed in the gel casting apparatus. The addition of TEMED and APS to the gel solution induced the polymerization of the gel. Thus, after addition of these two additives the gel was immediately poured between the glass plates. The separation gel was poured up to 3/4 of the height of the glass plates. The gel was overlaid with isopropanol to prevent oxidation of acrylamide which would have, otherwise, led to incomplete polymerization. After 30 minutes the gel was totally polymerized, and the isopropanol was removed. The stacking gel was then complimented with TEMED and APS and poured to the rim of the glass plates. The comb was immediately inserted. After total polymerization of the gel, it was removed from the casting apparatus and wrapped in damp paper towels and stored at 4°C for a maximum of five days. Additionally, a Tricine-SDS-PAGE system (according to Schägger and von Jagow, 1991) was used for the separation of small proteins and peptides (1 -100 kD). In this study, Tricine-SDS-PAGE (16 % (w/w) acrylamide) was used to analyze the small Tom proteins Tom5, Tom6, and Tom7. The Tricine-SDS gels were prepared in a similar man-

ner as described above. Simply, an additional 1 cm wide spacer gel was poured between the separating gel and stacking gel.

In our laboratory two different gel apparatus were used – the BioRad Protean III system for fast analysis of protein, and a custom-made setup that uses larger gels for a better separation of proteins with similar molecular mass and for gel elution experiments. The electrophoresis conditions for the Protean III system were 20 mA and 200 V, and 100 mA, 200 V for the custom-made apparatus.

Composition of SDS-PAGE (14.5 % (w/w) acrylamide)

	Separating gel	Stacking gel	Bottom gel
Acrylamide (Rotiphorese Gel A*)	14.5 % (w/v)	5 % (w/v)	20 % (w/v)
Bisacrylamide (Rotiphorese Gel B*)	0.03 % (w/v)	0.03 % (w/v)	0.13 % (w/v)
Tris-HCl pH 8.8	380 mM	–	475 mM
Tris-HCl pH 6.8	–	60 mM	–
10 % SDS	0.1 % (w/v)	0.1 % (w/v)	0.1 % (w/v)
TEMED	0.05 % (v/v)	0.05 % (v/v)	0.05 % (v/v)
APS	0.05 % (w/v)	0.25 % (w/v)	0.25 % (w/v)

*Roth, Karlsruhe, Germany

Composition of Tricine-SDS-PAGE (16 % (w/w))

(according to Hunte et al., 2003, chapter 4)

	Separating gel	Stacking gel	Spacer gel
"Acrylamide-mix"	10 ml	1 ml	3 ml
Gelbuffer	10 ml	3 ml	5 ml
Glycerol	3 g	–	–
H₂O	30 ml	12 ml	15 ml
TEMED	100 μ l	80 μ l	90 μ l
APS	10 μ l	8 μ l	9 μ l

4.4.11 Documentation of polyacrylamide gels

- **Buffers and reagents**

Coomassie stain

(30 % (v/v) methanol, 10 % (v/v) acetic acid, and 0.1 % (w/v) Coomassie-Brilliant-blue R250 (Serva, Heidelberg, Germany))

Destaining buffer

(30 % (v/v) methanol, 10 % (v/v) acetic acid)

Silver staining

(Silver Stain kit – Fluka, Buchs, Switzerland)

- **Devices and material**

Shaker

(GFL 3005 – Gesellschaft für Labortechnik, Burgwedel, Germany)

Scanner

(Epson perfection 1250 – Epson, Meerbusch, Germany)

Whatman paper

(3MM, GB002 – Schleicher and Schuell GmbH, Dassel, Germany)

Gel dryer

(MGD-5040 – VWR, Darmstadt, Germany)

Coomassie staining

For the detection of 1 μg and more protein the SDS- polyacrylamide gels as well as Tricine-SDS gels were stained with a Coomassie dye. For this, the gels were incubated for 30 minutes in staining solution at room temperature. The irreversibly stained protein bands became visible after removing the background stain with destaining buffer. For this, the destained buffer was exchanged with fresh buffer every 15 minutes. Approximately after 2 hours the gel was sufficiently destained.

Silver staining

Smaller amounts of protein separated on a polyacrylamide gel were visualized with silver staining. For this, the silver stain kit based on Swain and Ross (1995) was used at room temperature according to the manufacture's directions. After fixation of the protein bands in the ethanol/ acetic acid solution (10 minutes), the gel was rinsed with water (10 minutes) before the proteins were sensitized with a sodium dithionite solution (5 minutes). Thereafter, the gel was washed with 40 % (v/v) ethanol solution (20 minutes) and with water (20 minutes). A further sensitizing of the gel was induced with the sodium thiosulphate solution (1 minute). The gel was quickly rinsed in water (2 x 1 minute), before the color reaction was

induced by incubating the gel in the silver nitrate solution (20 minutes) and subsequently in a sodium carbonate/formaldehyde detection solution (5 - 15 minutes). The color reaction was stopped by incubating the gel in 2.5 % (v/v) acetic acid solution (15 minutes).

Drying polyacrylamide gels

The gels were scanned for documentation using a flat bed scanner. For this, they were placed between saran wrap to protect the scanner. Afterwards, they were dried with vacuum and heat (65°C) for 90 minutes onto a sheet of Whatman paper with a gel dryer.

4.4.12 Elution of proteins separated by SDS-PAGE

- **Buffers and reagents**

pre-stained protein standard marker

(Roti-Mark PRESTAINED – Roth, Karlsruhe, Germany)

(Myosin (245 kD); β -Galactosidase (123 kD); Serum albumin (77 kD); Ovalbumin (42 kD); Carboanhydrase (30 kD); Trypsin inhibitor (25.4 kD); Lysozyme (17 kD))

SE buffer

(50 mM potassium acetate, 10 mM MOPS pH 7.2, 10 % (v/v) glycerol, 0.1 % (w/v) DDM)

- **Device**

Overhead shaker

(34528 E – NeoLab Migge, Heidelberg, Germany)

As an additional purification step, proteins were separated with SDS-PAGE or Tricine-SDS-PAGE and were then eluted thereof by diffusion (Hunte et al., 2003, chapter 4). For this, proteins were separated by electrophoresis along with pre-stained protein standards to estimate the migration distance of the protein sample. After gel electrophoresis the gel band was excised with a scalpel blade. The removed band was placed in a reaction tube and incubated in 300 μ l SE buffer for 48 hours at 4°C in an overhead shaker. Samples were analyzed with SDS-PAGE and subsequent silver staining.

4.4.13 Blue-native polyacrylamide gel electrophoresis (BNGE)

- **Buffers and reagents**

- “Acrylamide-mix”*

- (48 % (w/v) acrylamide, 1.5 % (w/v) bisacrylamide)

- Bottom gel*

- (see 4.4.10)

- Solution A*

- (13 % (v/v) “Acrylamide-mix”, 25 mM imidazole pH 7.0, 0.5 M 6-aminocaproic acid, 20 % (v/v) glycerol, 0.05 % (w/v) APS, 0.0055 % (v/v) TEMED)

- Solution B*

- 5 % (v/v) “Acrylamide-mix”, 25 mM imidazole pH 7.0, 0.5 M 6-aminocaproic acid, 0.05 % (w/v) APS, 0.0005 % (v/v) TEMED)

- Stacking gel*

- (4 % (v/v) “Acrylamide-mix”, 25 mM imidazole pH 7.0, 0.5 M 6-aminocaproic acid, 0.08 % (w/v) APS, 0.008 % (v/v) TEMED)

- Cathode buffer*

- (15 mM bis-Tris pH 7.0, 50 mM Tricine, 0.02 % (w/v) Coomassie-Brilliant-blue G250 (Serva, Heidelberg, Germany))

- Slightly blue cathode buffer*

- (the same as cathode buffer, dye concentration is reduced to 0.002 % (w/v))

- Anode buffer*

- (50 mM bis Tris-HCl pH 7.0)

- BNGE-loading buffer (5x)*

- (10 % (v/v) glycerol solution supplemented with 0.002 % (w/v) Ponceau S)

- Marker proteins*

- (Thyroglobulin (Thy, 667 kD); Apoferritin (Apo, 440 kD); Alcohol dehydrogenase (ADH, monomer: 50 kD, dimer: 100 kD trimer: 150 kD); Bovine serum albumin (BSA, monomer: 66 kD, dimer: 132 kD); from Sigma Aldrich (Munich, Germany) and GE Healthcare (Munich, Germany))

- **Devices**

- Glass plates*

- (see above)

- Gradient mixer*

- (custom-made)

- Power supply*

- (Consort E861 – Sigma Aldrich, Munich, Germany)

The blue-native polyacrylamide gel electrophoresis (BNGE) approach (Schägger and von Jagow, 1991) was used for the separation of native proteins (10 kD - 10000 kD). Binding of Coomassie dye to a protein shifts the isoelectric point of

the latter resulting in a more negative net charge at neutral pH. Length of migration is dependent on the mass of the protein complex when using a uniform native gel. In most cases, however, a gradient gel was used. Here, the decreasing pore size of the gel caused an almost complete migration stop when the various proteins reach the pores that were too small for them to pass.

For this, a polyacrylamide gel was cast with an acrylamide gradient from 18 % (w/v) to 5 % (w/v) acrylamide, thus, allowing a wide range of separation (10 kD - 500 kD). Larger glass plates with a 1 mm thick spacer were used. After sealing the plates with a bottom gel, the separating gel was poured between them with the help of a gradient mixer. Solution A was placed in the front compartment, and Solution B was placed in the back compartment. Solution A slowly left the tube by gravity flow. At the same velocity solution B flowed into the front chamber and, thus, dilution of buffer A took place and an acrylamide gradient was built up between the glass plates. After complete polymerization of this gel a stacking gel was poured on top. This too, was allowed to polymerize. Gels were stored at 4°C for a maximum of 14 days until use. BNGE-loading buffer was added to the samples before they were loaded onto the gel. Gel electrophoresis was performed at 4°C, resulting in sharper bands.

The initial electrophoresis settings were 100 V and 10 mA. Once the migration front reached two thirds of the gel the cathode buffer was replaced by the slightly blue cathode buffer, and the voltage was increased to 500 V.

4.4.14 Elution of proteins separated by BNGE

- **Buffers and reagents**

SE buffer

(50 mM potassium acetate, 10 mM MOPS pH 7.2, 10 % (v/v) glycerol, 0.1 % (w/v) DDM)

- **Device**

Overhead shaker

(34528 E – NeoLab Migge, Heidelberg, Germany)

Similar to the protocol for the isolation of proteins by elution from SDS- gels in section 4.4.12, protein samples were loaded onto a native gel and separated by electrophoresis. Due to the blue color, the desired protein band was easily identified and removed with a scalpel blade, placed into a reaction tube, and incubated

in 300 μ l of SE buffer for 48 hours at 4°C on an overhead shaker. The successful elution of the protein was verified with SDS-PAGE.

4.4.15 Transfer of proteins to nitrocellulose or PVDF membranes

- **Buffers and reagents**

- Transfer buffer*

- (20 mM Tris, 150 mM glycine, 20 % (v/v) methanol, 0.08 % (w/v) SDS)

- Ponceau S solution*

- (0.2 % (w/v) Ponceau S in 3 % (w/v) trichloroacetic acid solution)

- **Devices and material**

- nitrocellulose*

- (Protran nitrocellulose membrane – Schleicher and Schuell GmbH, Dassel, Germany)

- PVDF membrane*

- (Roti-PVDF-membrane – Roth, Karlsruhe, Germany)

- Whatman paper*

- (3MM, GB002 – Schleicher and Schuell GmbH, Dassel, Germany)

- Transfer device*

- (custom-made)

- Power supply*

- (Consort E861 – Sigma Aldrich, Munich, Germany)

Proteins separated by SDS-PAGE, Tricine-SDS-PAGE, or BNGE were transferred either onto a nitrocellulose or PVDF membrane, using the semi-dry blotting method (Kyhse-Andersen, 1984; Towbin et al., 1979). The choice of membrane depended on the detection method preferred for immunodecoration (see below). Whatman filter paper (six sheets) and the membrane were soaked in transfer buffer. When using PVDF membranes, these were soaked in methanol and rinsed well with water before use. Three sheets of filter paper were laid on the anode. The membrane was placed on top. This was followed by the gel and another three sheets of filter paper, before placing the cathode on top. The transfer was performed at 200 mA and 5-15 mV for 50 minutes for the larger gels (16 x 14 cm). When smaller gels (8 x 6 cm) were used, the current was adjusted accordingly to 50 mA. Reversibly staining the membrane with Ponceau S solution allowed the determination of the transfer efficiency. For this, the membrane was incubated in Ponceau S solution for 5 minutes. After rinsing the membrane with water, the protein bands became visible.

4.4.16 Immunodecoration

- **Buffers and reagents**

TBS

(50 mM Tris-HCl pH 7.2, 150 mM NaCl)

TBS-Tween

(50 mM Tris-HCl pH 7.2, 150 mM NaCl, 0.1 % (v/v) Tween-100)

Blocking solution

(5 % (w/v) milk powder in TBS-T , or 5 % (w/v) BSA in TBS-T)

Primary antibodies

(Polyclonal antisera were made in rabbits and were kindly provided by Dr. Doron Rapoport – Institut für Biochemie, Universität Tübingen, Germany)

Secondary antibody

(Anti-rabbit, AP - conjugated; Rockland (BioMol GmbH, Hamburg, Germany))

AP-buffer

(100 mM Tris-HCl pH 9.6, 100 mM NaCl, 5 mM MgCl₂*6 H₂O).

NBT (Nitro blue tetrazolium chloride)

(50 mg/ml in 70 % (v/v) dimethylformamide)

BCIP (5-Brom-4-chloro-3-indolyl-phosphat)

(50 mg/ml in 100 % (v/v) dimethylformamide)

CDP-Star

(5 µl of the chemiluminescence substrate (Roche, Mannheim, Germany) in 500 µl AP-Puffer)

- **Devices**

Overhead shaker

(34528 E – NeoLab Migge, Heidelberg, Germany)

Horizontal shaker

(GFL 3005 – Gesellschaft für Labortechnik, Burgwedel, Germany)

X-ray film

(Fuji Photo Film Co., Ltd., Tokyo, Japan)

Automatic developing machine

(Curix 60, Agfa, Cologne, Germany)

After having transferred the separated proteins from the SDS-PAGE onto a membrane various proteins were identified with specific antibodies. First, the areas of the membrane that did not have protein attached were saturated with blocking solution to avoid non-specific binding of the primary and secondary antibody. For this, the membrane was either incubated in blocking solution for 90 minutes at room temperature or overnight at 4°C. The next step was the binding of the

specific primary antibody. Sera containing polyclonal antibodies were diluted between 1:500 and 1:5,000 in blocking solution. The membrane was either incubated for one hour at room temperature or overnight at 4°C with the primary antibody. Excess antibody was removed with six washing steps (with TBS-T, 5 minutes each) before incubating the membrane with the secondary antibody. In this study, the secondary antibody was directed against the Fab fragments of rabbit IgG and coupled with alkaline phosphatase (AP). The secondary antibody was also diluted in blocking buffer (1:10,000) and added to the membrane for one hour at room temperature. Again, excess antibody was removed with three washing steps with TBS-T and three washing steps with TBS. The latter washing steps were important to remove the detergent Tween-100, which would have otherwise prevented the substrate from binding to the enzyme. The membrane was then equilibrated with AP-buffer. Two different detection systems were applied:

(i) color reaction: 66 μ l NBT, 33 μ l BCIP were freshly mixed in 10 ml AP-buffer. The membrane was covered with the solution, and after 3-10 minutes the decorated proteins became visible as dark-purple precipitate. The color reaction was stopped by adding water to the solution.

(ii) CDP-Star reaction: the membrane was covered with the CDP-Star solution, and the chemiluminescence reaction was visualized on X-ray film.

4.5 Structural biological methods

4.5.1 Reconstitution of membrane proteins for 2-D crystallization

- **Buffers and reagents**

- Lipids*

- (DMPC, EPC, DOPC, Cardiolipin, DMPE, DMPG, DOGS-Ni-NTA – Avanti Polar Lipids, Alabaster, USA)

- Bio-beads*

- (Bio-Beads SM-2 – BioRad, Munich, Germany)

- Uranly acetate*

- (2 % (w/v) solution – Merck, Darmstadt, Germany)

- **Devices**

- Carbon grids*

- (Plano, Wetzlar, Germany)

- Electron microscope*

- (Philips CM 120 electron microscope operating at 120 kV)

- “monolayer method” device*

- (custom-made)

- Hamilton syringe*

- (VWR, Darmstadt, Germany)

For reconstitution of TOM core complex into lipid membranes, two different approaches were applied – the “bulk method” and the “monolayer method”. In the first method, lipid vesicles were formed in which the proteins are tightly packed. For this, isolated membrane proteins in detergent solution were incubated with lipids and bio-beads. These macroporous polystyrene beads absorbed detergent. The detergent surrounding the protein was replaced with lipids. This led to formation of the protein-embedded lipid vesicles. In the second method, quasi crystalline sheets of protein surrounded by lipids are formed at an air-water interface. For this, lipid was spread over a cavity containing isolated membrane proteins in a detergent solution. Here too, the detergent was removed with bio-beads and the proteins incorporated into the monolayer formed at the air-water interface. For structure analysis of these “2-D” crystals electron microscopy techniques were applied. Electron micrographs of reconstituted protein were taken with a video

printer. These were then scanned and analyzed with ImageJ 1.38x (Wayne Rasband, National Institutes of Health, USA; <http://rsb.info.nih.gov/ij/>). For this, a Fourier transform was performed to check if the reconstituted proteins are ordered in a crystal like lattice.

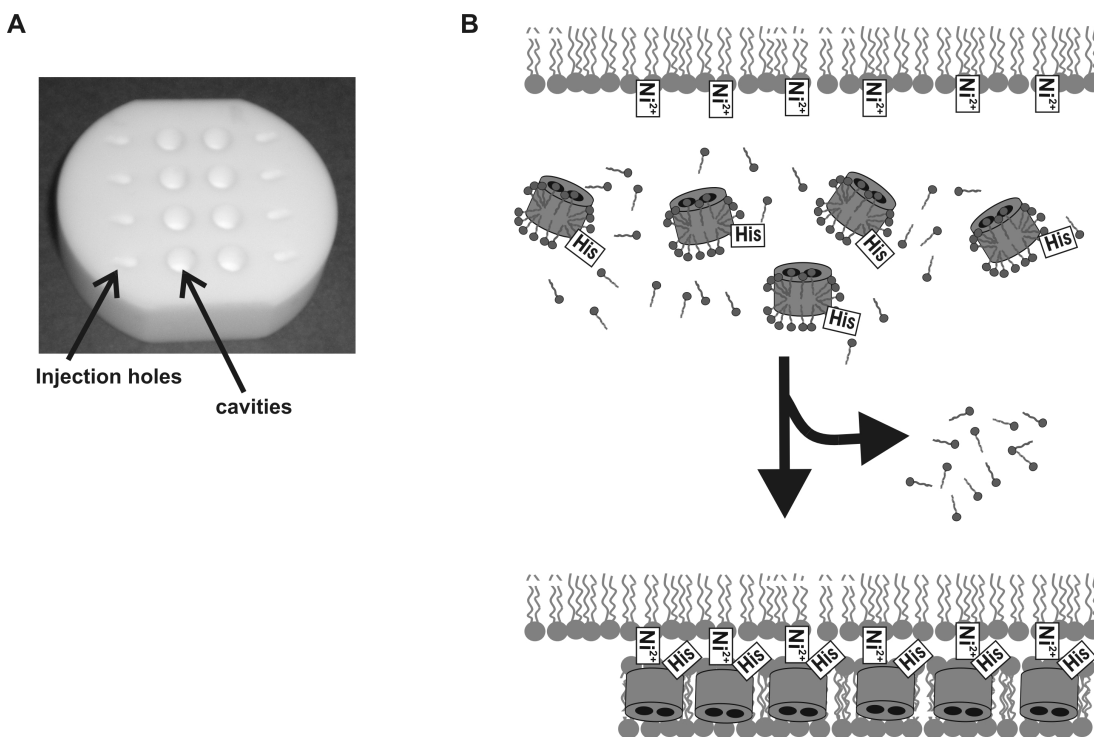


Figure 4.2: 2-D crystallization – Monolayer method

A) Photograph of the monolayer method device. Injection holes are placed next to Teflon wells with 60 μl volume and 4 mm diameter. 1 μl (0.5 μg) DOGS-Ni-NTA is spread on the surface of the solution in the cavity. Protein preincubated with lipids as well as bio-beads are added through the injection holes.

B) Schematic drawing of the principle of the method. Proteins bind to the monolayer with their specific tag. With the addition of bio-beads the detergent is removed from the sample. The lipids and proteins form crystalline sheets.

Bulk method

50 μl sample with a protein concentration of 0.5 mg/ml was incubated with various concentrations of different lipids for one hour. 5 mg of bio-beads were added to the solution. This was allowed to incubate for 1 hour. Thereafter, another 5 mg bio-beads were added. After another incubation for one hour 5 μl of sample were spread onto a carbon coated grid and stained with uranyl acetate (2 % (w/v) in distilled water). The grids were analyzed with standard electron microscopy tech-

niques (in collaboration with Dr. Daniél Levi and Dr. Jean-Louis Rigaud – Institut Curie, Paris, France).

Monolayer method

The surface of the apparatus (see Fig.4.2) was washed with methanol and warm water and subsequently rinsed with distilled water. Small magnet stirrers were put into the holes, and 60 μl of buffer were added through the injection holes (thereby air bubbles were removed). Next, 1 μl DOGS-Ni-NTA (0.5 mg/ml) was spread on the surface of the solution in the cavity. DOGS-Ni-NTA is a lipid derivatized with a Ni-NTA head group. The protein sample (0.5 mg/ml) was incubated with the respective lipid for one hour. This solution (6 μl) was then carefully added to the setup through the injection holes. The setup was allowed to relax for some time. Thereafter, bio-beads were added to the system through the injection holes. The solution was stirred with a magnet stirrer. A carbon-coated grid was laid onto the cavity allowing the monolayer to transfer to the grid. The grid, was analyzed with electron microscopy techniques (in collaboration with Dr. Daniél Levi and Dr. Jean-Louis Rigaud – Institut Curie, Paris, France).

4.5.2 3-D crystallization

- **Buffers and reagents**

protein

(Tom40 protein isolated with the protocol described in section 4.4.4)

dialysis buffer

(10 mM Hepes pH 7.2; 1 % (w/v) β -D-glucopyranoside)

crystallization screens

from Jena Bioscience GmbH, Jena, Germany: Jena Classic (1+2)

Ozma PEG-Series 48-Salt

(1K, 4K, 8K and 10 K)

Emerald Cryo (I + II)

Emerald Wizard (1,2,3)

Hampton Research, Aliso Viejo, CA, USA: Hampton Index

Hampton Crystal Screen HT

Hampton Salt Rx HT

Hampton Membfac HT

Hampton Cryo (1 - 48)

- **Devices**

concentrator

(Vivaspin concentrator, cut-off 10 kD – Vivascience, Hannover, Germany)

dialysis membrane

(VISKING; cut-off 10 kD – Roth, Karlsruhe, Germany)

pipetting robot

(Honeybee 961 crystallization robot – Genomic Solutions, Huntingdon, United Kingdom)

documentation device

(RockImager 54 – Formulatrix, Amsterdam, the Netherlands)

sitting-drop plates

(96 well Corning 3550 plates – Hampton Research, Aliso Viejo, CA, USA)

The aim of X-ray crystallography is the determination of the atomic structure of a protein. The atomic structure of the sample can then be determined by analyzing diffraction patterns from X-ray scattering. The challenging task in X-ray crystallography of biological samples is the generation of a protein crystal. To obtain crystals, protein samples have to be isolated in large amounts and with high purity. By screening various conditions the optimum buffer and additives are determined that prompt crystallization.

For the crystallization trials of Tom40 at least 10 mg protein was isolated and concentrated to a concentration of 10 mg/ml. The protein solution was dialyzed against 1 % (w/v) β -D-glucopyranoside in a 10 mM Hepes (pH7.2) solution for at least 24 hours.

With the aid of an automatic pipette robot 400 nl sample was subjected to 96 well plates of commercial crystallization screens. In the sitting-drop technique which was applied in this study, the sample was mixed with equal volume of precipitation solution and was placed next to a liquid reservoir of the same solution. As the drop contained a lower precipitant concentration, water left the drop towards the reservoir to achieve vapor equilibrium. This led to a higher concentration of protein within the drop and sometimes resulted in the formation of crystals. On day 1, 7, and 28 drop images were obtained with the RockImager.

The obtained crystals were analyzed at the synchrotron radiation facility SLS (PSI Villigen, Switzerland) by Dr. Reinhard Albrecht (Max-Plank-Institut für Entwicklungsbiologie, Tübingen, Germany).

4.6 Spectroscopical methods

- **Buffers and reagents**

FCS buffer

(25 mM HEPES pH 7.2, 2 % (v/v) DMSO, 0.03 % (w/v) DDM)

Chromophores

(Alexa Fluor 488 C5-maleimide, Alexa Fluor 546 C5-maleimide – Molecular Probes, Leiden, the Netherlands; these were dissolved in DMSO (20 mM) and stored at -20°C)

DMSO

(Sigma Aldrich, Munich, Germany)

TCEP

(Sigma Aldrich, Munich, Germany)

- **Devices and material**

Bio-beads

(Bio-Beads SM-2 – BioRad, Munich, Germany)

Desalting column

(PD10 column – GE Healthcare, Munich, Germany)

Micro desalt spin columns

(Zeba from Perbio Science, Bonn, Germany)

Vivaspin concentrator

(Vivascience, Hannover, Germany; cut-off 10 kD)

In fluorescence correlation spectroscopy (FCS) light is focused on the sample (Haustein and Schwille, 2003, 2007). The high energy of the laser beam excites fluorescently labeled proteins within the focus. With a detection system the fluorescent fluctuations are measured. These fluctuations can originate from fluorescent molecules that diffuse in and out of the laser focus. Large molecules with a slower diffusion time reside longer in the focus volume than molecules with a shorter hydrodynamic radius. For FCS measurements the detection volume is normally 1 - 6 fl small.

The fluorescent fluctuations $\delta F(t)$ within the defined volume at time t is:

$$\delta F(t) = F(t) - \langle F(t) \rangle \quad (4.1)$$

where $F(t)$ is the measured fluorescent count at time t and $\langle F(t) \rangle$ is the expected fluorescent count determined from the fluorescent count measured over a given total time T and can be described with:

$$\langle F(t) \rangle = \frac{1}{T} \int_0^T F(t) dt \quad (4.2)$$

Periodic fluctuations which are overlaid by a general background are determined by calculating the correlation of the fluorescent fluctuation function $\delta F(t)$ with a time-shifted version of itself. This autocorrelation function $G(\tau)$ is:

$$G(\tau) = \frac{\langle \delta F(t) * \delta F(t + \tau) \rangle}{\langle F(t) \rangle^2} \quad (4.3)$$

where τ is the time span by which the function is shifted.

The recorded autocorrelation functions are fitted with a model function for three-dimensional diffusion:

$$G(\tau) = G(0) \frac{1}{\left(1 + \frac{\tau}{\tau_D}\right) \sqrt{1 + \frac{1}{\omega^2} \frac{\tau}{\tau_D}}} + G(\infty) \quad (4.4)$$

where ω is the form factor and describes the ratio of the axial to radial radii of the focus volume, τ_D is the expected diffusion time of the fluorescent molecule inside the detection volume. Due to the normalization of autocorrelation function (equation 4.3), the mean average of number of fluorophores $\langle N \rangle$ inside the detection volume can be determined from $G(0)$:

$$G(0) = \frac{1}{\langle N \rangle} \quad (4.5)$$

FCS was applied to analyze the dynamics underlying the interaction of pre-protein with the translocase of the mitochondrial outer membrane. A binding of a fluorescent labeled preprotein to the large TOM complex would have resulted in slower diffusion time of the preprotein and therefore an increase in the time span spent in the focus volume τ_D . For this experiment Su9_{1–69}DHFR, a model preprotein, was fluorescently labeled.

Preparation of Su9_{1–69}DHFR or FCS measurements

Recombinant Su9_{1–69}DHFR was isolated from *E. coli* (as in section 4.4.6). During the isolation 1 mM DTT was added to SB buffer to avoid disulfide formation of Su9_{1–69}DHFR. Before labeling the protein with a thiol reactive reagent, however,

the DTT had to be removed. For this, the protein sample was passed over a small gravity-flow gel filtration column (PD10 column).

Labeling with Alexa Fluor 488 C5-maleimide was performed according to the manufacture's directions at room temperature. The protein sample (0.5-1 mg/ml) was incubated with 40 μ M Alexa Fluor 488 C5-maleimide and a time series was performed to determine the optimal binding time. For this, at 0, 5, 10, 40, 60, 90, and 120 minutes an aliquot was removed, and the labeling of the sample was stopped by adding the reducing agent TCEP (5 mM). The samples were analyzed with SDS-PAGE. For quantification of the fluorescent intensity of the samples, the gels were analyzed with the gel documentation system from SERVA, or micrographs of the gels excited with UV light were analyzed with ImageJ 1.38x (Wayne Rasband, National Institutes of Health, USA; <http://rsb.info.nih.gov/ij/>).

For binding studies with FCS, labeling of the smaller binding partner is sufficient. For fluorescent cross correlation spectroscopy (FCCS), however, both binding partners have to be labeled. During the measurements the sample is excited with two different laser beams, and two different emission spectra are recorded. The cross correlation of the fluctuations for both wavelengths is then determined. Fitting this curve with the function for three-dimensional diffusion (equation 4.4) allows the determination of τ_D which corresponds to the expected time span that both fluorophores and, therefore, both binding partners spend in the detection volume.

Preparation of TOM core complex for FCCS measurements

Preliminary FCS measurements had indicated that the isolation buffer of TOM core complex (50 mM potassium acetate, 10 mM MOPS pH 7.2, 10 % (v/v) glycerol, 0.03 % (w/v) DDM) was not very suitable for FCS and FCCS measurements. Both MOPS and glycerol changed the spectroscopic properties of the solution. Therefore, the isolation of TOM core complex (see section 4.4.3) was performed in 25 mM HEPES pH 7.2, 2 % (v/v) DMSO, 0.03 % (w/v) DDM.

TOM core complex (1 mg/ml) was incubated with 40 μ M Alexa Fluor 546 C-maleimide at room temperature. A time-dependent binding assay was performed as described above.

Removal of free label

A critical but tricky step in the preparation of proteins for FCS measurements is the removal of free dye. In this study, various methods were applied to accomplish this task.

- Size exclusion chromatography (Superose 6 column – GE Healthcare, Munich, Germany)

This method, as described in section 4.4.7, was used to separate the labeled sample from free dye by size exclusion with a Superose 6 column and the Äkta Purifier system. The buffer used for elution of the protein was 25 mM HEPES, 10 mM MOPS pH 7.2, 2 % (v/v) DMSO , 0.1 % (w/v) DDM

- Desalting column (PD10 column – GE Healthcare, Munich, Germany)

Similar to the Superose 6 column, different molecules were separated with PD10 columns by size. The column was equilibrated with 20 ml FCS buffer. After applying the labeled sample, the protein was eluted by adding further buffer and collecting samples.

- Micro desalt spin columns (Zeba – Perbio Science, Bonn, Germany)

Similar to the PD10 columns, the spin columns were used to remove small molecules like salt and dye. After spinning the column (tabletop centrifuge, 1,500xg for one minute) to remove storage solution, the sample was loaded onto the column. This was spun again for two minutes, before the sample was collected.

- Vivaspin concentrator (Vivascience, Hannover, Germany; cut-off 10 kD)

The principle behind a concentrator is a membrane that acts as a molecular sieve, as small molecules can pass the pores with a distinct size, while larger molecules are concentrated above the membrane. The sample was loaded above the membrane and centrifuged in a table top centrifuge at 10,000xg until the desired volume was left.

- Bio-beads (Bio-Beads SM-2 – BioRad, Munich, Germany)

These macroporous polystyrene beads absorb hydrophobic molecules and are often used in 2-D crystallization trials for the removal of detergent. In this study, they were also used to remove free dye from the sample. For this, they were added to a protein solution, and the solution was stirred for two hours while the free dye was adsorbed by the bio-beads.

FCS measurements

FCS measurements were performed with a commercial ConfoCor 2 combination system (Carl Zeiss, Jena, Germany; Weisshart et al., 2004) in collaboration with Dr. Elke Haustein (TU Dresden, Germany, laboratory of Dr. Petra Schwille). The measurements were performed at room temperature. The sample was transferred to the specimen stage. The laser beam was focused with the objective. The fluorescent molecules were excited with the Argon-laser beam at 488 nm and the HeNe laser-beam at 546 nm, respectively.

For the analysis of the collected data, the autocorrelation function $G(\tau)$ was derived from the measured fluctuations. Ten measurements of ten seconds each were averaged. The resulting curve was fitted with a one- or two-component fit function to estimate the diffusion times for the fast (free dye) and slow (labeled protein) components.

4.7 Electrophysiological Methods

4.7.1 Setup

- **Buffers and reagents**

- Buffer*

- (10 mM HEPES pH 7.2 with 125 mM, 250 mM, 1000 mM, and 3000 mM KCl, respectively)

- Lipid*

- (diphytanoyl-phosphatidylcholine, DiphPC – Avanti Polar Lipids, Alabaster, USA)

- n-Decan*

- (Sigma Aldrich, Munich, Germany)

- Butanol*

- (Merk, Darmstadt, Germany)

- Chloroform*

- (Merk, Darmstadt, Germany)

- Methanol*

- (VWR, Darmstadt, Germany)

- **Devices and material**

- Amplifier*

- (EPC-8 patch clamp amplifier – HEKA Electronics, Lamprecht, Germany)

A/D converter

(NI-USB-6251 interface – National Instruments, Munich, Germany; controlled by programs of the Strathclyde electrophysiology suite (WinEDR 2.8 or WinWCP 3.6, J. Dempster, University of Strathclyde, Glasgow, UK <http://spider.science.strath.ac.uk/sipbs/page.php?show=software>))

Oscilloscope

(HM 504 – HAMEG Instruments, Mainhausen, Germany)

Chamber

(During this study two types of chambers were used. (i) a custom-made setup (according to Hanke and Schlue, 1993), in which both chambers were identical in size (5 ml). (ii) a cylindrical Delrin cup with a flattened side (BCH-13a – Warner Instruments, Hamden, CT, USA))

Electromechanical shielding

(Electromechanical shielding was created by using a vibration isolation table (TMC, Peabody, USA) and a Faraday cage made from chicken wire.)

Ag/AgCl electrode

(WPI, Berlin, Germany)

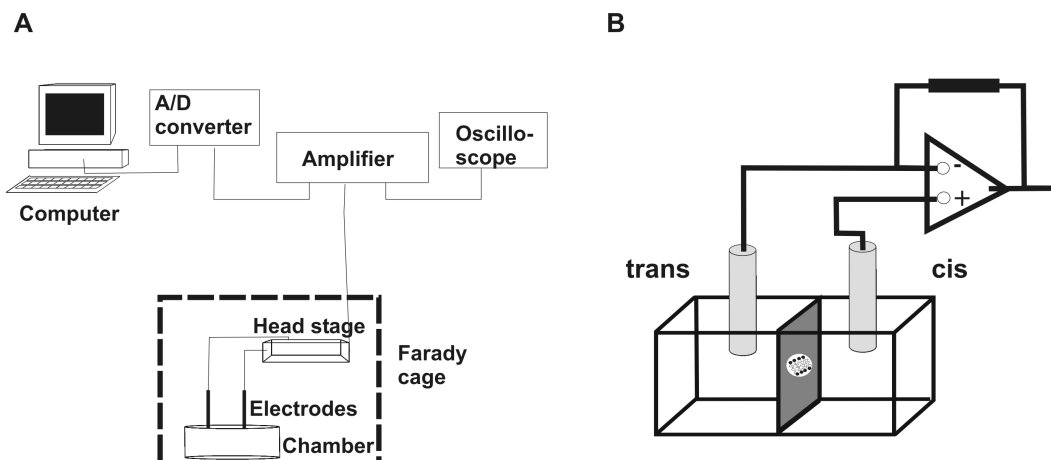


Figure 4.3: Schematic drawing of black lipid membrane setup

A) Complete bilayer setup with its main components (Computer, A/D converter, amplifier, oscilloscope, headstage, electrodes, chamber, and Faraday cage.

B) Extract of the setup – amplifier and chamber.

4.7.2 Painted bilayer membranes

In this study a black lipid membrane (BLM) setup was used (Fig.4.3). It consisted of a chamber with a partition dividing it into two compartments. These were filled

with a saline solution, and a Ag/AgCl electrode was placed in each side. A membrane was drawn across the hole with the “painting-bilayer method” according to Mueller et al. (1962). For this, the hole in the partition of the Teflon chamber was “primed” with 1 % (w/v) DiphPC dispersion in chloroform:methanol (1:1 (v/v)). This served as a reservoir of lipids during the formation of a membrane. A 1 % (w/v) DiphPC dispersion in *n*-decane:butanol (9:1 (v/v)) was painted across the hole with a glass rod or Teflon loop. The initial “membrane” was up to several μm thick at first, but after a short time, it thinned out, and a bilayer was formed. Isolated protein was added to the cis side of the chamber after formation of a stable bilayer.

Aliquots of 1 % (w/v) DiphPC in chloroform were stored at -20°C . Lipid working solutions were freshly prepared approximately every five days. For this, the chloroform of the lipid stock solution was evaporated under a stream of nitrogen, and the dried lipid was resuspended in the respective organic solution.

4.7.3 Single channel measurements

The protein was added to the cis side of the chamber and a constant voltage was applied to the membrane (-50 mV). Incorporation of a channel was observed as a step-like increase of current. The current trace was then recorded. The data were low-pass filtered at 3 kHz using the built-in Bessel-filter of the amplifier and digitized at a sampling rate of 10 kHz using an A/D converter and recorded on a PC. For current-voltage analysis, either linear voltage ramps or stepwise voltage changes were applied.

4.7.4 Data analysis

Visualization and first analysis of the digitized data were performed with the Strathclyde electrophysiology suite (WinEDR 2.8 or WinWCP 3.6, J. Dempster, University of Strathclyde, Glasgow, UK; <http://spider.science.strath.ac.uk/sipbs/page.php?show=software>), as well as the pClamp-Suite (Version 8, from Axon-Instruments). Further analysis was conducted with a software program developed in our laboratory (SANALYSIS, by Dr. R. Eckert) and standard scientific graphic software (Microcal Origin 7.5, OriginLab, Northampton, MA, USA).

The following analysis procedures were used:

- All-point histogram

To define the current level amplitudes of single channels, amplitude histograms were generated (Sachs, 1983; <http://www.moleculardevices.com/pdfs/AxonGuide.pdf>). For this, all the recorded data points (current values) from steady state measurements were divided into bins of a specific size. The frequency of points within the individual bins were normalized to the bin width and plotted against the corresponding bin center. If more than one channel, or if a channel with subconductance states was reconstituted in the membrane the histogram revealed more than one peak (Colquhoun and Sigworth, 1983; Sachs, 1983). These peaks were fitted with Gaussian functions, and the mean position (current amplitude) and the peak area (occupancy probability) were determined. The conductance for the various states was calculated as:

$$\gamma = \frac{i}{V} \quad (4.6)$$

where γ is the chord conductance, i is the current amplitude, and V is the holding potential.

- I-V curves

For the generation of I-V curves, single channel measurements were performed by recording steady state measurements at different holding potentials. All-point histograms were created for each voltage. The current levels were determined by fitting the histograms with Gaussian peaks. Peak means were plotted against the respective holding voltage. This was done for each state. The slope of the I-V characteristic (chord conductance) was then determined by fitting a linear fit function to the data in Microcal Origin 7.5.

- I-V surfaces

Current traces generated with linear voltage ramps were analyzed with I-V surfaces (Eckert, 1993; Sansom and Mellor, 1990). For this, 10 - 20 voltage ramps were applied to a membrane with a single channel incorporated, and the current traces were recorded. 2-D histograms were calculated from these data points in Microcal Origin 7.5. or with SANALYSIS. In the latter program, the slope conductance could be determined with the tools supplied.

- Fitting of non-linear I-V relationships

Non-linear I-V curves were fitted with model equations for energy barriers. Such barriers are located within a channel and are to be surmounted by ions passing through the channel (Hall et al., 1973). Examples of model equations describing such barriers are given in section 6.1. The respective function was fitted to the generated I-V curves in Microcal Origin 7.5.

- Occupancy probability

The steady state occupancies were determined by generating total current amplitude all-point histograms. The area under each peak in these histograms were taken as proportional to the time spent in that state (occupancy probability) and were plotted against the respective holding voltage (Sachs, 1983). For this, several measurements were averaged. The occupancy probability of the main conductance state corresponds to the probability of the channel being open. This plot was fitted with a double Boltzmann equation (see section 6.2)

- Transitions between conductance states

Variance-mean plots were created according to Patlak (1993). For this, the mean current and variance of a set of data points within a sliding window were determined and plotted against each other (see 6.3). Stable current levels were represented as clusters of points with low variance. The transition between two such stable current levels was indicated as a parabolic arch between clusters.

- Transition frequencies

For a kinetical analysis of single channels the transition frequencies between the various conductance levels were determined (according to McManus and Magleby, 1988). This was done with tools provided with the SANALYSIS program. First, the current data was idealized to a series of open and closed states (Colquhoun and Sigworth, 1983). For this, current level all-point histograms were created from stationary measurements, and the current levels of the present states were determined. Transitions between these open and closed states were detected by setting a threshold level (50 % of the height between two levels). With this “threshold idealization” the data was reduced to a list of events corresponding to the transitions between the

present levels. Analysis of the event list allowed the determination of the transition frequency between the various states.

4.7.5 Determination of the ion selectivity

The ion selectivity of a channel can be determined by measuring the channel activity in asymmetric saline solution. For this, both chambers were initially filled with 250 mM saline solution. After the incorporation of several channels, aliquots of 250 μ l of 3 M KCL solution were added to the trans side. I-V curves were generated as described above and the new reversal potential was determined as the zero intercept of the current on the voltage x-axis. The reversal potential was plotted against the salt concentration.

The resulting curve was fitted with a modified Goldman-Huxley-Katz voltage equation (Hille, 1992):

$$V_{rev} = \frac{RT}{zF} \ln \left(\frac{[K^+]_o + \kappa [Cl^-]_i}{[K^+]_i + \kappa [Cl^-]_o} \right) \quad (4.7)$$

where V_{rev} = reversal potential,

R = relative gas constant,

T = absolute temperature,

F = Faraday constant,

κ = permeability of potassium ions / permeability of chloride ions

$[K]_o$ = concentration of potassium ions – outside,

$[K]_i$ = concentration of potassium ions – inside,

$[Cl]_o$ = concentration of chloride ions – outside,

$[Cl]_i$ = concentration of chloride ions – inside

5 Results

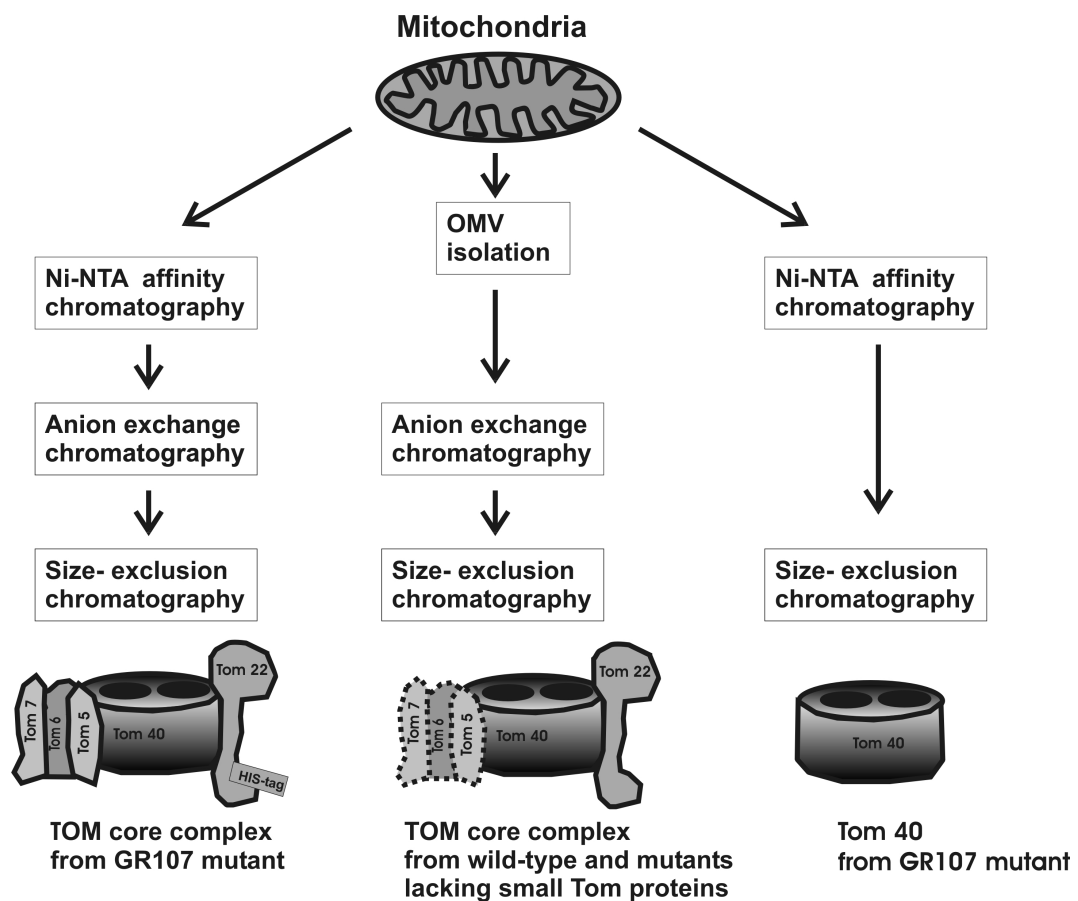


Figure 5.1: Biochemical isolation procedures

Overview of the various biochemical procedures used in this study for the purification of TOM core complex and Tom40 from the *N. crassa* GR107 mutant (which has a hexahistidinyl-tagged form of Tom22) as well as TOM core complex from mutants deficient in Tom5, Tom6, or Tom7.

The aim of my project was to gain further insights into the structure and dynamics of the TOM machinery from *N.crassa*. For this, (i) biochemical protocols were established for the isolation of TOM core complex from wild-type mitochondria and from various mutants, as well as Tom40 protein and the most abundant protein of the mitochondrial outer membrane – VDAC (voltage dependent anion channel). The isolated protein samples were then further analyzed in a number of biophysical experiments. These were (ii) structural studies (2-D crystallization, 3-D crystallization), (iii) binding studies, and (iv) electrophysiological studies.

5.1 Biochemical characterization

The basis for many biophysical applications is the isolation of pure protein in relatively high amounts. In this study existing protocols were improved and new procedures developed to achieve this task. An overview of the different biochemical procedures, which I applied, is given in Fig.5.1.

5.1.1 Isolation of TOM core complex from mitochondria

The *N. crassa* mutant GR107 contains a hexahistidiny1-tagged form of Tom22. This has allowed the purification of TOM core complex in high amounts in the past (Ahting et al., 1999). In the following section, I describe an improvement to the existing protocol, as well as the determination of the molecular mass of the TOM core complex with gel filtration and blue native gel electrophoresis (BNGE). Additionally, TOM core complex was eluted from the BNGE.

For the isolation of TOM core complex from GR107 cells, Ni-NTA affinity chromatography and anion exchange chromatography were applied. In the past, the Ni-NTA affinity chromatography was conducted by using Ni-NTA superose from Qiagen (Hilden, Germany). For each gram of mitochondria, 5 ml Ni-NTA superose was required, and from 5 g mitochondria 2-8 mg TOM core complex could be obtained (Schmitt, 2005). In this study, I exchanged the Ni-NTA material with a prepacked Ni-NTA column of only 1 ml resin from GE Healthcare (Munich, Germany). With the improved binding capacity of the new column, the smaller volume was sufficient to isolate 2-4 mg TOM core complex from 2 g mitochondria (Fig.5.2A). Tom40, Tom22, and the small Tom proteins, but no other distinct protein bands were detected in the collected sample. This new column allowed a

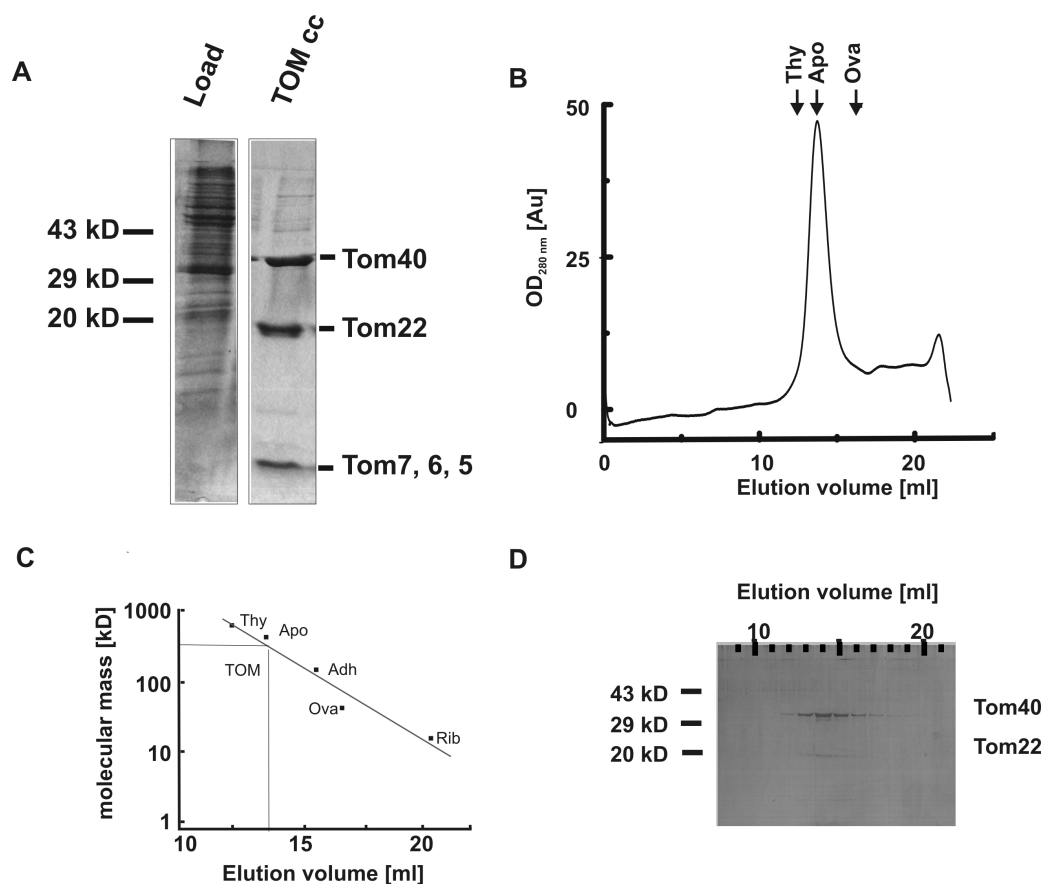


Figure 5.2: Purification of TOM core complex

A) Mitochondria from GR107 mutant were solubilized in 0.1 % (w/v) DDM. Subsequently, TOM core complex was isolated in a two-step purification procedure – by Ni-NTA affinity chromatography and anion-exchange chromatography. The purified sample was analyzed with a Coomassie stained SDS gel (14.5 % (w/v) acrylamide). For this, 50 μ g solubilized mitochondria (load) and 10 μ g isolated TOM core complex (TOMcc) were loaded onto the gel. An enrichment of the components of the TOM core complex can be seen in the right lane.

B) Elution profile of TOM core complex loaded onto a Superose 6 gel filtration column. The elution volumes of the protein standards are indicated with arrows. Elution speed: 0.25 ml/min; sample volume: 500 μ l; buffer: 50 mM potassium acetate, 10 mM MOPS, pH 7.2, 10 % (v/v) glycerol, 0.1 % (w/v) DDM. TOM core complex eluted from the column at approximately 14 ml.

C) For the generation of a calibration curve of the Superose 6 column, the molecular mass of the protein standards was plotted versus the elution volume. Protein standards: Thy, thyroglobulin (669 kD); Apo, apoferritin (443 kD); Adh, alcohol dehydrogenase (150 kD); Ova, ovalbumin (43 kD); Rib, ribonuclease A (13.7 kD). An elution volume of 14 ml corresponds to a molecular mass of 400 kD for TOM core complex.

D) The peak fractions collected from the gel filtration with TOM core complex (B) were analyzed on a silver stained 14.5 % (w/v) acrylamide SDS gel. Bands corresponding to Tom40 and Tom22 were detected.

faster and more efficient isolation. On average, the yield was improved by a factor of two.

To analyze the oligomeric state of purified TOM core complex, the sample was passed over a gel filtration column (Superose 6, GE Healthcare). The increase of absorption at 280 nm indicated the elution of TOM core complex after 14 ml (Fig.5.2B). Analyzing the peak fractions with SDS-PAGE and subsequent silver staining verified the existence of TOM core complex in these samples. To estimate the molecular mass of the complex, protein standards were passed over the same column. Their elution profiles were fitted with Gaussian functions to determine their elution volumes. The molecular mass of the protein standards was then plotted against the elution volume (Fig.5.2C). The elution volume of 14 ml for TOM core complex corresponded to a molecular mass of approximately 400 kD, which was in line with previous studies (Ahting et al., 1999).

As an alternative method to estimate the molecular mass of the complex, a blue native polyacrylamide gel electrophoresis (BNGE) was performed. For this, the sample was separated within a polyacrylamide gel under native conditions. The Coomassie stain, which was used to give the proteins a negative charge, allowed the detection of the sample in the gel. Furthermore, Tom40 was identified in the BNGE by Western blotting. For this, a TOM core complex sample as well as a sample treated with denaturing Laemmli-loading buffer were loaded onto a BNGE. With this the difference of the native complex (400 kD) and denatured sample (40 kD; Fig.5.3) was displayed.

BNGE of TOM core complex was also used as an additional purification step. For this, isolated TOM core complex was loaded onto a native gel and was allowed to enter the gel. The visible blue band was removed and incubated in SE buffer (50 mM potassium acetate, 10 mM MOPS pH 7.2, 10 % (v/v) glycerol, 0.1 % (w/v) DDM) for 48 hours at 4°C. The components of the TOM core complex (Tom40, Tom22, and the small Tom proteins) were detected in the sample with SDS-PAGE and subsequent silver staining (Fig.5.3A). The functionality of the eluted TOM core complex was demonstrated with electrophysiological measurements.

In summary, I have improved the protocol used in our laboratory for the isolation of TOM core complex by exchanging the Ni-NTA material. By applying size exclusion chromatography and BNGE, the molecular mass of the TOM complex was estimated to be 400 kD. Both these applications could be performed as ad-

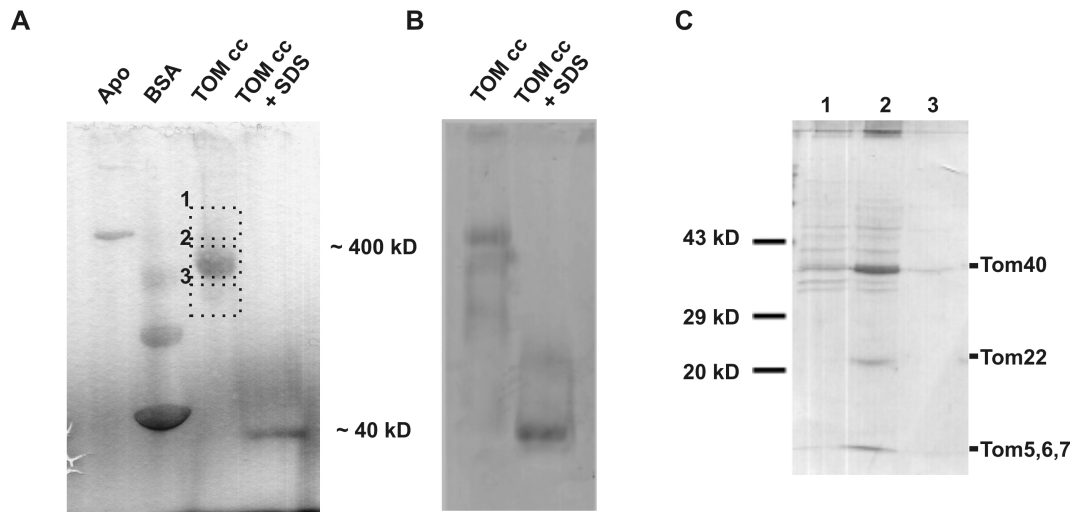


Figure 5.3: BNGE of TOM core complex

TOM core complex and TOM core complex treated with Laemmli-loading buffer were subjected to a BNGE with an acrylamide gradient from 5 % to 18 % (w/v). 20 μ g protein were loaded. Marker proteins: Apo (apoferritin, 443 kD); BSA (bovine serum albumin, 66 kD (and multiples of this)).

A) Coomassie stained gel. TOM core complex migrated as a band slightly below the apoferritin band, whereas the SDS treated band migrated slightly below the monomeric BSA band. The indicated inlays were removed from the gel and incubated in elution buffer (see (C)).

B) Proteins separated with BNGE were transferred to a PVDF membrane and Tom40 was detected with a specific antibody and visualized with NBT-BCIP substrate. With this, the 400 kD and 40 kD bands detected in (A) were identified as Tom40 containing bands.

C) Elution of TOM core complex from BNGE with gel elution. After migration of TOM core complex in a native gel, the band as indicated in (A) was excised and incubated in SE buffer (50 mM potassium acetate, 10 mM MOPS pH 7.2, 10 % (v/v) glycerol, 0.1 % (w/v) DDM) at 4°C. After 48 hours TOM core complex was detected with Tricine-SDS-PAGE (16 % (w/v) acrylamide) and subsequent silver staining (lane 2). Bands in the BNGE above and below the TOM core complex were treated in the same manner (lane 1 and lane 3, respectively). Lane two contains the components of the TOM core complex (Tom40, Tom22, and the small Tom proteins).

ditional purification steps, which was particularly important to avoid contamination of the sample with partially dissociated or oligomerized TOM core complex.

5.1.2 Isolation of TOM core complex from OMVs

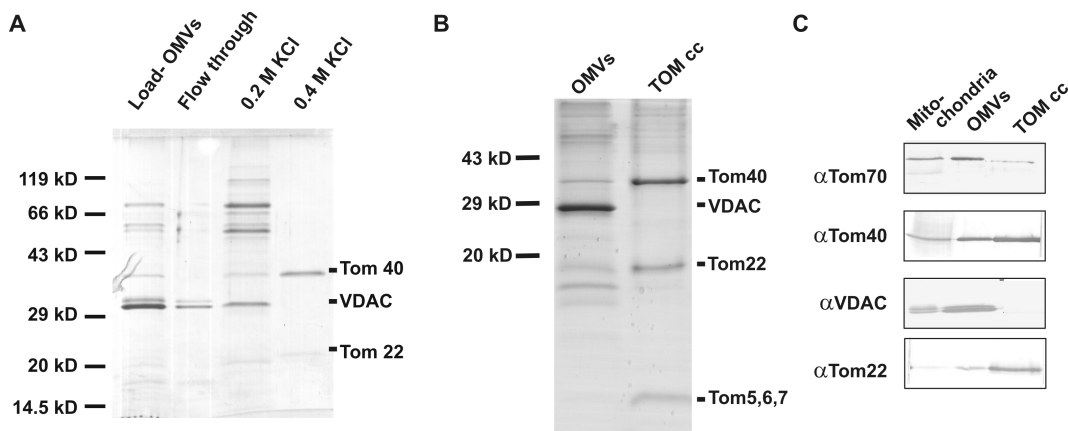


Figure 5.4: Isolation of TOM core complex from mitochondrial outer membrane vesicles (OMVs)

A) Isolation of TOM core complex from OMVs by anion exchange chromatography (Δ Tom7 mutant). 10 mg OMVs were solubilized in 0.1 % (w/v) DDM and loaded onto a ResourceQ column (1ml). After washing the column with 20 column volumes, bound protein was eluted from the column with salt concentrations of 0.2 M and 0.4 M. The samples were analyzed with a Coomassie stained 14.5 % (w/v) acrylamide SDS gel. Lane 1, solubilized OMVs (12.3 μ g); lane 2, flow through (10 μ g); lane 3, proteins eluted with 0.2 M KCl (10 μ g); lane 4, eluted TOM core complex (5 μ g). No contaminations were visible in the latter lane. VDAC was mostly found in the flow through sample as well as in the sample eluted with 0.2 M salt.

B) Purification of TOM core complex isolated from OMVs obtained from frozen mitochondria. Coomassie stained gel comparing OMVs (lane 1, 20 μ g protein) with the isolated TOM core complex (lane 2, 10 μ g protein). Here too, only Tom40, Tom22, and the small Tom proteins and no other distinct protein bands were detected in the purified TOM core complex sample.

C) Immunodecoration of mitochondria, OMVs, and isolated TOM core complex with various antibodies against proteins of the outer membrane. Lane 1, mitochondria (20 μ g protein); lane 2, OMVs (20 μ g protein); lane 3, TOM core complex (10 μ g protein). Tom40 and Tom22 accumulated in the TOM core complex sample. Only little Tom70 was detected in this sample and no VDAC.

For the analysis of TOM core complex from wild-type *N. crassa* as well as from mutants lacking the hexahistidinyI-tagged form of Tom22, I have developed a

new protocol to isolate these complexes in high amounts.

For this, mitochondrial outer membrane vesicles (OMVs) were obtained from freshly isolated mitochondria. These were solubilized in DDM and loaded onto a ResourceQ 6 anion exchange column. Various proteins were washed from the column with 0.2 M KCl. TOM core complex could be eluted from the column with 0.4 M KCl (Fig.5.4A). No additional distinct protein bands were detected in the isolated sample. VDAC was detected in the flow through sample and in the sample eluted with 0.2 M KCl.

Different opinions existed on the effect of freezing and thawing on the mitochondrial outer membrane. It was believed that freezing might destroy the integrity of the membrane structure and, therefore, swelling of the mitochondria, which is an essential step in the isolation of OMVs, would no longer be possible. To test for this hypothesis, I conducted an experiment with frozen mitochondria. As shown in Fig.5.4B freezing did not have an effect on the isolation of OMVs and, most important, on the subsequent isolation of TOM core complex. Besides the components of the TOM core complex no other proteins were detected in the sample with Tricine-SDS-PAGE. The proteins from mitochondria, OMVs, and TOM core complex were separated with SDS-PAGE and subsequently decorated with antibodies against proteins of the outer membrane (Fig.5.4C). An increase in the amount of Tom70 and VDAC was observed in the OMV fraction compared with the mitochondrial fraction. Tom70 was hardly, and VDAC was not detectable in the TOM core complex fraction. On the other hand, an enrichment of Tom40 and Tom22 was seen in the TOM core complex sample in this fraction.

Taken together, I have developed a procedure to isolate and purify TOM core complex from OMVs and have shown that frozen mitochondria could also be used to obtain the OMVs. On average, 2 g mitochondria (freshly prepared or frozen) yielded 10-20 mg OMVs from which 0.5 - 1 mg TOM core complex was isolated.

5.1.3 Isolation of TOM core complex lacking one of the small Tom proteins from outer membrane vesicles

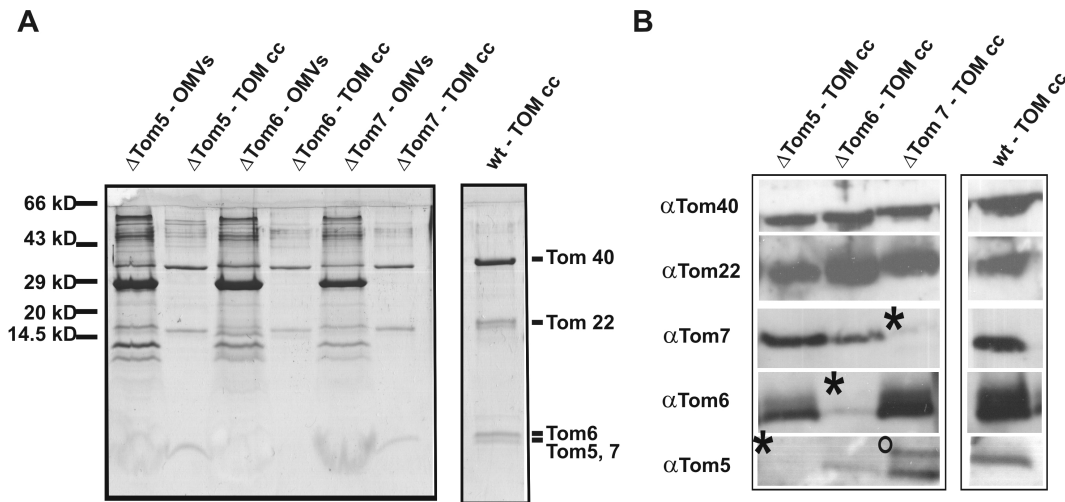


Figure 5.5: Isolation of TOM core complex lacking one of the small Tom proteins

TOM core complex from *N. crassa* mutants was isolated from OMVs and analyzed by polyacrylamide gel electrophoresis.

A) Comparison of isolated TOM core complex from Δ Tom5, Δ Tom6, and Δ Tom7 mutants with wild-type TOM core complex. 20 μ g OMVs and 10 μ g TOM core complex were analyzed with a Coomassie stained 16 % (w/v) acrylamide Tricine-SDS gel. An accumulation of the components of the TOM core complex was observed.

B) Immunodecoration against all five components of the TOM core complex (10 μ g protein loaded). All the components of the TOM core complex except the respective knock-out protein (indicated with *) were detected. Δ Tom6 mutant showed a decrease in the amount of Tom5 and Tom7. Note that the double band at ° resulted from cross reaction of anti-Tom5 antibody with Tom6.

To analyze the function of the different subunits, TOM core complex was isolated from *N. crassa* knock-out mutants lacking one of the small Tom proteins (Tom5, Tom6, and Tom7). Only these knock-out mutants could be examined, as Tom40 and Tom22 are essential in *N. crassa* (Baker et al., 1990; Hönlinger et al., 1995; Nargang et al., 1995).

N. crassa mutants Δ Tom5, Δ Tom6, and Δ Tom7 were kindly provided by Dr. Frank Nargang (University of Alberta, Canada). Since these knock-out mutants did not contain a hexahistidinyI-tagged form of Tom22, TOM core complex was isolated from OMVs with the method described above (Fig.5.5A). The purity of these complexes was comparable with that of wild-type TOM core complex. West-

ern blot analysis of all the components of the TOM core complex confirmed the absence of the respective small Tom protein, as well as the presence of the other components (Fig.5.5B). The Δ Tom6 mutant, however, showed a decrease in the amount of Tom7 and Tom5. This is in agreement with previous studies (Sherman et al. 2006), which suggest that Tom6 plays a role in the integrity of the whole complex.

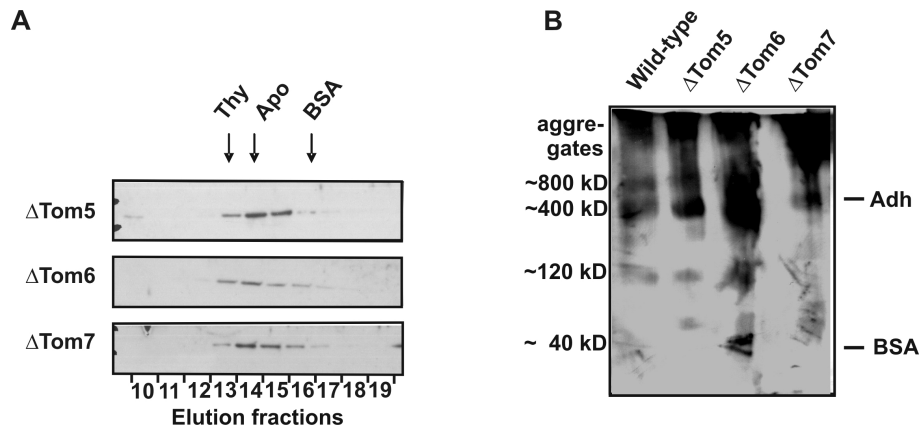


Figure 5.6: Molecular mass estimation of TOM core complex from mutants lacking one of the small Tom proteins (Tom5, Tom6, and Tom7)

A) Purified TOM core complex from Δ Tom5, Δ Tom6, and Δ Tom7 mutants, respectively, were passed over a Superose 6 gel filtration column under standard conditions, and the peak fractions were analyzed with Western blot with specific antibodies against Tom40. Elution maxima of protein standards are indicated with arrows. Thy, thyroglobulin (669 kD); Apo, apoferritin (443 kD); BSA, bovine serum albumin (66 kD). All mutants eluted in a similar elution volume as apoferritin indicating a molecular mass of 400 kD. This is in agreement with the elution volume of wild-type TOM core complex.

B) Analysis of molecular mass by BNGE (18 - 5 % (w/v) acrylamide gradient) with subsequent Western blot analysis with Tom40 antibodies in comparison with wild-type complex. The migration distances of the protein standards are indicated. TOM core complex from all *N. crassa* strains were identified as a 400 kD complex. Additionally, an 800 kD complex as well as aggregates were identified. Especially in the Δ Tom6 mutant, Tom40 was detected as a 120 kD complex and as a monomer.

Size exclusion chromatography experiments were performed to estimate the molecular mass of the TOM core complex lacking one of the small TOM proteins. Comparison of the elution profiles obtained with the elution profiles of protein standards (see Fig.5.2B) revealed a molecular mass of approximately 400 kD for these TOM core complex samples (Fig.5.6A). This was in agreement with BNGE analysis. Immunodecoration with antibodies against Tom40 revealed a

distinct complex of approximately 400 kD in agreement with wild-type TOM core complex (Fig.5.6B). Additionally, some Tom40 was detected as an approximately 120 kD complex, as well as in highly oligomeric structures. The latter population was especially increased for the TOM core complex lacking Tom7. TOM core complex lacking Tom6, however, showed an increase in the 120 kD fraction. Monomeric Tom40 was also detected.

In summary, I was able to isolate TOM core complex lacking one of the small Tom proteins from *N. crassa* knock-out mutants. The presence of the remaining TOM core complex components was verified, and the estimated molecular mass of the complex was in agreement with wild-type TOM core complex. However, the performed BNGE revealed a slight inhomogeneity of the isolated samples as not only 400 kD complexes were detected but monomeric and other oligomeric complexes as well.

5.1.4 Isolation of monomeric Tom40 from mitochondria

For the analysis of the biophysical properties of Tom40, the major subunit of the TOM core complex, I optimized a previous protocol to purify native Tom40 protein from isolated mitochondria (Ahting et al., 2001).

For the isolation of about 1-2 mg Tom40, 2 g mitochondria of *N. crassa* strain GR107 were solubilized in DDM and loaded onto a Ni-NTA column. After the removal of excessive proteins by washing the column with 50 column volumes washing buffer, Tom40 was eluted from the column by adding 3 % (w/v) n-octyl β -D-glucopyranoside. Octylglucoside is a non-ionic detergent that reduces the binding interaction between Tom40 and Tom22, leading to a disassociation of the complex. Tom40 eluted from the column, while the hexahistidiny-tagged Tom22 remained bound. The latter and other proteins bound to the column were eluted by adding 300 mM imidazole. Purity of the eluted Tom40 protein was analyzed by Tricine-SDS-PAGE (Fig.5.7A). Virtually no other proteins besides Tom40 were detected. Immunodecoration with anti-Tom40 antibodies showed little loss of Tom40 during the binding to the nickel column (lane 2, flow through). Additionally, some Tom40 was still bound to Tom22, even after extensive washing with octylglucoside (lane 4, imidazole fraction). Immunodecoration against all other TOM core complex components showed that the isolated sample only contained Tom40 (Fig.5.7B). The molecular mass of the isolated sample was determined with size exclusion chromatography and BNGE. Size exclusion chromatography

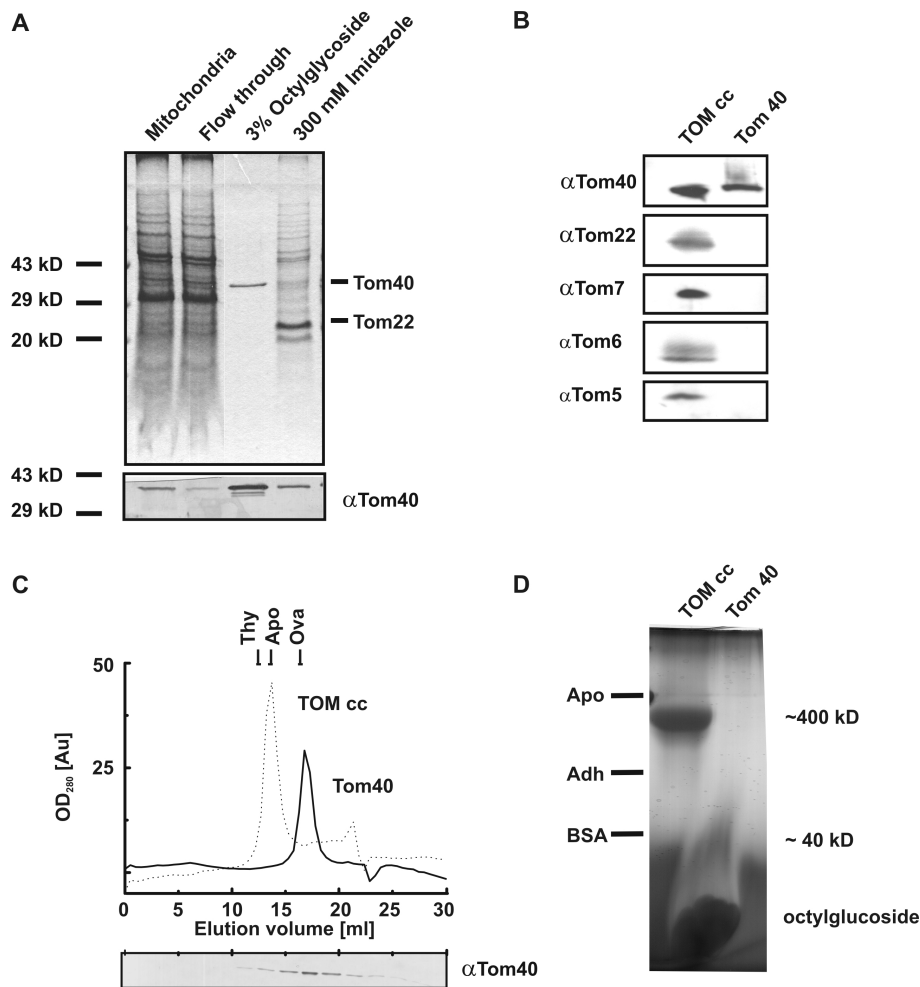


Figure 5.7: Analysis of purified Tom40 protein from *N. crassa* GR107 mitochondria

A) Isolated Tom40 samples were analyzed with a Coomassie stained Tricine-SDS-PAGE (16 % (w/v) acrylamide) and Western blot with anti-Tom40 antibodies (lower panel). Lane 1, solubilized mitochondria (50 μ g); lane 2, flow through (50 μ g); lane 3, isolated Tom40 (5 μ g); lane 4, eluted proteins with imidazole (20 μ g). In the purified Tom40 sample virtually no other proteins were detected. Western blot analysis confirmed that the purified protein was Tom40.

B) Immunodecoration of isolated TOM core complex and purified Tom40 protein with antibodies against Tom40, Tom22, Tom7, Tom6, and Tom5. Lane 1, TOM core complex (10 μ g); lane 2, Tom40 (5 μ g). In the latter lane, only Tom40 was detected.

C) Size exclusion chromatography of Tom40 (continuous line). 200 μ g of protein were passed over a Superose 6 column and 1 ml fractions were collected and analyzed with Western blot analysis with anti-Tom40 antibodies (lower panel). The elution volume of 17 ml indicated that Tom40 was isolated in its monomeric state.

D) Western blot analysis of TOM core complex and Tom40 separated by BN-PAGE (10 μ g each) with anti-Tom40 antibodies. This indicated a molecular mass of 40 kD for the purified Tom40 sample. Marker proteins: thyroglobulin, Thy (669 kD); apoferritin, Apo (443 kD); alcohol dehydrogenase, Adh (150 kD); bovine serum albumin, BSA (66 kD); ovalbumin, Ova (43 kD).

of Tom40 revealed a similar molecular mass as ovalbumin (43 kD), indicating that Tom40 was in its monomeric state (Fig.5.7C). This was in agreement with the BNGE (Fig.5.7D).

The newly established protocol allowed the isolation of highly pure monomeric Tom40. This sample was then examined with electrophysiological approaches and used in crystallization trials.

5.1.5 Isolation of VDAC

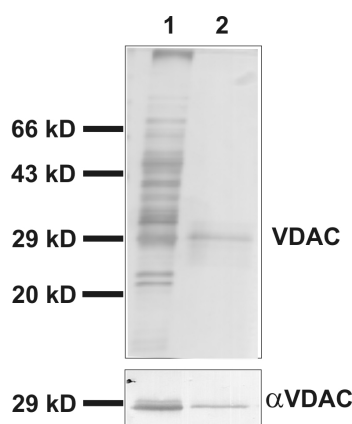


Figure 5.8: Purification of VDAC with gel elution

Silver stained SDS-PAGE (14.5 % (w/v) acrylamide) of isolated VDAC with corresponding immunodetection (lower panel). *N. crassa* mitochondria were solubilized in 0.1 % (w/v) DDM and were passed over a Ni-NTA column. The VDAC containing flow through was separated on a 14.5 % (w/v) acrylamide SDS gel. The band containing VDAC was excised from the gel, and VDAC was eluted by incubation in SE buffer (50 mM potassium acetate, 10 mM MOPS pH 7.2, 10 % (v/v) glycerol, 0.1 % (w/v) DDM) at 4°C for 48 hours. Lane 1, Ni-NTA flow through; lane 2, isolated VDAC. In the latter lane only VDAC was detected and no other proteins. Western blot analysis confirmed that the protein was VDAC.

For a comparison of the channel properties of TOM core complex with a β -barreled protein of the mitochondrial outer membrane, I established a new protocol for the isolation of VDAC.

Detergent-solubilized mitochondria were passed over a Ni-NTA column and the VDAC containing flow through (500 μ g protein) was separated by SDS-PAGE, and the corresponding slice of the gel was cut-out. Protein was recovered by elution in SE buffer at 4°C for two days. The presence of eluted VDAC in the

eluate was confirmed with SDS-PAGE and subsequent silver staining (Fig.5.8). No other distinct protein bands were visible. Western blot analysis confirmed that the eluted protein was VDAC. The functionality of the refolded protein was analyzed with electrophysiological techniques.

Taken together, the isolation protocols that I developed during this study and have described above are the basis for the further biophysical characterization of TOM core complex from wild-type and various mutants, as well as Tom40, and VDAC.

5.2 Crystallization of the TOM machinery

Only very few structural details of the TOM machinery have been revealed so far. In this study, two different approaches were undertaken to crystallize the TOM machinery. The first was the 2-D crystallization of TOM core complex. In this method, isolated membrane proteins are reconstituted within a lipid bilayer in which the lipid to protein ratio is adjusted so that proteins come into contact forming a 2-D crystalline array. With electron diffraction of such patches structural information of the protein can be obtained.

The second approach was the generation of 3-D crystals. In this method proteins are tightly packed in three dimensional lattices, which can be examined by X-ray diffraction. As it is hard to obtain 3-D crystals from large oligomeric complexes, only 3-D crystallization trials of purified Tom40 protein were undertaken.

5.2.1 Reconstitution of TOM core complex into lipid membranes for 2-D crystallization

The lack of hydrophilic surfaces in membrane proteins is responsible for the difficulty in obtaining three dimensional crystals. The possible contact sites are reduced, since membrane proteins are isolated in protein-detergent micelles. An alternative method for the structural analysis of membrane proteins is the reconstitution into two dimensional crystals in the presence of lipids (Levy et al., 2001; Stahlberg et al., 2000). Membrane patches, in which the protein is highly ordered, can then be used to gain structural information by analyzing electron diffraction patterns. The aim of the next study was to determine conditions in which TOM core reconstitutes into lipid membranes.

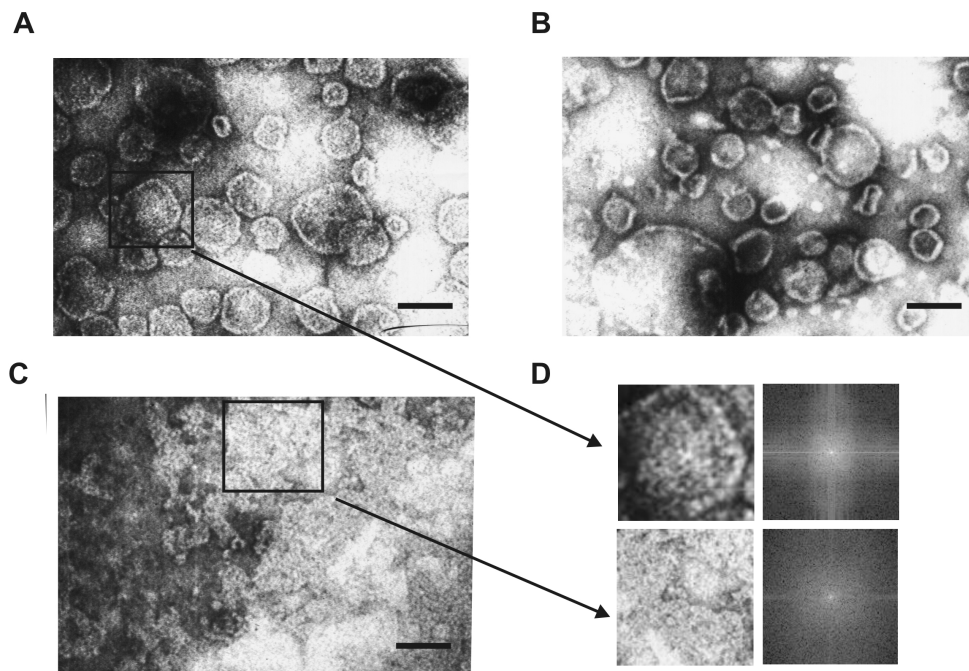


Figure 5.9: Reconstitution of TOM core complex into lipid membranes

Electron micrographs of TOM core complex reconstituted in DMPC (L:P (w/w) = 0.3) with 10 % (w/v) cardiolipin. Samples were transferred to carbon coated grids and stained with 2 % (w/v) uranylacetate. The EM images were taken at 36.000 x magnification. Scale bar = 0.25 μm .

A) Vesicles obtained with the “batch method”. These were between 2 - 4 μm in diameter with incorporated protein.

B) Vesicles obtained with the “batch method” without stirring during bio-bead incubation. Here too, the vesicles were between 2 - 4 μm in diameter.

C) Sheets obtained with the “monolayer method”. DOGS-NTA-Ni with 50 % (v/v) DMPC spread at the air-water interface.

D) Fourier spectra of indicated inlays performed with ImageJ. No prominent reflections on the reciprocal lattice were detected. Thus, the reconstituted protein did not form ordered 2-D crystals.

After purification of the native membrane protein in detergent micelles, the difficult step in reconstitution is the removal of detergent, as this step controls the micelle to bilayer phase transition as well as the incorporation of the protein (Levy et al., 2001). Many different methods for the removal of detergent have been proposed so far. One promising method for the removal of DDM (the detergent in which TOM core complex has been isolated) and other detergents with a low cmc (critical micelle concentration) is the adsorption of detergent to bio-beads (Rigaud et al., 1997). These macroporous polystyrene beads absorb the detergent from the free micelles and micelles surrounding the protein. In this study, two different approaches were applied – the “bulk method” and the “monolayer method”. In the former, the proteins are incubated with lipids and by addition of bio-beads the detergent micelles surrounding the hydrophobic patches are removed and replaced by lipids added to the system. Thus, protein containing vesicles are formed. In the monolayer method, proteins are crystallized in a lipid monolayer spread at the air-water interface.

Reconstitution of TOM core complex with the “bulk method”

For the reconstitution of isolated TOM core complex into lipid membranes with the bulk method, the optimal lipid was determined with initial trials. Three different lipids were tested: DMPC, EPC, and DOPC. The largest protein containing vesicles were obtained with DMPC (0.2 μm). This was the only lipid tested with saturated fatty acid chains. With EPC, only very small vesicles were obtained ($< 0.2 \mu\text{m}$). The samples prepared with DOPC showed a separation into two phases – lipid aggregation on the one hand and protein aggregation on the other hand. Thus, for the subsequent experiments DMPC was used.

In the first DMPC approach the lipid to protein ratio (L:P (w/w)) had been 0.75. Besides the formed vesicles, an excess of lipid was visible. Thus, in the next approach the L:P (w/w) was reduced to 0.3 in one trial and 0.6 in another trial. However, even for the L:P (w/w) of 0.3, an excess of lipid was observed. Additionally, the DMPC was supplemented with additives such as cardiolipin (10 % (w/v)), DMPE (30 % (w/v)), and DMPG (25 % (w/v)). The sample containing cardiolipin led to homogenous vesicles, which were, however, still small (0.2 - 0.4 μm ; Fig.5.9A). In a further approach, 0.5 M NaCl was added to the sample (L:P (w/w) = 0.3; 10 % (w/v) cardiolipin). The vesicles obtained were, however, even smaller than the vesicles formed by the sample without additional salt.

During the formation of vesicles the detergent removal with bio-beads is an essential step. In the next trial, incubation with bio-beads occurred without stirring to reduce the speed of detergent removal. The vesicles obtained with this trial were, nevertheless, similar to the samples obtained with stirring (Fig.5.9B).

Table 5.1: Parameters tested with the “bulk method”

Choice of lipid		
DMPC	EPC	DOPC
Lipid to protein ratio, L:P(w/w)		
0.3	0.6	0.75
Additives		
Cardiolipin (10 % (w/v))	DMPE (30 % (w/v))	DMPG (25 % (w/v))
Additional approaches		
0.5 M NaCl no stirring while bio-bead incubation		

Testing the above parameters resulted in the best reconstitution of TOM core complex into vesicles with DMPC, L:P (w/w) = 0.3, 10 % (w/v) Cardiolipin. Improvement of the size of the vesicles and the packing of the proteins within the vesicles can be obtained by trying different methods of detergent removal such as detergent dialysis or detergent dilution (Hunte et al., 2003, chapter 15). In future studies, the influence of the pH and temperature may be analyzed. Also the addition of different salts, such as MgCl₂, which modify the head group packing of the lipids, and different concentrations of glycerol, which competes with the protein hydration layers, should be tested.

Reconstitution of TOM core complex with the “monolayer method”

With the “monolayer method” trials were undertaken to fuse the small protein-containing vesicles obtained by the “bulk method”. For this, 1 μ l of DOGS-NTA-Ni was spread on the buffer filled cavities of the “monolayer setup”. The vesicles were then added to the setup through the injection holes. Due to the hexahistidiny-tag on Tom22, the TOM core complex containing vesicles bound to this lipid monolayer. However, the analysis of this monolayer showed that no fusion between the separate vesicles had occurred.

In another approach the “monolayer method” was applied to samples preincubated with DMPC (L:P (w/w) = 0.25, and L:P (w/w) = 0.5, respectively). Additionally, 10 % (w/v) cardiolipin had been added to the sample. The lipids that were scattered on the surface were either pure DOGS-NTA-Ni or DOGS-NTA-Ni/DOPC (50 % (v/v)). All samples showed little patches of protein-containing sheets that were linked together (Fig.5.9C). The largest patches were observed with the combination 50 % (v/v) DOGS-Ni-NTA and an L:P (w/w) of 0.25. However, these patches were still small and did not show crystalline packing.

In summary, with both methods TOM core complex was reconstituted into lipid bilayers. However, the obtained vesicles were too small for structure determination by electron crystallography (Walz and Grigorieff, 1998). Fourier transform of reconstituted TOM core complex did not show reflections. This strongly indicates that the reconstituted proteins in both methods were not ordered yet (Fig.5.9). Optimization of the conditions will have to be performed with the methods suggested above.

5.2.2 3-D crystallization

The development of the Tom40 isolation procedure described in section 5.1.4 allowed a large scale purification of monomeric Tom40 protein. With the next experiment the trial was undertaken to obtain three dimensional crystals that can be used for determining its atomic structure by X-ray diffraction.

Isolated Tom40 protein was concentrated to a protein concentration of approximately 10 mg/ml and dialyzed against 10 mM HEPES pH 7.2, 1 % (w/v) octylglucoside for at least 24 hours at 4°C. In collaboration with Dr. Reinhard Albrecht (Max-Planck-Institut für Entwicklungsbiologie, Tübingen, Germany), this sample was then subjected to 12 commercial crystallization screens (see section 4.5.2). With the help of a pipette robot samples of 0.4 μ l were added to the “sitting-drop” of each of the 96 wells in one screen. The droplets were automatically photographed on days 1, 7, and 21 after pipetting. In various samples formation of 3-D crystals was observed. Almost all of the crystals turned out to be salt crystals, except for the crystals obtained with 0.5 M potassium sodium tartrate tetrahydrate, 0.1 M CHES pH 9.5, 50 % (v/v) ethylene glycol (CryoII sparse matrix crystallization screen, Emerald Bio Systems). With this condition a triangular crystal and a crystal aggregate were observed (Fig.5.10).

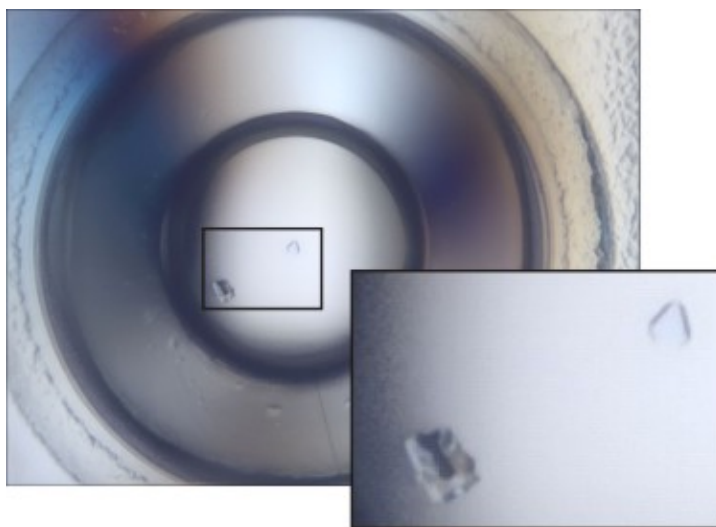


Figure 5.10: Droplet from 3-D crystallization trial

Photograph of protein crystals obtained with 0.5 M potassium sodium tartrate tetrahydrate; 0.1 M CHES pH 9.5; 50 % (v/v) ethylene glycol on day 7. An aggregation of crystals is located in the bottom left corner of the enlarged inlay, and a triangular crystal in the upper right corner.

The single crystal and crystal bits from the aggregate were analyzed for X-ray diffraction at the synchrotron radiation facility SLS (PSI Villigen, Switzerland) by Dr. Reinhard Albrecht. Diffraction patterns with a resolution of 0.8 \AA were collected.

5.3 Binding studies of precursor protein with TOM core complex

With fluorescence correlation spectroscopy (FCS) diffusion constants of fluorescently labeled proteins can be determined. For this, a laser is focused on the sample and the temporal fluctuations in the fluorescent counts are determined within the detection volume. These fluctuations can result from fluorescently labeled molecules that diffuse in and out of the defined volume. An interaction of a fluorescently labeled protein with another protein larger in size results in a lower mobility which can be measured as a slower diffusion time. For proteins with a molecular mass $m > 1 \text{ kD}$ the diffusion constant is proportional to $\frac{1}{\sqrt[3]{m}}$.

If the second population of proteins is labeled with a different fluorescent dye the interaction between the two proteins can be determined with fluorescence cross correlation spectroscopy (FCCS). Here, the temporal correlation between the diffusion constants for both fluorescent wavelengths is determined.

For a better understanding of the binding and threading of a polypeptide through the TOM machinery, such measurements would be helpful. The TOM core complex is a suitable protein for this kind of measurements, as the molecular mass of this complex is 400 kD, and typical protein substrates that bind to the TOM machinery have a mass which is significantly smaller. The classical mitochondrial model protein Su9₁₋₆₉DHFR for example has a molecular mass of 29 kD. The binding of such a small protein to the TOM core complex would be accompanied by an obvious increase in diffusion time for the small protein resulting in a longer time span spent in the detection volume.

The initial step for such experiments is the correct labeling of protein with a fluorescent dye. In this study I have established protocols for the binding of chromophores to TOM core complex and to Su9₁₋₆₉DHFR. These labeled substrates were the basis for FCS measurements that I performed with members of the group of Dr. Petra Schwille (Institut für Biophysik, TU Dresden, Germany).

The green fluorophore Alexa Fluor 488 C5-maleimide and the orange dye Alexa Fluor 546 C5-maleimide were chosen as chromophores, since FCS and FCCS measurements can be performed with these dyes. Both dyes display emission spectra with only a small overlap (Panchuk-Voloshina et al., 1999). Alexa Fluor 488 C5-maleimide was used for the labeling of the preprotein Su9₁₋₆₉DHFR and Alexa Fluor 546 C5-maleimide for the TOM core complex.

Initial FCS experiments revealed that the buffer commonly used in our laboratory for the isolation of TOM core complex (10 % (v/v) glycerol, 0.03 % (w/v) DDM, 50 mM potassium acetate, 10 mM MOPS pH 7.2) was not suitable, as a calibration of the FCS setup for the chosen wavelengths with an Argon-laser beam at 488 nm and with a HeNe-laser beam at 546 nm was not possible in these conditions. Both MOPS and glycerol changed the spectroscopic properties of the solution. Additionally, glycerol changed the viscosity of the sample and was prone to minor pipetting errors. FCS experiments in which free dye was measured in various buffer solutions indicated that 25 mM HEPES pH 7.2, 2 % (v/v) DMSO, and 0.03 % (w/v) DDM is a suitable buffer (data is presented below). The preparation of Su9₁₋₆₉DHFR and TOM core complex were, therefore, performed in this

buffer.

The next section is divided into three parts. First, the isolation and labeling of Su9₁₋₆₉DHFR is described. This is followed by a listing of the results of the labeling of the TOM core complex. Finally, preliminary data collected with FCS measurements is given.

5.3.1 Labeling of Su9₁₋₆₉DHFR

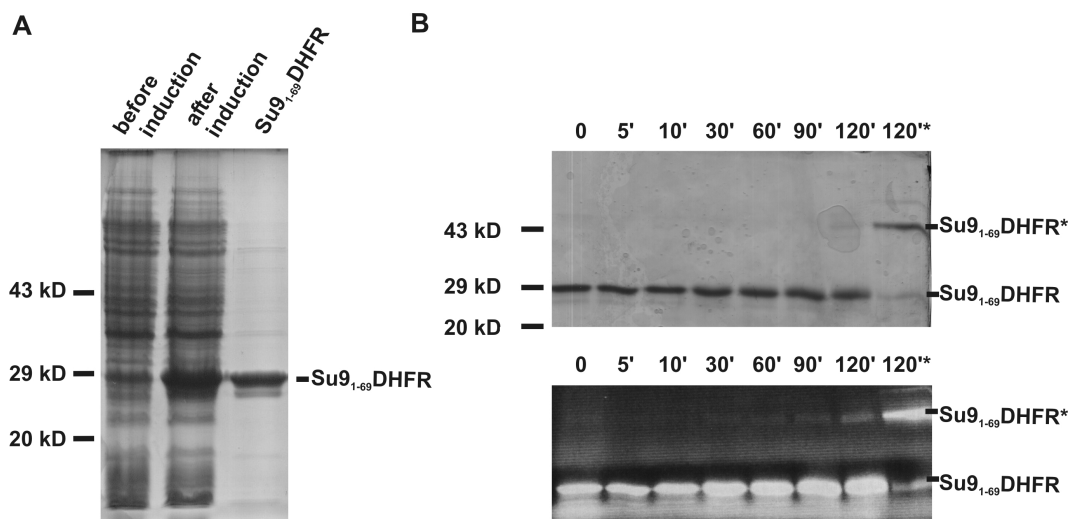


Figure 5.11: FCS- isolation of Su9₁₋₆₉DHFR and time-dependent labeling with fluorescent dye

A) Isolated Su9₁₋₆₉DHFR from *E.coli* cells analyzed with Coomassie stained SDS-PAGE (14.5 % (w/v) acrylamide). For this, 50 μ g cell lysate before (lane 1) and after induction of protein synthesis (lane 2) as well as 10 μ g purified protein were loaded onto the gel. An increase in Su9₁₋₆₉DHFR was visible in lane 2 and an enrichment in lane 3. No other protein bands were visible in the purified sample.

B) SDS-PAGE (14.5 % (w/v) acrylamide) of time-dependent labeling series: Su9₁₋₆₉DHFR was incubated with Alexa Fluor 488 C5-maleimide (Molecular Probes) and at the indicated time-points an aliquot was removed and supplemented with Laemmli-loading buffer. After 120 minutes Laemmli-loading buffer lacking β - mercaptoethanol was added to the sample (last lane, marked with *). Upper panel: Coomassie stained, lower panel: detection of the fluorescent labeled protein with exposure of the gel to UV-light. A time-dependent increase in the fluorescent intensity of the labeled Su9₁₋₆₉DHFR band was observed. The non reduced sample migrated as a dimer.

From 300 ml bacteria culture about 20 mg recombinant Su9₁₋₆₉DHFR was isolated (Fig.5.11A). To prevent aggregation of the protein due to disulfide-formation, DTT

had been added to the buffers during isolation. This was removed with a PD10 column before protein labeling with cysteine-specific label could occur. During the removal of DTT less than 10 % of the protein was lost.

Time course of binding of Alexa Fluor 488 C5-maleimide to Su9_{1–69}DHFR was determined. After distinct incubation periods, aliquots of the sample were removed, and further binding of the label was stopped by adding Laemmli-loading buffer containing β -mercaptoethanol. These samples, as well as a sample taken after 120 minutes and complemented with Laemmli-loading buffer lacking β -mercaptoethanol were separated on a 14.5 % (w/v) acrylamide SDS gel and binding efficiency was determined by analyzing the fluorescent intensity on exposure of the gel to UV-light (Fig.5.11B). The time series showed an increase in the fluorescent intensity of Su9_{1–69}DHFR with time. For later experiments a reaction time of 120 minutes was chosen. Interestingly, the non-reduced sample that was loaded on the gel revealed a dimerization of Su9_{1–69}DHFR (Fig.5.11B, last lane).

An important step after the labeling of protein is the removal of free dye. The diffusion time of the free dye is faster than the diffusion time of the sample (by a factor 5 - 10). Free dye could, however, react with the second protein during the binding studies. Furthermore, the curve fitting of the correlation functions would be less efficient. Whereas dialysis is a commonly performed method to remove small additives from the solution, this method is not appropriate for the removal of free dye from Su9_{1–69}DHFR due to the long time which is required for the complete removal of the dye. Therefore, a number of other methods were applied. After removal of the dye the sample was analyzed with SDS-PAGE. With UV excitation the fluorescently labeled proteins were made visible. For quantification of the amount of free dye (Fig.5.14), the gels or pictures thereof were either analyzed with the gel documentation system from SERVA (Heidelberg, Germany) or ImageJ.

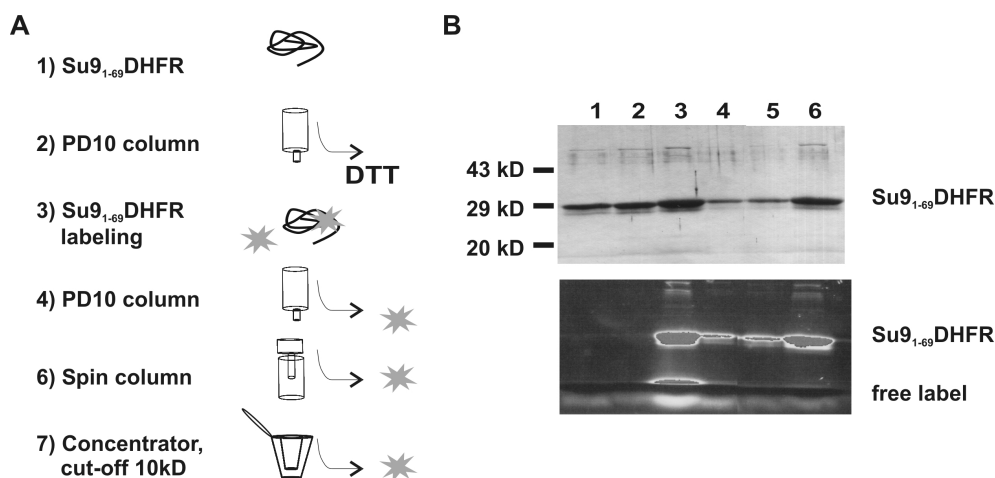


Figure 5.12: Preparation of Su9₁₋₆₉DHFR for FCS measurements

Su9₁₋₆₉DHFR was incubated with Alexa Fluor 488 C5-maleimide and various methods for the removal of free dye were performed.

A) Schematic drawing of the different steps. Recombinant Su9₁₋₆₉DHFR was isolated from *E. coli* cultures (1). The isolated protein was passed over a PD10 column to remove the reducing agent DTT (2) before labeling the protein (0.5 mg/ml) with 40 μ M Alexa Fluor 488 C5-maleimide for two hours at room temperature (3). Excessive dye was removed by passing the labeled protein over a PD10 column (4). Further dye was removed by either applying the sample to a Spin column (5) or to a concentrator with a 10,000 kD cut-off (6).

B) Aliquots of the different steps listed in (A) were analyzed on a 14.5 % (w/v) acrylamide SDS gel. Upper panel: Coomassie stained gel. Lower panel: Detection of the fluorescently labeled protein. For this, the gel was exposed to UV light. The best ratio of labeled protein to free dye is observed with the concentrator.

- **Gel filtration**

Separation of the 29 kD protein Su9₁₋₆₉DHFR from the free dye was possible by passing the sample over a gel filtration column. For this, either a Superose 6 column or a disposable PD10 column was used. Due to the very high dilution of the sample with the Superose 6 column, the PD10 column was used routinely. Free label was reduced to 45 % of original amount of free dye but was still detectable in the sample after passing it over the column (Fig.5.12B, lane 4).

- **Spin column**

Similar to the PD10 columns, micro desalt spin columns can be used to remove small molecules such as salt and dye. The advantage of this procedure

is the possibility to apply small volumes and the accelerated procedure by using centrifugal force instead of gravity. The sample is also less diluted. Subjecting labeled Su9_{1–69}DHFR to such a spin column resulted in a similar decrease in the amount of free dye compared to the sample which was subjected to gel filtration (41 % of original amount of free dye; Fig.5.12B, lane 5).

- **Vivaspin concentrator**

The principle behind a concentrator is a membrane that acts as a molecular sieve. Pores of a distinct size allow small molecules as well as the solution to pass, while larger molecules are concentrated above the membrane. For these experiments concentrators with cut-off of 10 kD were used. In Fig.5.12B (lane 6) an increase in Su9_{1–69}DHFR without an increase of free label (45 % of original amount of free dye) can be observed.

- **Bio-beads**

Bio-beads are polystyrene beads that adsorb hydrophobic molecules. They are often used for the removal of detergent in 2-D crystallization approaches (see section 5.2.1). After labeling Su9_{1–69}DHFR with Alexa Fluor 488 C5-maleimide, bio-beads were added to the sample. After one and two hours of incubation, aliquots of the sample were analyzed on a 14.5 % (w/v) acrylamide SDS gel, and the fluorescent intensity was quantified with the gel documentation system from SERVA (Heidelberg, Germany; Fig.5.13). A drastic decrease of free label was observed after 120 minutes incubation with bio-beads (< 6 % of original amount of free dye). This method showed the best result for the removal of free dye when compared with the other methods (Fig.5.14).

An interesting observation during the labeling of Su9_{1–69}DHFR was its high tendency to dimerize. In an additional experiment, the effect of the reducing agent TCEP (Tris (2-carboxyethyl) phosphine) on this dimerization was tested. For this, TCEP was added to labeled Su9_{1–69}DHFR. This sample was analyzed on a non-reducing SDS gel (14.5 % (w/v) acrylamide), with subsequent quantification of the fluorescent intensity (Fig.5.15). TCEP prevented the dimerization of Su9_{1–69}DHFR. Surprisingly, TCEP also increased the migration distance of the free dye.

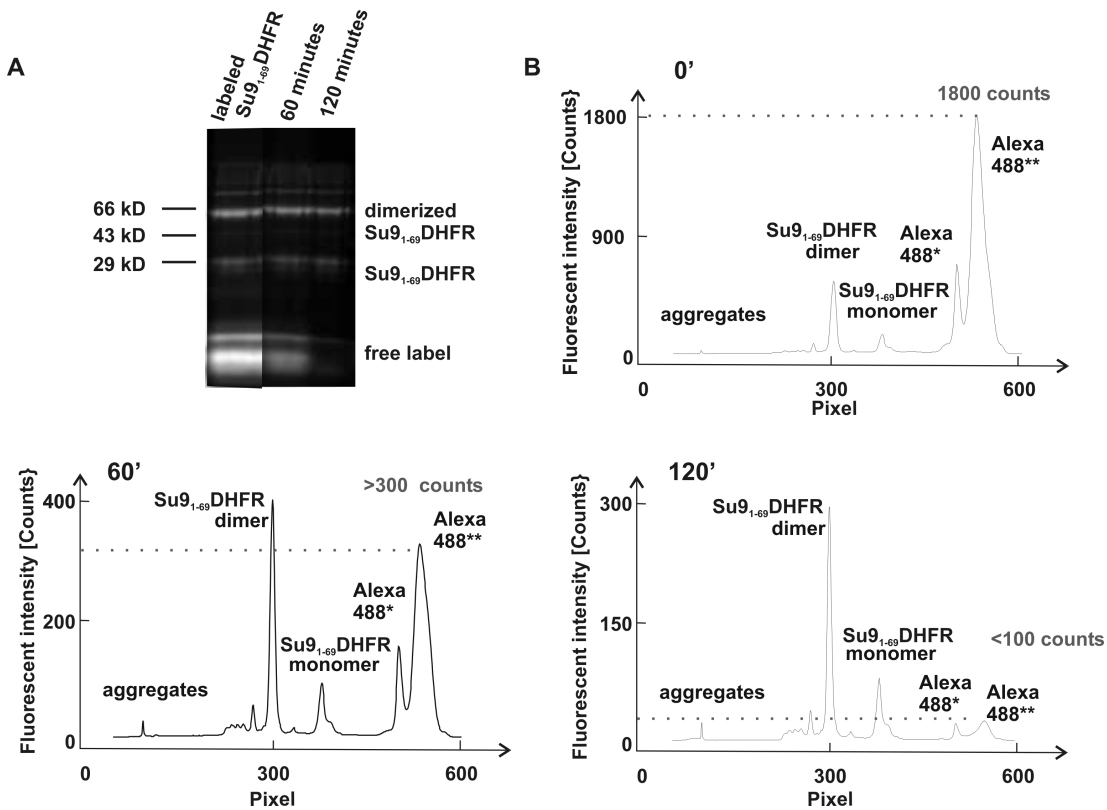


Figure 5.13: Removal of free dye from labeled Su9₁₋₆₉DHFR with bio-beads

300 μ l Su9₁₋₆₉DHFR (1 mg/ml) was labeled with 40 μ M Alexa Fluor 488 C5-maleimide and then incubated with bio-beads (10 mg). Samples were removed at 0, 60, and 120 minutes and were analyzed on a non-reducing SDS gel (14.5 % (w/v) acrylamide). After electrophoresis the gel was scanned with the gel documentation system from SERVA. This allowed a quantitative analysis of the intensity of the fluorescent bands.

A) Detection of the fluorescently labeled protein. For this, the gel was exposed to UV light.

B) Quantification of fluorescently labeled protein after 0, 60, and 120 minutes of bio-beads incubation. After the incubation of the samples with bio-beads for 120 minutes, a significant reduction of free dye was observed.

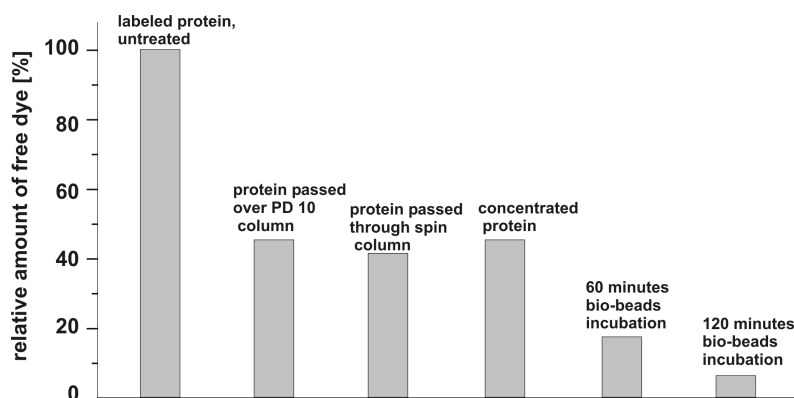


Figure 5.14: Quantification of removal of free dye

Su9₁₋₆₉DHFR was labeled with Alexa Fluor 488 C-5 maleimide and excessive dye was removed with various methods. For quantification of the remaining free dye the samples were analyzed with SDS-PAGE. Photographs thereof were analyzed with ImageJ. The relative amount of free dye compared to the untreated labeled sample is plotted. Incubation of the sample with bio-beads for 120 minutes led to the highest reduction of free dye.

In summary, I successfully labeled Su9₁₋₆₉DHFR with Alexa Fluor 488 C5-maleimide. The removal of unbound dye could be performed with various methods. The removal of free dye with bio-beads led to the best result. Only 5 % of the original amount of free dye remained after two hours of incubation.

5.3.2 Labeling of TOM core complex

For the analysis of the binding of Su9₁₋₆₉DHFR to TOM core complex with FCS the labeling of Su9₁₋₆₉DHFR would be sufficient. For FCCS measurements, however, both binding partners have to be labeled. As there is only one cysteine in the TOM core complex from *N. crassa* (residue 294 of Tom40) a specific labeling of Tom40 was expected.

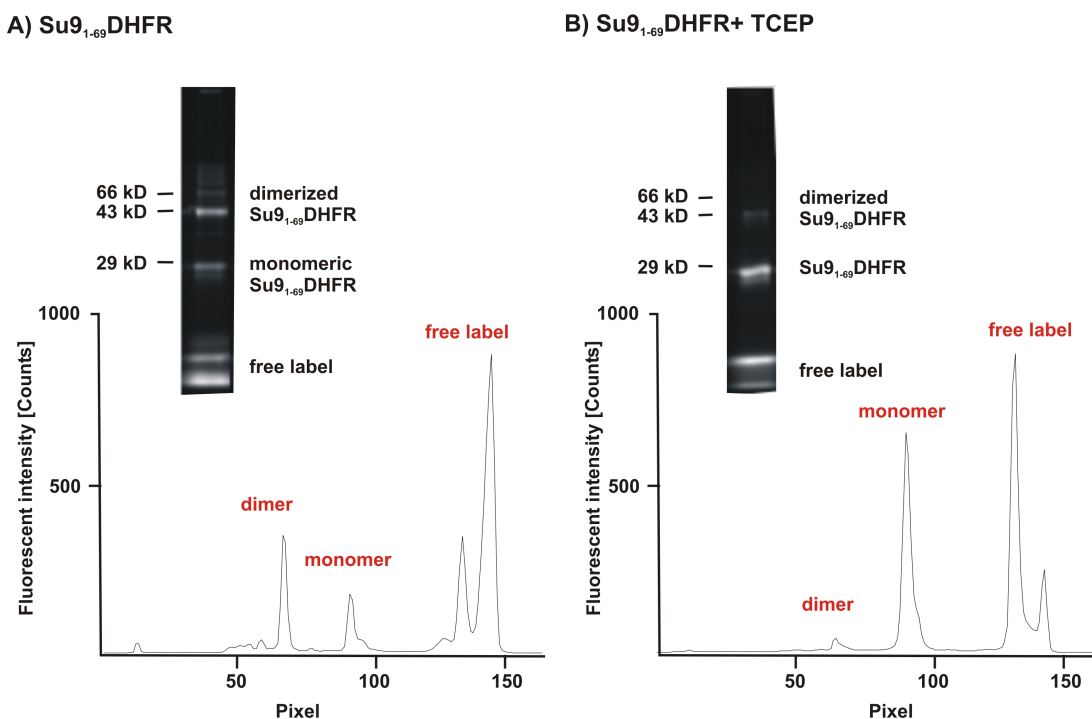


Figure 5.15: Effect of TCEP on labeled Su9₁₋₆₉DHFR

Su9₁₋₆₉DHFR was labeled with Alexa Fluor 488 C-5 maleimide. A sample was supplemented with TCEP and analyzed on a non-reducing SDS gel (14.5 % (w/v) acrylamide). After electrophoresis the fluorescent bands were detected with UV exposure, and a line scan allowed a quantitative analysis of the intensity of the fluorescent bands.

A) Untreated Su9₁₋₆₉DHFR. The dimeric band was enhanced compared to the monomeric band.

B) Su9₁₋₆₉DHFR with TCEP. Addition of TCEP led to a higher amount of monomeric Su9₁₋₆₉DHFR.

Similar to the time series described for Su9₁₋₆₉DHFR (see section 5.3.1), the time-dependent binding of Alexa Fluor 546 C5-maleimide to TOM core complex was analyzed. Isolated TOM core complex was incubated with Alexa Fluor 546 C5-maleimide and samples were taken after certain time-points. Labeling of the complex was stopped with the addition of Laemmli-loading buffer containing β -mercaptoethanol. These samples were analyzed on a 14.5 % (w/v) acrylamide SDS gel (Fig.5.16A). For subsequent experiments the binding time was set to 120 minutes. A longer incubation time at room temperature would have been bad for the stability of the protein complex.

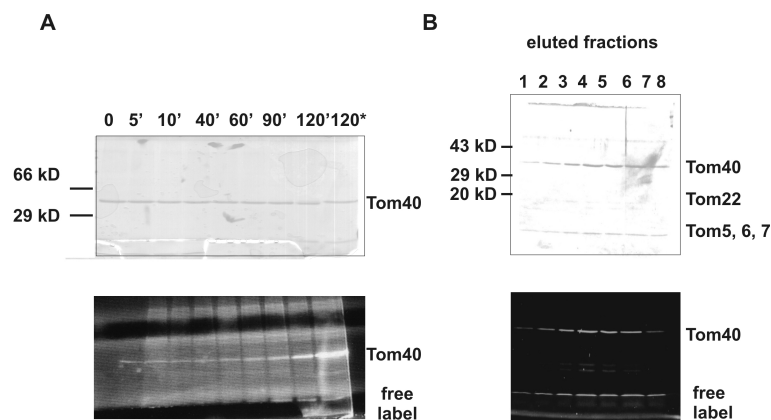


Figure 5.16: Labeling of TOM core complex

A) SDS-PAGE (14.5 % (w/v) acrylamide) of time-dependent labeling series: TOM core complex was incubated with Alexa Fluor 488 C5-maleimide (Molecular Probes) and at the indicated time-points an aliquot was removed and supplemented with Laemmli-loading buffer. After 120 minutes Laemmli-loading buffer lacking β -mercaptoethanol was added to the sample (last lane, marked with *). A time-dependent increase in the fluorescence intensity of Tom40 was observed.

B) Removal of free dye with size exclusion chromatography. Labeled TOM core complex was passed over a Superose 6 gel filtration column. The fractionated peak samples were analyzed on a 14.5 % (w/v) acrylamide SDS gel.

Upper panels: Coomassie stained, lower panels: detection of the fluorescently labeled proteins after exposure of the gel to UV-light. The eluted fraction contained fluorescently labeled Tom40 and a small amount of free dye.

To prevent binding of free dye to the precursor protein during the subsequent binding studies, the excessive free dye was removed from the sample with various purification procedures. First, the sample was passed over a Superose 6 gel filtration column. Fluorescently labeled TOM core complex eluted as a 400 kD complex (Fig.5.16B). Free dye eluted in the later fractions. However, a small per-

centage of free dye was detected in the TOM core complex sample. For further removal of the free dye, the sample was passed over the gel filtration column a second time. For this, the Superose 6 column was excessively washed with buffer (> 4 column volumes) in between. Furthermore, a trial was undertaken to reduce the free dye by subjecting the sample to a micro desalt spin column. The relative amount of free dye that remained in the samples was determined with FCS measurements (data presented below).

5.3.3 FCS Measurements

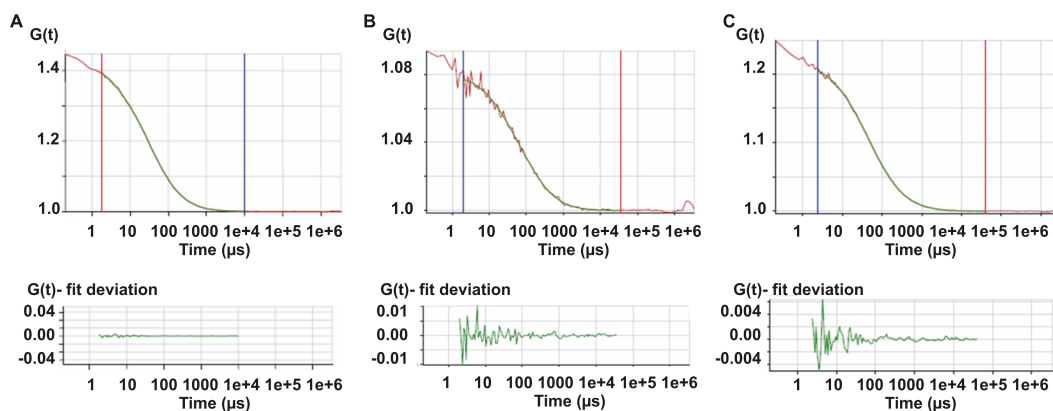


Figure 5.17: Autocorrelation of fluorescent dye in different buffers

FCS measurements were conducted from 1 nM Alexa Fluor 546 C5-maleimide in different buffers. The averaged autocorrelation curves generated from 10 single measurements (red curve) were fitted with a one-component fit function (green curve). The lower panel displays the corresponding fit residuals.

A) FCS measurements were performed with Alexa Fluor 546 C5-maleimide in water. The fitting of the generated autocorrelation curve with a one-component fit function revealed a diffusion time τ_{D_1} of 33 μs .

B) FCS measurements were performed with Alexa Fluor 546 C5-maleimide in 50 mM potassium acetate, 10 mM MOPS pH 7.2, 10 % (v/v) glycerol, 0.03 % DDM. The fitting of the generated autocorrelation curve with a one-component fit function revealed a diffusion time τ_{D_1} of about 76 μs . However, there was a high discrepancy in these measurements.

C) FCS measurements were performed with Alexa Fluor 546 C5-maleimide in 25 mM HEPES pH 7.2, 2 % (v/v) DMSO, 0.03 % (w/v) DDM; The fitting of the generated autocorrelation curve with a one-component fit function revealed a diffusion time τ_{D_1} of 50 μs .

To characterize the diffusion properties of labeled Su9₁₋₆₉DHFR and TOM core complex FCS measurements were performed on a commercial ConfoCor 2 combination system (Carl Zeiss, Jena, Germany). For calibration of the system, free dye was measured in buffer. Fitting the obtained autocorrelation curve with a one-component fit allowed the determination of the structure parameter ω and the diffusion time τ_D for free dye. Furthermore, the diffusion constant D for both Alexa dyes was set as $D = 4.14 \times 10^{-6} \text{ cm}^2 / \text{s}$. This is the value that has been determined for a similar dye, Rhodamin (Culbertson et al., 2000). With this, the dimensions of the parameters for axial to radial radii (r_0 and z_0), and detection volume V_{eff} were calculated with:

$$\tau_D = \frac{r_0^2}{4D} \iff r_0 = 2\sqrt{D\tau_D} \quad (5.1)$$

and

$$\omega = \frac{z_0}{r_0} \iff z_0 = r_0\omega \quad (5.2)$$

as well as

$$V_{eff} = \pi^{\frac{3}{2}} r_0^2 \omega \quad (5.3)$$

Calibration of the detection volumes in the green and orange channel were performed by comparing measurements from free dye in pure water and in the selected buffer. Measurements conducted with buffer containing 50 mM potassium acetate, 10 mM MOPS pH 7.2, 10 % (v/v) glycerol, 0.03 % DDM showed high variation within the repetitive measurements. Both MOPS and glycerol shifted the optical properties of the buffer. For the buffer containing 25 mM HEPES pH 7.2, 2 % (v/v) DMSO, 0.03 % (w/v) DDM a significant improvement was observed (Fig.5.17). Therefore, this buffer was used for all subsequent measurements and preparation of the fluorescently labeled proteins. With the equations described above the effective detection volumes of $V_{eff} = (1.2 \pm 0.1) \text{ fl}$ for 546 nm and $V_{eff} = (1.5 \pm 0.01) \text{ fl}$ for a 488 nm were determined. Laser power settings were 13 μW for the 488nm Argon-ion laser line and 2 μW for the HeNe laser (543 nm). No artificial reduction of the diffusion through photobleaching was observed with the applied laser intensities.

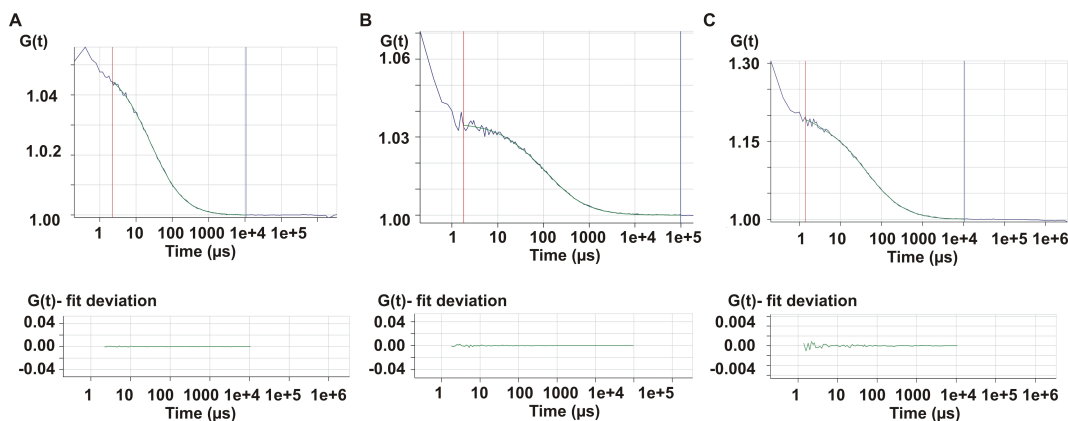


Figure 5.18: Autocorrelation of fluorescently labeled Su9_{1–69}DHFR

FCS measurements of Su9_{1–69}DHFR were performed in 25 mM HEPES pH 7.2, 2 % (v/v) DMSO, 0.03 % (w/v) DDM. Ten autocorrelation curves generated from single measurements were averaged (blue curve). This was fitted with a one-component or two-component fit function (green curve). The lower panel displays the corresponding fit residuals.

A) FCS measurements were performed with Alexa Fluor 488 C5-maleimide in buffer solution. Fitting of the generated autocorrelation curve with a one-component fit function revealed a diffusion time τ_{D_1} of 30 μs .

B) FCS measurements were performed with GFP in buffer solution. Fitting of the generated autocorrelation curve with a one-component fit function revealed a diffusion time τ_{D_1} of 120 μs .

C) FCS measurements were performed with Alexa488-Su9_{1–69}DHFR in buffer solution. Fitting of the generated autocorrelation curve with a one-component fit function revealed a diffusion time τ_{D_1} of 30 μs and a diffusion time τ_{D_2} of 130 μs . This is in agreement with the diffusion time determined for GFP. The relative amount of the former population was 80 % and of the latter population 20 %.

Next, the FCS measurements were performed with labeled Su9_{1–69}DHFR (Fig.5.18). These were compared with control measurements conducted with green fluorescent protein (GFP). This protein fluoresces green when exposed to blue light (Shimomura et al., 1962) and has a similar molecular mass (26.9 kD) as Su9_{1–69}DHFR (29 kD). For GFP a diffusion time of 120 μs was determined and for the labeled Su9_{1–69}DHFR diffusion times of about 130 μs were measured. However, Su9_{1–69}DHFR seemed to aggregate, and many of the measurements had to be discarded as aggregated particles with high fluorescent intensities were detected. In the remaining measurements the population of free dye was very high (80 %).

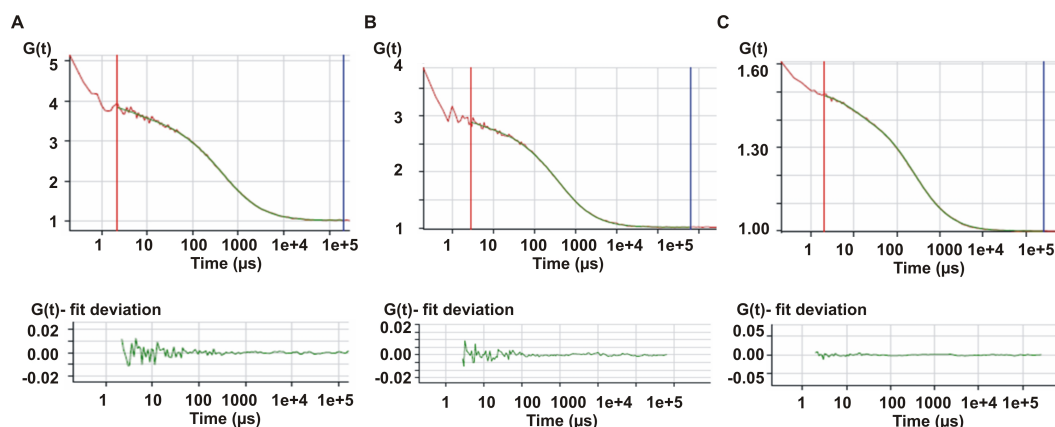


Figure 5.19: Autocorrelation of fluorescently labeled TOM core complex

FCS measurements of labeled TOM core complex with Alexa Fluor 546 C5-maleimide were performed in 25 mM HEPES pH 7.2, 2 % (v/v) DMSO, 0.03 % (w/v) DDM. Ten autocorrelation curves generated from single measurements were averaged (red curve). This was fitted with a two-component fit function (green curve). The lower panel displays the corresponding fit residuals.

A) FCS measurements were performed with TOM core complex labeled with Alexa Fluor 546 C5-maleimide and passed over a Superose 6 column. Fitting of the generated autocorrelation curve with a two-component fit function revealed a diffusion time τ_{D_1} of 50 μs and τ_{D_2} of 530 μs . The relative amount of the former population was 21 % and of the latter population 79 %.

B) FCS measurements were performed with TOM core complex labeled with Alexa Fluor 546 C5-maleimide and passed over a Superose 6 column twice. Fitting of the generated autocorrelation curve with a two-component fit function revealed a diffusion time τ_{D_1} of 50 μs and τ_{D_2} of 469 μs . The relative amount of the former population was 23 % and of the latter population 77 %.

C) FCS measurements were performed with TOM core complex labeled with Alexa Fluor 546 C5-maleimide and subjected to a micro spin column. Fitting of the generated autocorrelation curve with a two-component fit function revealed a diffusion time τ_{D_1} of 50 μs and τ_{D_2} of 250 μs . The relative amount of the former population was 4 % and of the latter population 96 %. The lower value for $G(0)$ indicated that a reduction of the chromophores had taken place.

To determine the diffusion time of TOM core complex, FCS measurements were performed with fluorescently labeled TOM core complex (Fig.5.19). Alexa Fluor 546 C5-maleimide was used as a chromophore. At least ten autocorrelation curves generated from FCS measurements were averaged and fitted with a two component fit to determine the diffusion times and relative amount of the two fluorescent populations. First, labeled TOM core complex, which had been passed over a Superose 6 column, was measured. About 20% of the measured

fluorescence fluctuations derivated from free dye (Fig.5.19A). Repeating the gel filtration showed no significant reduction of the amount of free dye (Fig.5.19B). However, the repetitive gel filtration lead to an improvement of the homogeneity of the sample. Whereas, in the first measurements aggregated TOM core complex was sometimes detected during the measurements (with a frequency of 0.03 per second), no aggregation of the sample was observed after the second gel filtration step. Measurements of up to 30 minutes were possible. The diffusion times determined for the slow component were between 470- 530 μs . This is in excellent agreement with the theoretical value for the diffusion time of the TOM core complex under the given conditions which is about 500 μs . After applying the labeled TOM core complex to a spin column the free label was reduced to a negligible fraction of 4 % (Fig.5.19C). Interestingly, the longer diffusion time was reduced to 250 μs . This dramatical reduction of the diffusion time after using the spin column indicates severe damage to the protein complex. However, the actual shape (and thus the diffusion coefficient) of the measurement indicates an extremely homogeneous sample. It must be noticed that the amount of fluorescent molecules ($G(o) = 1.6$, see equation 4.5) was strongly decreased after the use of the micro spin column (Fig.5.19C). This indicates that labeled TOM core complex was most likely removed from the sample with the spin column.

To analyze the binding between Su9₁₋₆₉DHFR and TOM core complex FCS measurements were performed. Either unlabeled or labeled TOM core complex was added to labeled Su9₁₋₆₉DHFR and the diffusion time of the preprotein was monitored. During a binding event of labeled Su9₁₋₆₉DHFR to TOM core complex an increase in diffusion time to >500 μs would be expected. However, the diffusion time of Su9₁₋₆₉DHFR stayed constant (about 130 μs) after the addition of unlabeled (Fig.5.20A) as well as labeled TOM core complex (Fig.5.20B). Furthermore, the aggregation problem of Su9₁₋₆₉DHFR was very severe. Thirty minutes after addition of labeled TOM core complex, only a negligible fraction of the slow component was detectable (Fig.5.20C). Labeled Su9₁₋₆₉DHFR obviously aggregated and precipitated. Due to these aggregation problems no FCCS measurements were performed.

In summary, I was able to label TOM core complex as well as the model precursor protein Su9₁₋₆₉DHFR with cysteine specific Alexa chromophores. FCS measurements of labeled TOM core complex revealed a diffusion time for the complex in agreement of the theoretical value estimated with the molecular mass of the complex. FCS measurements of the labeled Su9₁₋₆₉DHFR were, however, dif-

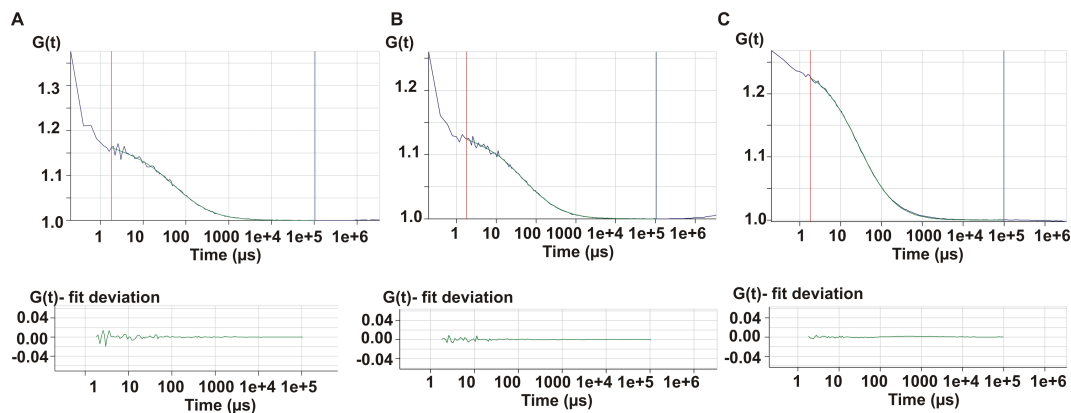


Figure 5.20: Autocorrelation of fluorescently labeled Su₉₁₋₆₉DHFR and added TOM core complex

FCS measurements of Su₉₁₋₆₉DHFR with purified TOM core complex added were performed in 25 mM HEPES pH 7.2, 2 % (v/v) DMSO, 0.03 % (w/v) DDM. Ten autocorrelation curves generated from single measurements were averaged (blue curve). This was fitted with two-component or three-component fit function (green curve). The lower panel displays the corresponding fit residuals.

A) FCS measurements were performed with Alexa488-Su₉₁₋₆₉DHFR and purified TOM core complex (unlabeled) in buffer solution. Fitting of the generated autocorrelation curve with a two-component fit function revealed the diffusion times τ_{D_1} of 32 μs and τ_{D_2} of 113 μs . The relative amount of the former population was 68 % and of the latter population 32 %. No third component was detected.

B) FCS measurements were performed with Alexa488-Su₉₁₋₆₉DHFR and purified TOM core complex (labeled with Alexa Fluor 546 C5-maleimide) in buffer solution. Fitting of the generated autocorrelation curve with a two-component fit function revealed diffusion times of τ_{D_1} of 32 μs and τ_{D_2} of 138 μs . The relative amount of the former population was 70 % and of the latter population 30 %. No third component was detected. This indicates that there was no binding between the two substrates.

C) FCS measurements were performed with Alexa488-Su₉₁₋₆₉DHFR and purified TOM core complex (labeled with Alexa Fluor 546 C5-maleimide) in buffer solution after 30 minutes of incubation. Fitting of the generated autocorrelation curve with a one-component fit function revealed a diffusion time τ_{D_1} of 32 μs . Neither a second nor a third component was detected. This indicates that Alexa488-Su₉₁₋₆₉DHFR aggregated and precipitated and was no longer detected in the detection volume.

difficult as a strong tendency for aggregation was observed. Furthermore, it was not possible to demonstrate the binding of this protein to TOM core complex. In the future, different model proteins will have to be tested. The protocols described here can be used as the basis for the labeling of these new proteins.

5.4 Electrophysiological measurements

To gain further insights into the dynamics of the TOM core complex, planar lipid bilayer experiments were performed. Previous studies have addressed the channel-forming properties of the TOM core complex. However, no comprehensive investigation of the exact number of sub-conductance levels, their occupancy probability, and the transitions between these states has been available. To exclude a contamination of the purified TOM core complex sample with VDAC, the electrophysiological properties of purified VDAC were determined as well.

5.4.1 Electrophysiological characterization of VDAC

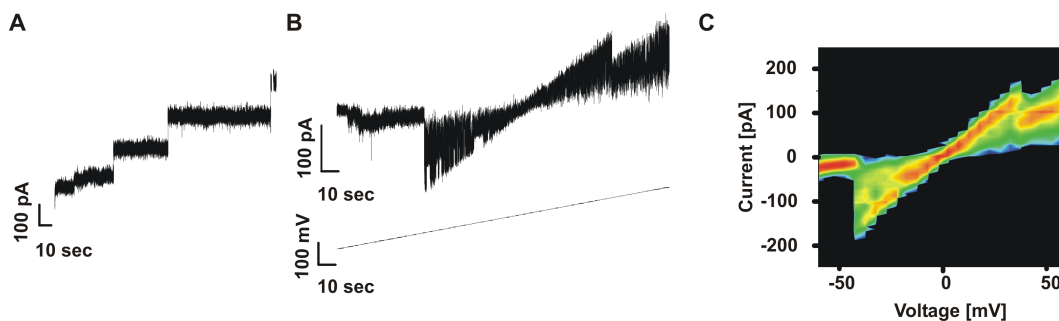


Figure 5.21: Electrophysiological characterization of VDAC

A) To determine the chord conductance purified VDAC was added to the cis side of the bilayer setup. Incorporation of VDAC into the bilayer was observed as step-like increases of the current level. The membrane potential was held at constant 20 mV.

B) Single channel measurement of a VDAC channel. For this, step-like increases in voltage were applied (from -70 to +70 mV in 1 mV increments and 1 sec duration) to an incorporated VDAC channel.

C) The recorded data displayed in (B) were imported into Microcal Origin 7.5 and a 2-D histogram was calculated. This is displayed as an I-V surface map. Increase in the probability that a data point is located within a given bin is presented by a color scheme (blue < green < yellow < red). VDAC channels occupied mainly two conductance levels.

VDAC, the voltage dependent anion channel, is the most abundant protein of the mitochondrial outer membrane (Colombini, 1979). To rule out any contamination with VDAC in the subsequent TOM core complex measurements, the electrophysiological properties of VDAC were analyzed. As both VDAC and TOM core complex are most likely β -barreled proteins, similar channel properties can be expected.

Isolated VDAC was added to an artificial bilayer, and step-like increases in current were observed indicating incorporation of channels. These channels displayed a conductance of approximately 4 nS (Fig.5.21A). Single channel recordings revealed a voltage-dependent gating behavior (Fig.5.21B). The corresponding I-V surface map (Fig.5.21C) showed the channel mainly in its open conductance state ($\gamma_1 = 4$ nS) and a half open state ($\gamma_2 = 2$ nS). This was in agreement with conductance values published for VDAC (Freitag et al., 1982). The analysis of channels formed by isolated VDAC indicated a main conductance state which is approximately twice the value for the channels measured for TOM core complex. The electrophysiological properties of TOM core complex are described in the following section.

5.4.2 Electrophysiological characterization of the channel properties of TOM core complex

First, an analysis of the channel properties of TOM core complex was conducted by performing stationary measurements of single channels incorporated in black lipid membranes. The current traces revealed fluctuations to different sub-conductance levels. The transition to these levels appeared to be voltage dependent. Amplitude all-point histograms were analyzed to estimate the number of conductance levels occupied by the TOM core complex. The conductance levels of the individual states were determined with I-V curves. Furthermore, occupancy probability plots were generated to describe the voltage dependent gating behavior of TOM core complex in the different conductance states. Thereafter, I have examined the influence of the KCl concentration on the channel properties of the TOM core complex.

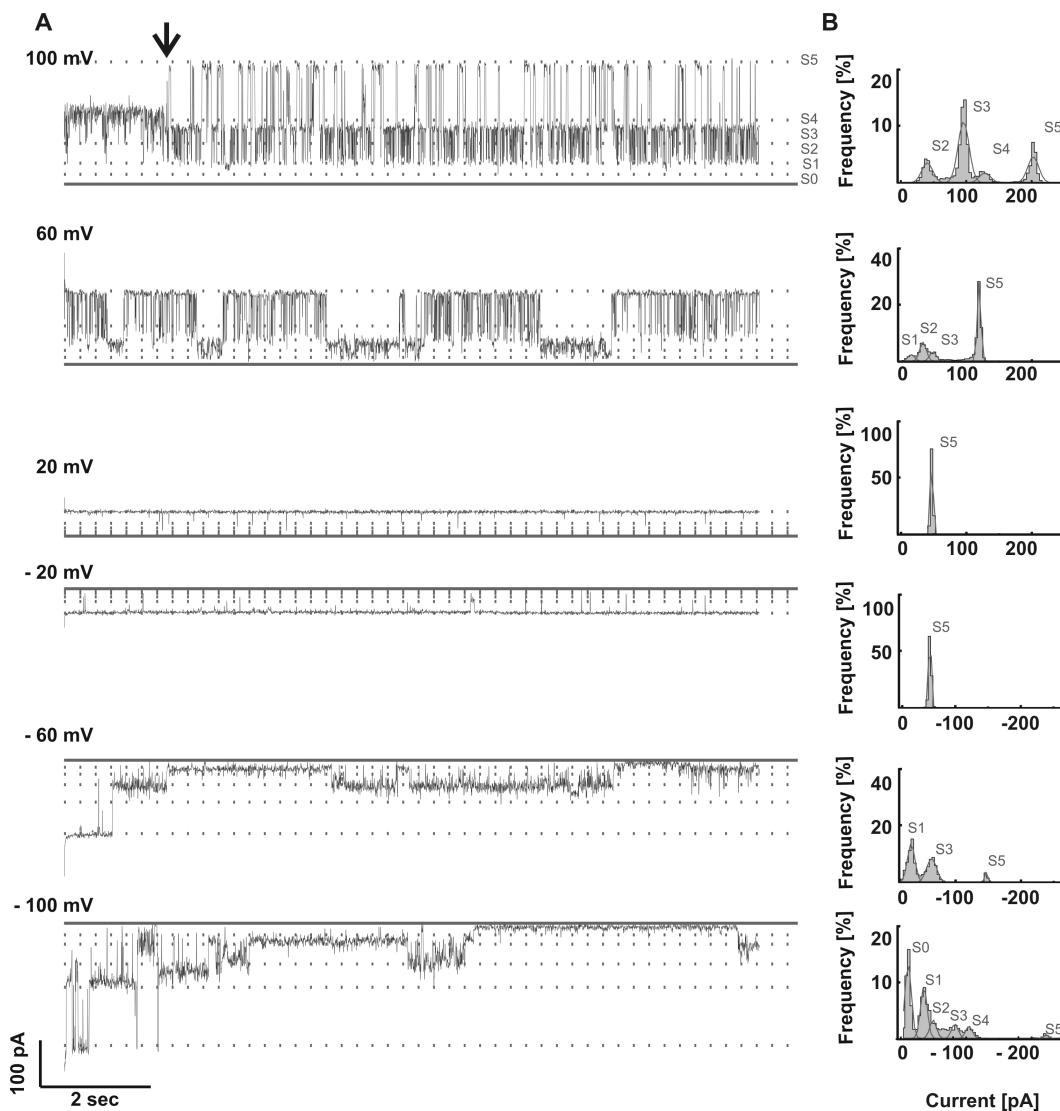


Figure 5.22: Single channel measurements of TOM core complex

Isolated TOM core complex was incorporated into planar lipid bilayers in symmetrical KCl solution (1M). Pulse measurements were recorded. For this, after applying 0 mV to the membrane for 10 sec, the voltage was increased like indicated, and a 10 sec stationary measurement was recorded.

A) Current traces. Dotted lines indicate the conductance levels S1-S5. The base line is presented with a continuous line. The arrow in the 100 mV current trace indicates a switch in the gating mode, which was often observed during single channel measurements.

B) Corresponding current all-point histograms of the 10 sec measurements. Bin size: 4 pA. Data were fitted with Gaussian functions, which could be assigned to the conductance levels S0-S5.

Determination of the conductance levels occupied by TOM core complex

The first step in a comprehensive characterization of the single channel properties of a pore-forming protein is the determination of the main conductance level and potential sub-conductance levels.

For this, isolated TOM core complex was added to a bilayer setup, and single channel measurements were conducted at symmetrical salt conditions (1 M KCl). The current traces of the measurements at +20 mV and -20 mV, respectively, showed the channel in its main conductance state for most of the time. Only occasional closing of the channel was observed as rare spikes in direction of the closed state (Fig.5.22A). The corresponding all-point histograms (Fig.5.22B), were each fitted with one Gaussian function. In agreement with previous studies, the chord conductance for a single channel was found to be $\gamma = 2.2$ nS (Ahting et al., 1999, 2001).

By increasing the voltage, an increase in the transition frequency to other conductance levels was observed (Fig.5.22A). A complete closure of the channel was rarely detected. The analysis of a large number of measurements ($n > 70$) pointed to the existence of at least six distinct conductance levels for TOM core complex. For clarity, these were named S0-S5 (S0 is the closed state, S1 = 0.16 ± 0.03 nS, S2 = 0.36 ± 0.06 nS, S3 = 0.67 ± 0.09 nS, S4 = 1.09 ± 0.15 nS, and S5 = 2.16 ± 0.34 nS) and are indicated in the current traces as dotted lines (Fig.5.22A).

The current traces revealed an asymmetric behavior of the channel regarding the polarity of the applied voltage. This has been described previously (Künkele et al., 1998b; Muro et al., 2003). For negative voltage the occupancy of the channel in the main conductance state (S5) was decreased. Transitions between lower conductance states were observed (Fig.5.22A, current traces -60 mV and -100 mV). For positive voltage (Fig.5.22A, +60 mV and +100 mV) fast flickering from the open state S5 to the sub-conductance levels was observed. This fast flickering was only detected for potentials of one polarity, indicating a random orientation of the TOM core complex in the artificial membrane. For further analysis and comparison of the measurements, the polarity of voltage of the measurements was aligned to adjust for the different insertion polarities of the channel.

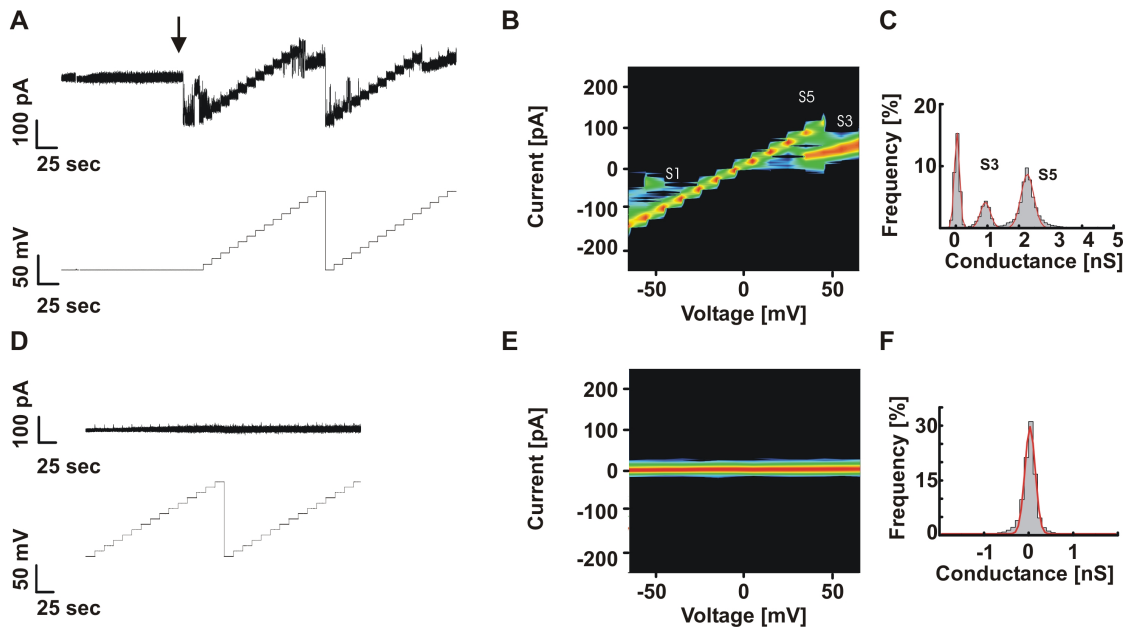


Figure 5.23: Conductivity of an empty membrane

A) Measurement of an empty membrane with subsequent insertion of a TOM core complex channel. Insertion event is indicated with an arrow. Thereafter, voltage sweeps from -70 mV to +70 mV in 10 mV increments and duration of 10 sec were applied to the membrane.

B) The recorded data shown in (A) were imported into Microcal Origin 7.5 and a 2-D histogram was calculated. This is displayed as an I-V surface map. Increase in the probability that a data point is within the respective bin is presented by a color scheme (blue < green < yellow < red). The slope conductance of about 2.2 nS for the S5 state confirmed that a single channel had incorporated.

C) All-point histogram of calculated chord conductance of the measurement shown in (A). This was fitted with three Gaussian functions. After insertion of the channel, conductance levels of 2.2 nS (S5 state) and 0.7 nS (S3 state) were detected. Before insertion of the channel, the conductance of the membrane was 0.03 nS. This corresponds to a membrane resistance of 33 G Ω .

D) Voltage sweeps applied to an empty membrane.

E) Corresponding I-V surface map of the measurement displayed in (D). Hardly any slope is detected.

F) All-point histogram of calculated chord conductance of measurement shown in (D). By fitting a Gaussian function to the histogram, the conductance of the empty membrane was determined to be 0.03 nS.

In the current trace record with a holding potential of 100 mV (Fig.5.22A), a typical behavior of TOM core complex channels was observed – a mode switching (indicated with an arrow). Here, the TOM core complex channel switched from a phase with hardly any transitions to a phase with fast flickering. Such a behavior indicated that there were not only different conductance states but also a number of kinetic states within the channel (McManus and Magleby, 1988).

To verify that the small S1 state (0.16 nS) was a real conductance state and not the result of a “leaky” membrane, the conductivity of an empty bilayer was measured. In Fig.5.23A a current recording of an empty membrane with a subsequent insertion of a TOM core complex channel is shown (see arrow). The membrane potential was held at constant -70 mV until the insertion of a channel was observed. Thereafter, voltage sweeps ranging from -70 mV to +70 mV (10 mV increments, 10 sec duration) were applied to this channel. The corresponding I-V surface map and the all-point histogram of calculated chord conductance values were generated ($\gamma = i/V$; Fig.5.23B and C). Fitting Gaussian functions to the histogram revealed a conductance of 0.03 nS for the empty membrane. This corresponded to 33 G Ω resistance. A similar result was achieved when applying voltage sweeps to an empty membrane (Fig.5.23D). Hardly any slope was detected in the corresponding I-V surface map (Fig.5.23E). In the all-point histogram of the chord conductance values, the conductance for the empty membrane was determined to be 0.03 nS or 33 G Ω .

In summary, the single channel measurements revealed at least six distinct conductance levels. The transitions between these were voltage dependent. The asymmetry of the voltage dependent switching between the conductance states allowed me to define an orientation of the reconstituted channel. In the following section, this voltage dependent occupancy of the various conductance states was examined in more detail by generating occupancy probability plots.

Voltage dependent gating

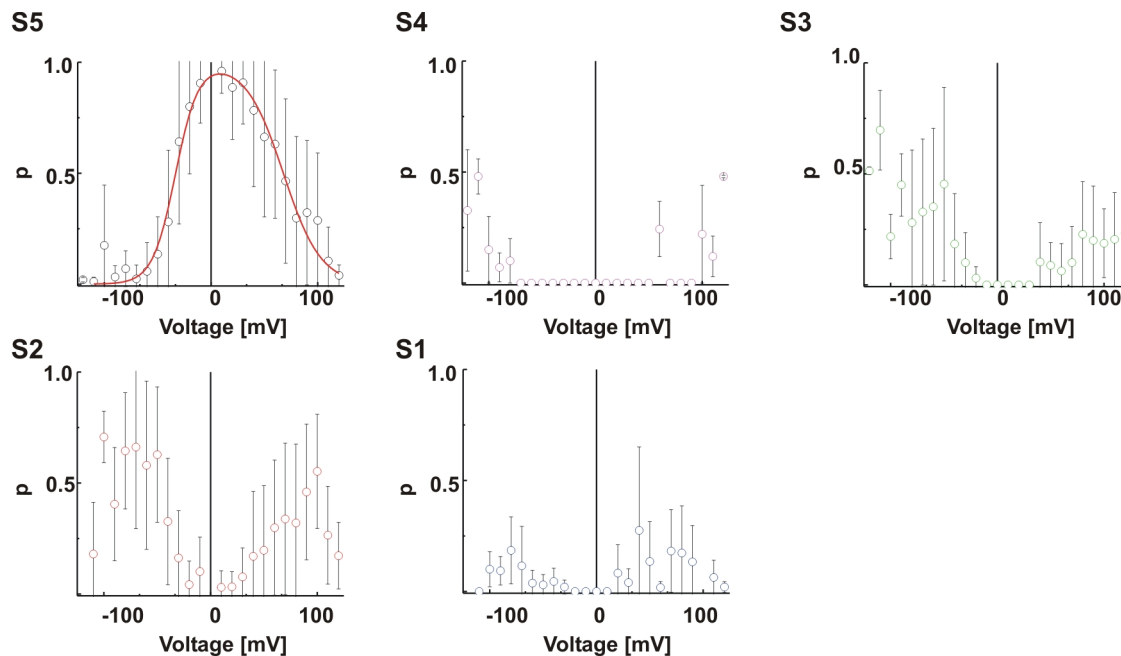


Figure 5.24: Occupancy probabilities of the conductance states occupied by TOM core complex channels

Single channel measurements of TOM core complex channels were conducted by applying voltage sweeps from -120 mV to +120 mV in increments of 10 mV and a duration of 10 sec. For each voltage all-point histograms were generated and fitted with Gaussian functions. Percentage of data points located within the peak areas (occupancy probabilities p) were determined and plotted against voltage. Occupancy probability of the S5 state corresponded to the open probability of the channel. This was fitted with a double Boltzmann equation (solid line). The average of eight measurements are displayed (\pm SEM). The S5 state was mainly occupied at voltages between -30 mV and +60 mV. An increase in voltage was accompanied by an increase in the occupation probabilities of the S3 and S2 state. The S4 and S1 states were hardly occupied.

For a better characterization of the voltage dependent gating behavior of a single TOM core complex channel, the occupancy probability of each conductance level was plotted against the respective voltage. For this, stationary single channel measurements were analyzed ($n = 8$), and all-point histograms were fitted with Gaussian functions. The peak area of the fitted peaks corresponded to the occupancy probability. The determined values were plotted against the respective voltage (Fig.5.24).

The generated curves indicated that the channel occupied the main conduc-

tance state (S5) between +20 mV and -20 mV. Increasing voltage was accompanied by population of mainly the S3 and S2 states. The occupancy probability for the S4 state was low for all voltages. The S1 state was mainly occupied at voltages higher than 80 mV. A complete closure of the channel (S0 state) was hardly ever observed.

For the S5 state the occupancy probability corresponded to the open probability of the channel. This was fitted with a double Boltzmann equation (see section 6.2).

$$p_o = \frac{1}{1 + e^{-a_l(V-V_l)}} * \frac{1}{1 + e^{-a_r(V-V_r)}} \quad (5.4)$$

where V_l (-33 ± 7 mV) and V_r (68 ± 10 mV) are the points of inflection of the curve. This corresponds to the voltage at which the probability that the channel is open is half maximal. The values a_l (0.1 ± 0.03 mV⁻¹) and a_r (-0.6 ± 0.02 mV⁻¹) correspond to the slope in these points and reflect the voltage sensitivity. From these $z\delta_l = 2.5 \pm 0.8$ and $z\delta_r = 1.5 \pm 0.5$ were determined as:

$$a = z\delta F / RT \quad (5.5)$$

The valence z and the fraction of membrane electric field δ cannot be separated. So without an atomic structure or mutant analysis, differentiation between e.g. one charge ($z=1$) across the whole membrane ($\delta=1$) and two charges ($z=2$) across half of the membrane ($\delta=0.5$) is not possible.

A bell-shaped open probability indicates that there are two different “gates” located in the channel. The parameters describing the gates reflected the asymmetric gating behavior of the channel. At -34 mV the open probability of the channel was already reduced to 0.5. For positive voltage, however, the open probability first reached the value 0.5 at +68 mV. Furthermore, the sensitivity to a negative voltage change of the electrical field over the membrane was double the value of the positive voltage change.

Analysis of I-V characteristics

The analysis of the I-V characteristics was performed with two different procedures. First, measurements generated by applying voltage ramps to reconstituted channels allowed the creation of I-V surface maps. Secondly, stationary single

channel measurements enabled the generation of I-V curves which allowed a more quantitative analysis of the I-V characteristics of the various conductance levels.

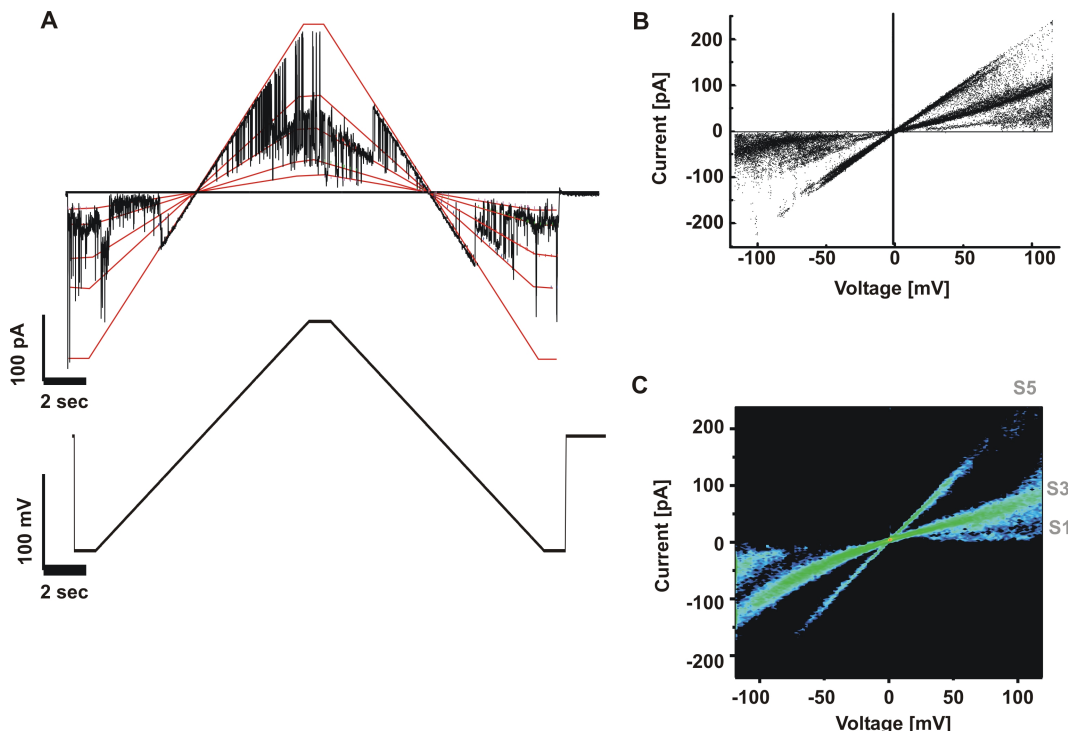


Figure 5.25: I-V characteristic analyzed with a voltage ramp protocol

Purified TOM core complex was incorporated into planar lipid bilayers and single channel measurements were recorded in symmetrical salt conditions (1 M KCl).

A) Voltage ramps from -120 mV to +120 mV were applied to an incorporated TOM core complex channel (see voltage trace, lower panel). Red lines in the current trace indicate the conductance levels S1-S5. The base line is presented as a continuous black line.

B) I-V scatter plot of ten voltage ramp measurements of the same channel as in (A).

C) The recorded data of ten voltage ramp measurements were imported into Microcal Origin 7.5 and a 2-D histogram was calculated. This is displayed as an I-V surface map. Increase in the probability that a data point is located within a given bin is presented by a color scheme (blue < green < yellow < red). Whereas the I-V characteristic of the S5 state was linear, those of the S2 and S3 states had the shape of an “inverted S.”

To further characterize the voltage dependency of the different conductance levels a new set of experiments were conducted using a bilayer setup with a smaller membrane surface. Thus, the membrane capacitance was decreased and capacitive current reduced. This allowed the application of faster voltage changes to a black lipid membrane. Ramps running from -120 mV to +120 mV in 10 sec

(0.024 V/sec) were applied (Fig.5.25A, lower panel). The five conductance states are indicated with red lines in the current traces (Fig.5.25A, upper panel). Each conductance level was occupied for at least a short period. Transitions between the states and the asymmetric voltage dependency were in agreement with the findings described above.

Conducting such measurements has the advantage that a number of measured voltage ramps of one channel were analyzed by creating I-V surface maps. Fig.5.25B shows such an I-V surface map resulting from ten ramps recorded from one membrane. Interestingly, only the main conductance level revealed a linear behavior. The sub-conductance levels S3 and S1 showed a non-linear behavior with the current increasing at higher voltages. The S4 and S2 states were hardly visible with this analysis method.

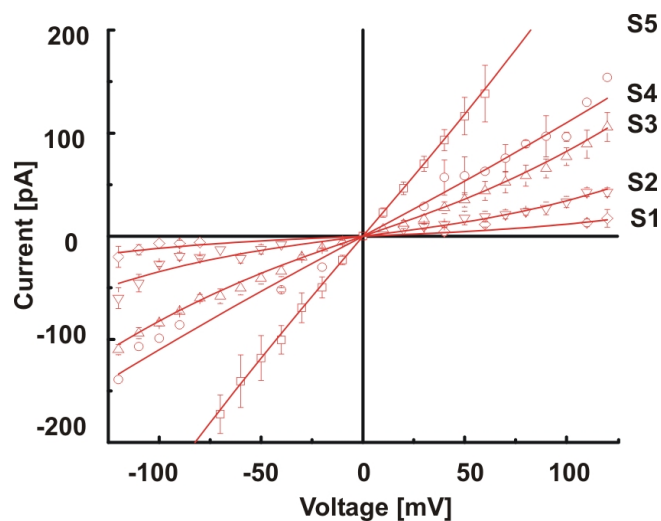


Figure 5.26: I-V characteristics of five conductance levels

Single channel measurements were recorded with step-like voltage increase of 10 mV and for 10 sec in symmetrical KCl solution (1 M). Mean currents were determined by fitting all-point histograms with Gaussian peaks and were plotted against the respective voltage. The peak current of eight measurements are displayed (\pm SD). The resulting I-V characteristics were fitted with a Nernst-Planck model assuming a single symmetrical triangular barrier (see equation 6.8). Whereas the S5 and S4 state revealed an Ohmic I-V characteristic, the I-V characteristics of the S1-S3 state were non-linear with the shape of an “inverted S”.

For a more quantitative analysis, the I-V characteristic generated from stationary measurements was analyzed. All-point histograms generated from current traces recorded at various voltages allowed the determination of the mean cur-

rent for each conductance state. The mean current was then plotted against the respective holding voltage. Only the conductance states S4 and S5 displayed a linear I-V characteristic (Fig.5.26). The other conductance states revealed non-ohmic I-V characteristics with increasing current at high voltages. These I-V curves were then fitted with a Nernst-Planck model assuming a single symmetrical triangular barrier (Hall et al., 1973, see section 6.1).

The barrier height ϕ and the cross sectional area A were set as free fitting parameters. The parameters that best fit the data for each conductance level are summarized in table 5.2.

Table 5.2: Parameters determined with Nernst-Planck barrier fit

Conductance state	energy barrier $\Delta\phi$ (kT)	pore diameter (nm)
S5	< 0.4	0.9
S4	< 0.4	0.7
S3	0.7	0.6
S2	2.0	0.5
S1	3.6	0.5

The determined parameters suggested that the ions passing through the channel occupying the states S1-S3 had surmounted an energy barrier. Ions passing the channel when it was occupying the states S4 and S5 did not have to surmount such barriers.

Dependency of KCl concentration

A set of experiments was conducted at lower KCl concentration to analyze if the conductance levels of the TOM core complex channel or its other channel properties were influenced by the ionic strength. For this, isolated TOM core complex was incorporated into black lipid membranes in symmetrical solution with 10 mM Hepes pH 7.2 and either 125 mM KCl or 250 mM KCl. Voltage ramps were applied as described and current traces were recorded (Fig.5.27). For both conditions, the current traces and the generated I-V surfaces indicated that all six conductance levels were occupied for at least a short period of time. The transition frequencies of the measured channels were similar to measurements conducted at 1 M KCl.

For both salt concentrations at least four experiments consisting of at least ten ramps were conducted. Values for the conductance levels were determined by

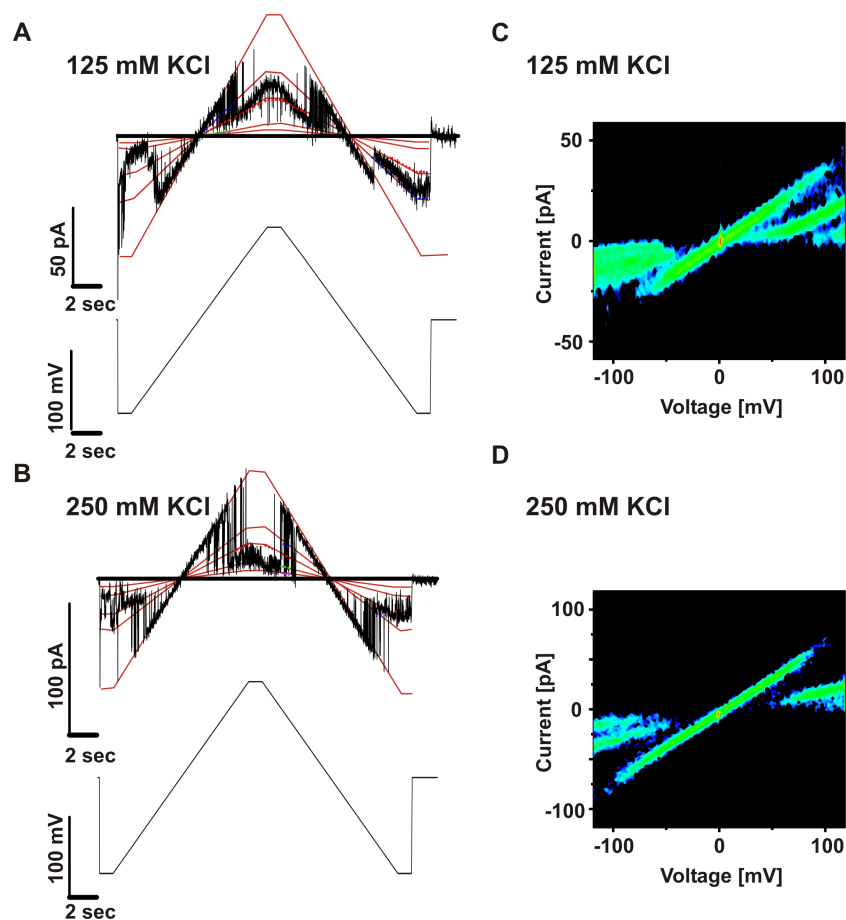


Figure 5.27: Single channel measurements at low salt concentrations

Isolated TOM core complex was incorporated into planar lipid bilayers in symmetrical 125 mM (A, C) and 250 mM (B, D) KCl solutions.

A, B) Current traces recorded while applying a voltage ramp from -120 mV to +120 mV. Red lines in the current trace indicate the conductance levels S1-S5. The baseline is represented with a continuous black line.

C, D) I-V surface maps. 2-D histograms were calculated from 10 ramps and are displayed as I-V surface maps. Increase in the probability that a data point is located within a given bin is presented by a color scheme (blue < green < yellow < red). Whereas the I-V characteristic of the S5 state was linear, those of the S2 and S3 states had the shape of an “inverted S.” The I-V surface maps were similar to that of 1 M KCl except for a decrease in the signal/noise ratio (see. Fig.5.25).

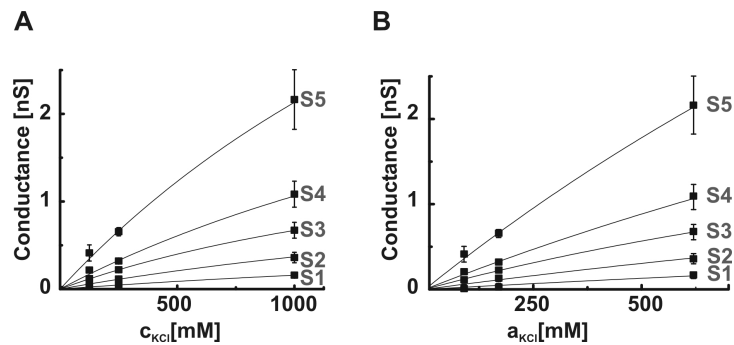


Figure 5.28: Dependency of KCl concentration and activity on the conductance levels

Single channel measurements were performed in 10 mM Heps pH 7.2 supplemented with 125 mM, 250 mM, or 1000 mM KCl. For each KCL concentration four measurements were performed. After incorporation of a single TOM core complex channel voltage ramps from -120 mV to +120 mV were applied to the membrane. I-V surface maps were generated in SANALYSIS and slope conductance values of the five most frequent conductance states were determined. These were plotted against the concentration of KCl (A) and activity of KCL (B). These data points were fitted with Michaelis-Menten functions (equation 5.6). Table 5.5 lists the parameters resulting in the best fit.

calculating the slope conductance.

Conductance was plotted against salt concentration as well as the activity of KCl (Fig.5.28). The resulting curves could be described with Michaelis-Menten functions (Hille, 1992):

$$\gamma = \frac{\gamma_{max} * a}{K_m + a} \quad (5.6)$$

where γ is the slope conductance, γ_{max} is the saturated conductance, a is the KCl activity, and K_m the Michaelis- Menten constant describing the salt activity value at which 50 % of γ_{max} is reached. As only a limited range of KCl concentrations was examined, the error estimates of the fit were extremely high. Further measurements at higher salt concentrations (closer to the expected K_m and γ_{max}) would have to be conducted for a more quantitative description of these channel parameters. However, the limiting factor of such experiments is the solubility constant for KCl (about 4.6 M; Lide, 2003).

In summary, analysis of the channel properties of TOM core complex revealed that the TOM core complex occupied at least six distinct conductance levels. I demonstrated that the occupancy probability of these conductance levels was voltage dependent. The analysis of the I-V characteristics of the individual con-

Table 5.3: Dependency of salt concentration

	S5	S4	S3	S2	S1
γ , 1000 mM (nS)	2.16 \pm 0.34	1.09 \pm 0.15	0.67 \pm 0.09	0.36 \pm 0.06	0.16 \pm 0.03
γ , 250 mM (nS)	0.65 \pm 0.05	0.32 \pm 0.01	0.22 \pm 0.02	0.11 \pm 0.02	0.05 \pm 0.01
γ , 125 mM (nS)	0.41 \pm 0.09	0.21 \pm 0.02	0.12 \pm 0.01	0.04 \pm 0.01	n.d.
γ_{max}	13 \pm 19	7 \pm 23	3 \pm 10	3 \pm 30	n.d.
K_m (mol/l)	3.2 \pm 5	3.6 \pm 12	2.2 \pm 8	4.2 \pm 6	n.d.

ductance levels indicated that the conductance levels could be divided into two classes. In the first class (S5 and S4 states) the channel followed Ohm's law and displayed a linear I-V characteristic. In the second class (S1 - S3) a non-linear I-V characteristic was observed. Measurements conducted at low KCl concentration demonstrated that all the described channel properties could still be observed. Only the conductivity was influenced by the salt concentration according to a Michaelis-Menten function.

5.4.3 Electrophysiological characterization of the kinetic properties of TOM core complex channels

The analysis of the channel properties of TOM core complex had revealed six distinct conductance levels. The occupancy of these conductance levels as well as the transitions frequencies between these states were voltage dependent. In the following section the kinetics of these transitions were further analyzed. To begin, variance-mean plots were created from single channel stationary measurements to visualize the existing transitions at various holding potentials. Thereafter, more detailed analysis of the transition frequencies were conducted at a holding potential of -60 mV and +60 mV, respectively.

Transitions between conductance states of TOM core complex visualized with variance-mean plots

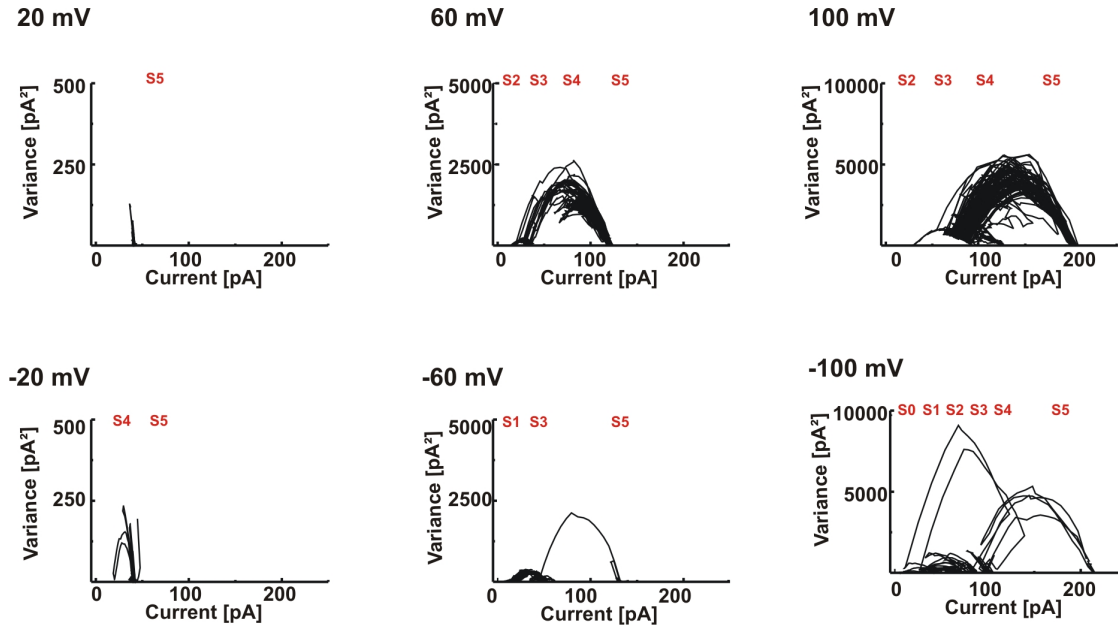


Figure 5.29: Variance-mean plots generated from single channel measurements of TOM core complex channels

Variance-mean plots according to Patlak (1988) were created from experimental data shown in Fig.5.22 revealing transitions between open and sub-conductance states for higher voltages. Mean current and variance were determined within a sliding window of 15 data points and plotted against each other.

Information on the transitions between various conductance levels was obtained by analyzing variance-mean plots. Plotting variance versus mean current calculated within a sliding window of 15 data points resulted in an inverted parabola for each transition between two states (Patlak, 1988, see section 6.3). Fig.5.29 shows the variance-mean plots for the current traces shown in Fig.5.22. From these and many other variance-mean plots ($n > 20$) I concluded that transitions between all six conductance levels are possible. Especially at higher voltage ($|V| > 40$ mV) transitions were detected between S5, S3, and S2. Transitions between the states S4, S1, and S0 occurred less frequent than transitions between the other states.

The variance-mean analysis of the single channel measurements did not reveal double arches – two parabolic connections between three equidistant nodes,

which would be expected for two independent channels.

Determination of transition frequencies at a holding potential of -60 mV and +60 mV

After determination of the observed conductance states (S0-S5), a description of the different transitions observed between these conductance states was possible. For a more quantitative analysis of the transition frequencies, multiple data sets from single TOM core complex channels were collected at -60 mV and +60 mV, respectively. The relative transition frequencies between the present sub-states were determined from event lists with SANALYSIS (see section 4.7; Colquhoun and Sigworth, 1983; Sachs, 1983). These are summarized in Tables 5.4.3 and 5.4.3. At a holding potential of -60 mV transitions were mainly observed between the S5 and the S3 state (70 %). Fewer transitions (26 %) were observed between the S3 and S2 state, and very little transitions (6 %) took place between the S5 and S2 state. At a holding potential of +60 mV, however, the transitions between the S5 and S3 state were reduced (6 %). Instead an increase in the transition frequency between the S3 and the S2 state was observed (70 %). Additionally, transitions between the S4 and S3 state could be observed (14 %).

Table 5.4: Relative transition frequencies determined at -60 mV

	S1	S2	S3	S4	S5
S1	X	0 %	0 %	0 %	0 %
S2	0 %	X	13 %	0 %	3 %
S3	0 %	13 %	X	0 %	35 %
S4	0 %	0 %	0 %	X	0 %
S5	0 %	3 %	35 %	0 %	X

Table 5.5: Relative transition frequencies determined at +60 mV

	S1	S2	S3	S4	S5
S1	X	0 %	0 %	0 %	0 %
S2	0 %	X	35 %	0 %	0 %
S3	0 %	35 %	X	7 %	3 %
S4	0 %	0 %	7 %	X	3 %
S5	0 %	0 %	3 %	3 %	X

Both, the variance-mean plots and the quantification of the transition frequencies at -60 mV and +60 mV, demonstrated the asymmetric voltage dependent gating behavior of the TOM core complex.

5.4.4 Electrophysiological characterization of the channel properties of Tom40

Previous studies have shown that Tom40 is the pore forming subunit of the TOM machinery. With the next experiments the channel properties of Tom40 were examined. The analysis included the determination of the conductance levels occupied by Tom40 channels. Furthermore, the ion selectivity of the channel was determined, and finally, the transition frequencies between the different conductance levels were examined.

Conductance levels occupied by Tom40 channels

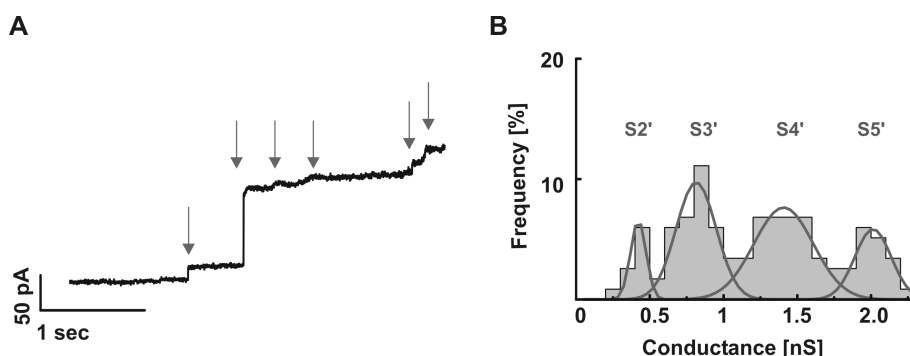


Figure 5.30: Electrophysiological measurements of Tom40 channels

Purified Tom40 was analyzed with planar lipid bilayer setup in symmetrical KCl solution (1M) and a holding potential of 70 mV.

A) Current trace displaying step-like increases (marked with arrows) resulting from incorporation of Tom40 channels.

B) Histogram showing the frequency of a given conductance increment $\Delta\gamma$. This was fitted with four Gaussian peaks (S2'-S5') leading to the conductance values listed in Table 5.6. 117 insertion events were examined. The bin size was 0.1 nS.

The first step in the characterization of Tom40 channels was the determination of the conductance levels occupied by Tom40 channels. For this, isolated Tom40 was added to a bilayer setup and the current trace was recorded at a constant

holding voltage. These measurements revealed step-like increases of the current indicating the incorporation of Tom40 channels into the membrane (Fig.5.30A). Chord conductance (γ) was calculated for each event as:

$$\Delta\gamma = \frac{\Delta i}{V} \quad (5.7)$$

where Δi is the increase in current during an insertion event, V corresponds to the applied voltage.

Tom40 channels displayed a wide range of conductance values. For statistical analysis, a histogram of the determined conductance values was generated and was fitted with four individual Gaussian functions (Fig.5.30B). The conductance levels of the Gaussian peaks are summarized in Table 5.6. Comparing these conductance levels with the conductance states from TOM core complex indicated that Tom40 channels occupied four conductance states, which were similar to the S2-S5 states described for the TOM core complex.

Table 5.6: Chord conductance levels for Tom40 compared with those presented for TOM core complex

TOM core complex	S5	S4	S3	S2	S1
G (nS)	2.16 ± 0.34	1.09 ± 0.15	0.67 ± 0.09	0.36 ± 0.06	0.16 ± 0.03
Tom40	S5'	S4'	S3'	S2'	-
G (nS)	2.01 ± 0.02	1.41 ± 0.02	0.81 ± 0.03	0.42 ± 0.03	-

Ion selectivity of Tom40 channels

To further compare the Tom40 channels with TOM core complex the ion selectivity for these channels was measured. Generating I-V characteristics from single channels or multiple channels in asymmetric salt concentrations allowed the determination of the ion selectivity of the channel from the shift in reversal potential.

For the determination of the ion selectivity of Tom40 channels, voltage ramps between -70 mV and +70 mV were applied to black lipid membranes with several channels incorporated and symmetrical saline solution (250 mM salt). Thereafter, the salt concentration was increased on the trans side of the chamber and further voltage ramps were applied to the membrane. This allowed the determination of the new reversal potential. The reversal potential was plotted against

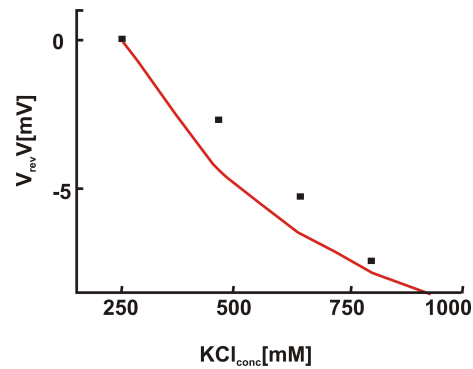


Figure 5.31: Cation selectivity of Tom40 channels

The reversal potential of Tom40 channels at various asymmetric salt concentrations was determined and plotted against KCl concentration of the trans side. The resulting curve was fitted with a derivation of the Goldman-Huxley-Katz voltage equation (see section 4.7.5).

the KCl concentration of the trans side (Fig.5.31). This could be fitted with a modified Goldman-Huxley-Katz voltage equation (see section 4.7.5). The best fit of the Goldman-Huxley-Katz voltage equation estimated a K:Cl permeability ratio of 1:1.8. This was in agreement with the ion selectivity of TOM core complex channels (1:3; Künkele et al., 1998a).

To further elucidate the channel properties of Tom40, I-V characteristics of single Tom40 channels were examined.

Transitions between conductance levels occupied by Tom40 channels

Single channel measurements of TOM core complex channels had revealed frequent transitions between the various conductance levels. To examine, if Tom40 showed a similar behavior, voltage ramps (-70 mV to +70 mV in 10 sec) were applied to single Tom40 channels incorporated into a black lipid membrane. These measurements showed virtually no transitions between conductance levels as demonstrated in the I-V surface maps shown in Fig.5.32. Channels with various slope conductance levels were observed but no switching between different conductance states.

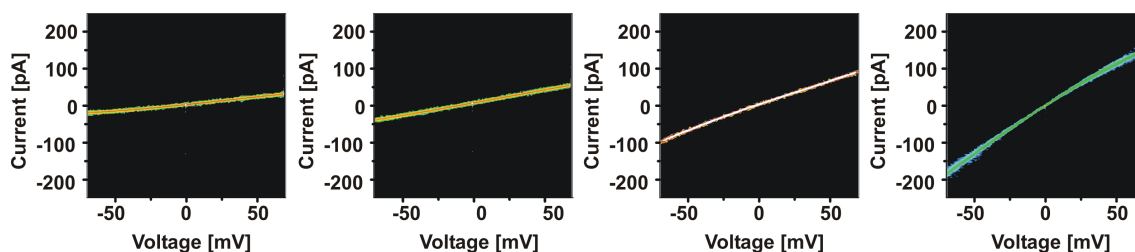


Figure 5.32: I-V surface maps of single channel measurements of purified Tom40

Purified Tom40 was analyzed with black lipid membranes in symmetrical KCl solution (1M). Four representative I-V surface maps are displayed. These were calculated from at least 10 voltage ramps applied to independent membranes after insertion of a single Tom40 channel. No transitions to different conductance levels were observed.

For a better comparison of the Tom40 channels with those from TOM core complex, the measurements from Fig.5.32 were overlaid in an I-V scatter plot (Fig.5.33). This was put in direct comparison with the I-V scatter plot of TOM core complex. The overlay showed similar I-V characteristics to TOM core complex channels.

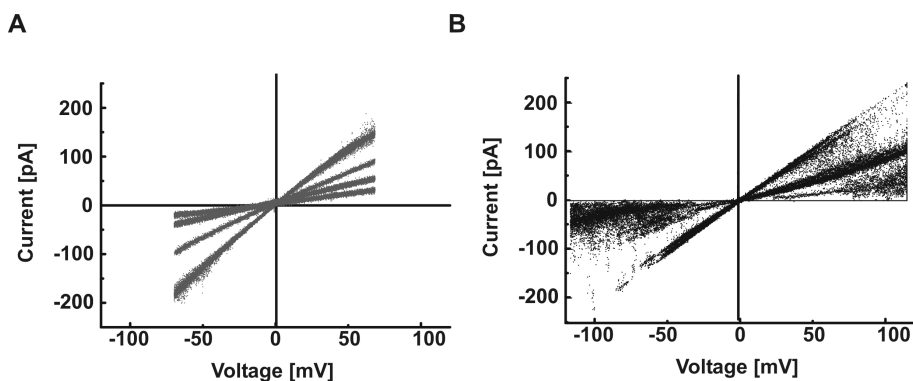


Figure 5.33: Overlay of single Tom40 channels compared with TOM core complex

A) The four independent single channel measurements of purified Tom40 channels from Fig.5.32 are presented as a scatter blot.

B) I-V scatter blot of a single channel measurement of purified TOM core complex. For this, ten voltage ramps from -120 mV to +120 mV were applied to a reconstituted channel. Both result in I-V characteristics with similar slope conductance values.

In summary, the measured Tom40 channels were similar to TOM core complex channels. The conductance levels and the cation selectivity were similar. However, the analysis of the transition frequencies between the different conductance levels indicated that Tom40 channels, in contrast to TOM core complex channels, did not change between conductance states.

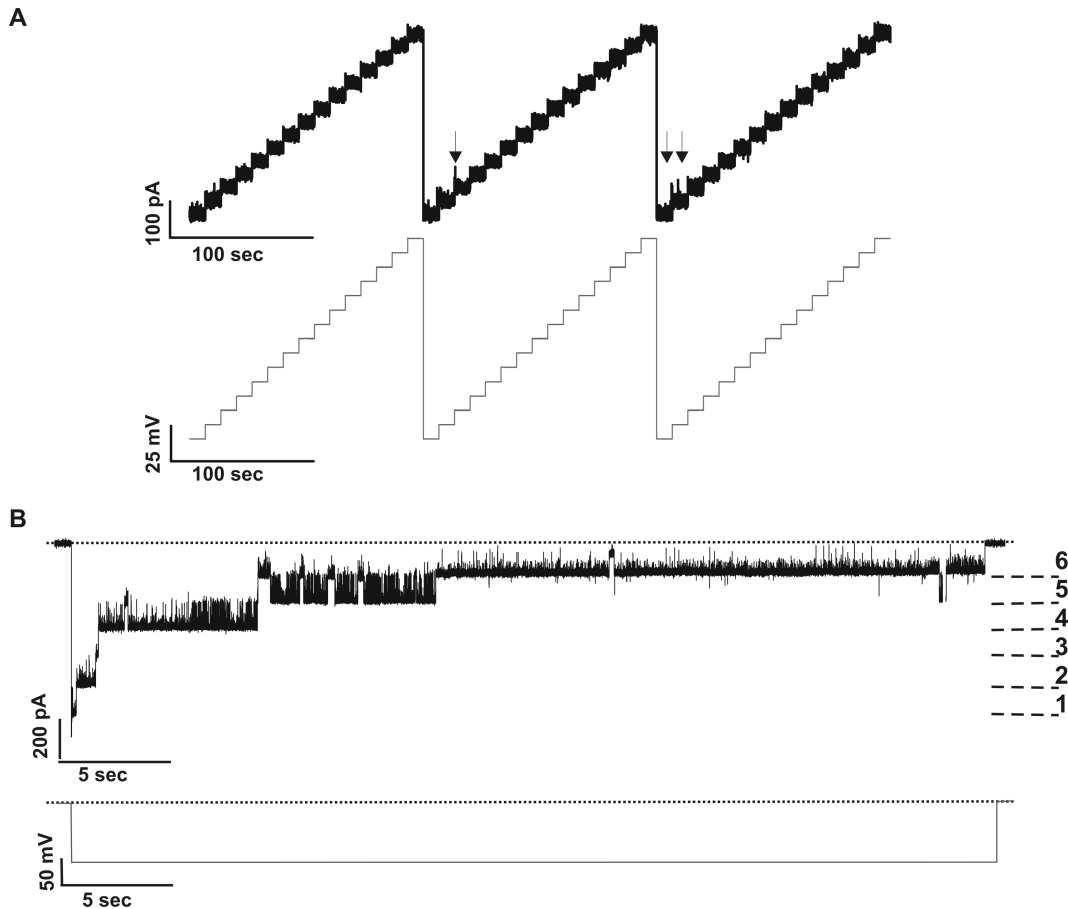


Figure 5.34: Influence of higher voltage applied to several Tom40 channels

After the reconstitution of several Tom40 channels into the artificial membrane current traces were recorded in symmetrical salt solution (1M KCl)

A) Application of step-like increase in voltage ranging from -70 mV to +70 mV in 10 mV increments and 10 sec duration. Very few (see arrows) transitions were observed.

B) Application of a pulse from 0 mV to -120 mV to the same membrane. This resulted in a subsequent closing of the single channels.

5.4.5 The influence of higher voltages on the channel properties of Tom40

When applying voltage ramps between -70 mV and +70 mV, Tom40 did not switch between conductance levels. Surprisingly this behavior changed when higher voltages (>100 mV) were applied.

Influence of higher voltages on a membrane with many channels incorporated

Current measurements were recorded by applying step-like increase of voltage to a membrane with several ($n > 4$) Tom40 channels incorporated. As described above, no transitions were observed when voltage sweeps between -70 mV and +70 mV were applied (Fig.5.34A). However, after applying a voltage pulse from 0 mV to -120 mV, a closing of the channels occurred.

Effect of higher voltages on a single channel measurement

To further investigate the effect of higher voltages to incorporated Tom40 channels, single channel measurements were conducted by applying voltage ramps. After insertion of a single Tom40 channel, voltage ramps from -70 mV to +70 mV were applied to the membrane (Fig.5.35; phase I). During several measurements few transitions were observed. Thereafter, the voltage range of the ramps was raised to -150 mV to +150 mV (phase II) leading to a behavior very similar to TOM core complex. After some time an increase in transition frequency was observed. This effect was reversible. After reducing the voltage range from -70 mV to +70 mV again (phase III), the channel gating decreased, and after some time the recorded current traces resembled the current traces in phase I.

Analysis of the transitions after the application of higher voltages

The transitions induced by the application of higher voltages to reconstituted Tom40 channels were analyzed with variance-mean plots. For this, purified Tom40 was incorporated into the bilayer. Fig.5.36A shows the resulting current trace at a constant voltage of -80 mV. The base line is indicated with dotted lines. Fig.5.36B displays the corresponding variance-mean plot. It indicated that at least two Tom40 channels were incorporated into the membrane, as individual gating of the single channels was observed.

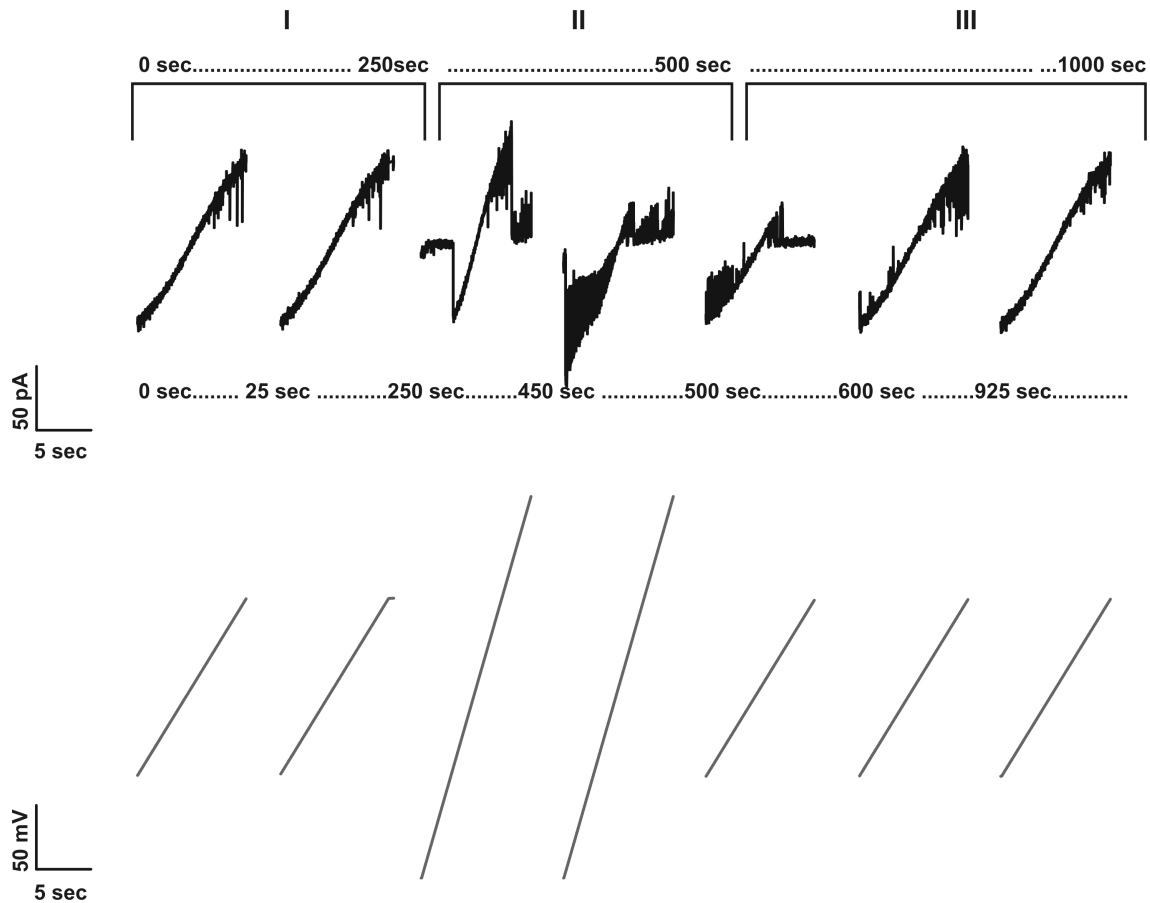


Figure 5.35: Influence of higher voltages on Tom40 channels

Single channel measurements of purified Tom40 were recorded in symmetrical KCl solution (1 M).

Phase I) voltage ramps from -70 mV to +70 mV were applied to a single Tom40 channel. Very few transitions between states were visible.

Phase II) voltage ramps from -150 mV to +150 mV were applied. An increase in transition frequency was visible.

Phase III) voltage ramps from -70 mV to +70 mV were applied. After some time, the transition frequency was reversibly reduced again.

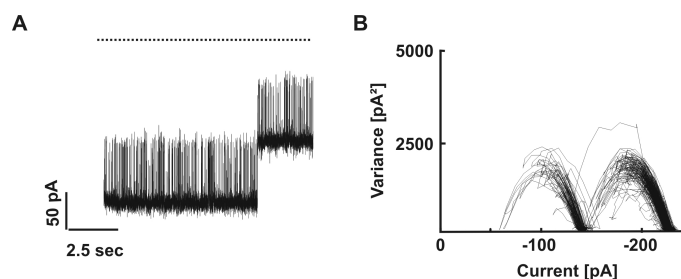


Figure 5.36: Transitions between two independent Tom40 channels

Purified Tom40 was incorporated into a planar lipid bilayer in symmetrical salt solution
 A) Current trace recorded at a constant holding voltage of -80 mV.

B) The corresponding variance-mean plot according to Patlak (1993) was generated. For this, the mean current and variance were determined within a sliding window of 10 data points and were plotted against each other. The observed arches indicated gating of two independent channels.

Comparison of the open probability plot of Tom40 channels with that of TOM core complex

Further experiments were conducted by generating stationary single channel measurements of Tom40. For this, either voltage sweeps from -70 mV to +70 mV or from -150 mV to +150 mV were applied. Current level all-point histograms were generated from this data. Fitting the histograms with Gaussian peaks allowed the determination of the voltage dependent open probability of Tom40 (Fig.5.37A). The open probability calculated from the first set of experiments (application of -70 mV to +70 mV voltage ramps; green squares) was significantly increased compared to the open probability of the second data set (black squares). The latter was comparable to the open probability determined for TOM core complex (Fig.5.37B; red circles). Furthermore, V_l for Tom40 with low voltage applied was estimated to be -90 mV. Assuming the same voltage sensitivity for TOM core complex, a Boltzmann fit curve (see equation 6.21) was calculated and is indicated in the figure as well (Fig.5.37A; green line).

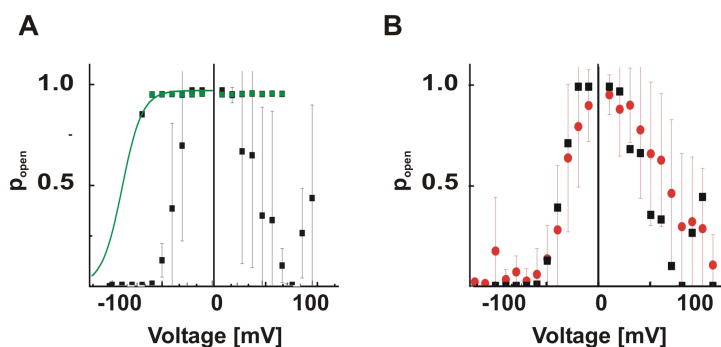


Figure 5.37: Open probability of Tom40 channels

Stationary measurements of purified Tom40 protein were conducted in symmetrical KCl solution (1 M). After insertion of a single Tom40 channel in the S5' state voltage ramps ranging from -70 mV to +70 mV or from -150 mV to +150 mV were applied. The generation of current level all-point histograms and fitting thereof with Gaussian functions allowed the determination of the open probability of the Tom40 channels.

A) Comparison of the open probability of Tom40 upon the application of lower voltages (green squares) and higher voltages (black squares). Tom40 upon application of lower voltages revealed a significantly increased open probability. This was fitted with a Boltzmann fit function for negative voltages (green line).

B) Comparison of the open probability of Tom40 after higher voltages were applied (black squares) and TOM core complex (circles). These were in good agreement with each other.

In summary, Tom40 channels displayed an interesting behavior. Although, the conductance levels and ion selectivity were comparable to that of TOM core complex channels, the transition frequencies between these conductance levels were reduced. Transitions between the conductance states were only observed after the application of higher voltages. This effect was reversible when the applied voltage was reduced again. The open probability for Tom40, however, was significantly increased when lower voltages were applied. The open probability plot of Tom40 channels after the application of higher voltages, however, was similar to that of TOM core complex.

5.4.6 Electrophysiological characterization of the channel properties of TOM core complex lacking one of the small Tom proteins

To elucidate which of the missing subunits was responsible for the difference between Tom40 and intact TOM core complex, channels of knock-out mutants lacking one of the small Tom proteins (Δ Tom5, Δ Tom6, and Δ Tom7 mutants) were analyzed. Conductance states, I-V characteristic of the conductance states, and transition frequencies and the open probability of the channel were compared to TOM core complex from wild-type.

Single channel measurements of TOM core complex lacking one of the small Tom proteins (Tom5, Tom6, or Tom7)

Single channel measurements of isolated TOM core complex from Δ Tom5, Δ Tom6, and Δ Tom7 mutants were conducted in the bilayer system. Recorded current traces showed that TOM core complex lacking one of the small Tom proteins occupied all six described conductance levels at least for a short period of time (Fig.5.38A; conductance levels indicated with red lines). The corresponding I-V surface maps were similar to the I-V surface map generated from wild-type TOM core complex (Fig.5.38B). The main conductance level, S5, revealed a linear I-V characteristic. At voltages $|V| > 40$ mV states S1-S4 were more frequently occupied. These states revealed a non-linear I-V characteristic. This was in agreement with the channel properties of wild-type TOM core complex.

Open probability of channels formed by TOM core complex lacking one of the small Tom proteins

Single channel measurements of TOM core complex lacking one of the small Tom proteins were conducted and the voltage dependent open probability of the channel was determined (Fig.5.39). This was compared with the Boltzmann function that was calculated as the open probability for wild-type channels (see section 5.4.2; indicated with a continuous line in Fig.5.39). No significant differences were observed between the open probability plots of the mutated TOM core complex and wild-type TOM core complex.

In summary, isolated TOM core complex from mutants lacking one of the small

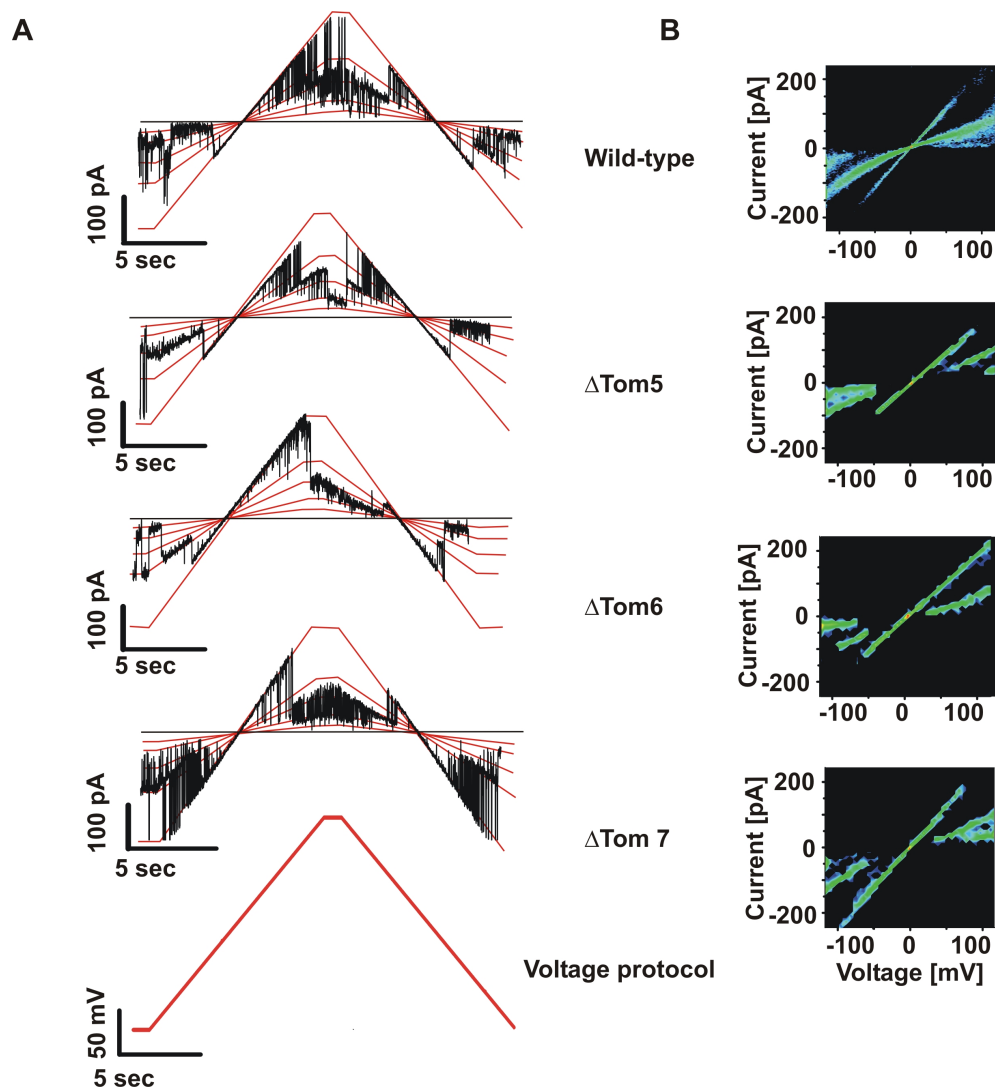


Figure 5.38: Single channel measurements of TOM core complex from knock-out mutants lacking one of the small Tom proteins

Purified TOM core complex from Δ Tom5, Δ Tom6, and Δ Tom7 mutants were incorporated into BLM in symmetrical conditions (1M KCl), and the results were compared with that of TOM core complex from wild-type.

A) Current traces resulting from the applied voltage ramp as shown in the lowest panel (-120 mV to +120 mV). The conductance levels S1-S5 are indicated with red lines. The base line is indicated with a black line. All conductance states were occupied for at least a short time for all four cases.

B) Corresponding I-V surface maps. 2-D histograms were calculated from 5 ramps for each mutant and are displayed as I-V surface maps. Increase in the probability that a data point is located within a given bin is presented by a color scheme (blue < green < yellow < red). Similar channel activity is observed for all four cases concerning the occupied conductance states, the linear I-V characteristic of main open state and the non-linear I-V characteristic of the other states.

Tom proteins revealed channels with similar properties as wild-type TOM core complex. All six conductance levels were occupied. The open probabilities of the channels and observed transitions between the various states were comparable with wild-type. This indicated that the individual small Tom proteins (Tom5, Tom6, and Tom7) were not responsible for the difference in transition frequencies of the channels formed by purified Tom40 and wild-type TOM core complex.

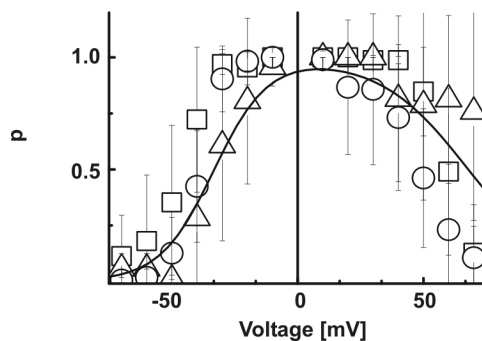


Figure 5.39: Open probability of knock-out mutants lacking one of the small Tom proteins

Open state occupancies of S5 state from all-point histograms of stationary records between -70 mV to +70 mV for TOM core complex purified from Δ Tom5 (\triangle), Δ Tom6 (\circ), and Δ Tom7 (\square) mutants were determined and compared with the Boltzmann fit function for wild-type TOM core complex. Except for the Δ 5 mutant these were virtually identical to TOM core complex.

6 Theory

The results showed that TOM core complex formed a pore that acted as a high-conductance channel allowing the passage of ions across lipid membranes. To be able to discuss the results in more detail, a brief theoretical overview of some of the important properties of ion channels is given in this chapter.

6.1 I-V relationships in ion channels

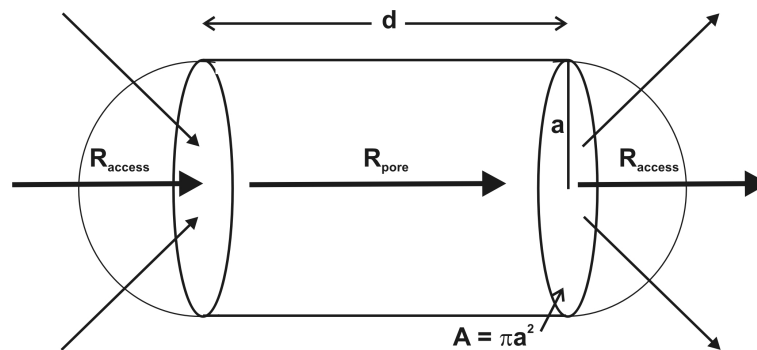


Figure 6.1: Schematic drawing of a channel represented by a cylindrical pore

Ion channels with a large radius a can be described as a cylinder of length d . The resistance that acts upon ions passing such a pore is the sum of the pore resistance and the access resistance. The latter describes the entrance of the ions into the channel and the exit out of the channel into bulk.

A common procedure to characterize ion conducting channels is to describe their current-voltage relationship. In the past, various models have been developed to explain the different I-V relationships observed in various ion channels.

The simplest model to describe ions passing a membrane is the idea of an Ohmic channel (Eckert, 1993; Hille, 1992). This can be described by a cylinder

of length d and cross section area A with radius a , which is filled with a saline solution of resistivity ρ (Fig.6.1). The single-channel conductance, γ , of such a cylindrical pore is given as:

$$\gamma = \frac{A}{\rho d} \quad (6.1)$$

and accordingly the pore resistance R_{pore} is:

$$R_{pore} = \frac{d}{\gamma} = \rho \frac{d}{A} = \rho \frac{d}{\pi a^2} \quad (6.2)$$

The measured resistance includes a second term, the access resistance. This considers the entry of the ions from bulk into the channel and their exit from the channel back into bulk (Fig.6.1). According to Hall (1975) this is:

$$R_{access} = \frac{\rho}{4a} \quad (6.3)$$

The total resistance of the channel $R_{channel}$ is therefore:

$$R_{channel} = R_{pore} + R_{access} = \left(d + \frac{a}{2}\right) \frac{\rho}{\pi a^2} \quad (6.4)$$

Thus, the length of the channel is "extended" by $\frac{a}{2}$.

Ions passing through such a channel are not influenced by any forces inside the channel except the force generated by the external electric field. Therefore, a linear relationship between voltage and current is described. This is, however, only true for low voltages. When higher voltages are applied ions accumulate at the exit of the pore. Thus, a concentration gradient is generated and the flux through the channel is, therefore, reduced. The resulting I-V characteristic of such a channel would be S-shaped as a reduction of the current is observed with higher voltages.

The above model is valid for channels with large pores. If the channel is narrow further forces such as attraction forces from charged amino acids lining the pore wall as well as image forces become more relevant (Hall et al., 1973; Hille, 1992; Jackson, 2006). An ion passing the channel senses these forces and is forced to surmount one or more energy barriers.

To be able to calculate the exact forces that act on an ion passing through a

narrow pore, one needs to know the atomic structure of the protein that forms the channel. For the cation-selective channel gramicidin A, Levitt was able to calculate the energy profile of the passing ions by adding image force and short-range attractions (Levitt 1978b). The sum revealed two potential energy wells, which function as ion binding sites. If the atomic structure is, however, not available course grain models have to be applied to obtain a first approximation of ion flux through the channel.

The equation for electrodiffusion (Nernst Planck equation) describes the flux of ions J in an external field. It includes a term considering the diffusion of the ions depending on the concentration c and a term considering the dependency of the voltage potential ψ on the ion flux J :

$$J = -D \left(\frac{\delta c}{\delta x} + \frac{ze}{k_B T} c \frac{\delta \psi}{\delta x} \right) \quad (6.5)$$

where D is the diffusion constant, z is the valence of the permeant species, k_B is the Boltzmann constant, e is the elementary charge, T is the temperature, and x is the position of the ion.

To include an energy barrier, this equation can be complemented with a third term, an invariant barrier function $\omega(x)$ (Hall et al., 1973; Neumcke and Lauser, 1969). Thus, current I is described as:

$$I = AzqD \left(\frac{\delta c}{\delta x} + c \frac{\delta \psi}{\delta x} + c \frac{\delta \omega}{\delta x} \right) \quad (6.6)$$

For this study the barrier was defined by a symmetrical triangular function $\omega(x)$ with height ϕ and width d as shown in Fig.6.2A and is described with:

$$\omega(x) = \phi \left(1 - \frac{2|x|}{d} \right), -\frac{d}{2} \leq x \leq \frac{d}{2} \quad (6.7)$$

Solving equation 6.6 with consideration of equation 6.7 leads to the following function for current I :

$$I = \frac{2Azq_e D}{d} * \frac{e^{-\phi} \left(c_1 e^{\frac{zqeV}{2k_B T}} - c_2 e^{-\frac{zqeV}{2k_B T}} \right)}{e^{\frac{\left(\frac{zqeV}{2k_B T} - \phi\right)}{2k_B T}} - 1 + \frac{1 - e^{\left(\frac{zqeV}{2k_B T} + \phi\right)}}{e^{\frac{zqeV}{2k_B T}} - \phi}} \quad (6.8)$$

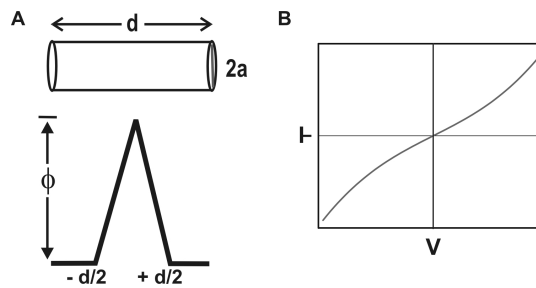


Figure 6.2: Schematic drawing of an energy barrier and the resulting I-V curve

A) For ion channels with a narrow pore the energy barrier that the ions have to surmount can be approximated by a symmetrical triangular function with height ϕ and width d .

B) Schematic drawing of I-V curve resulting from such a barrier. It has the shape of an “inverted S”.

where V is the voltage across the membrane, c_1 the concentration on the left, c_2 the concentration on the right side, and $k_B T$ was equal to 4.116×10^{-21} J.

In Fig.6.2B a schematic drawing is given of the I-V characteristic resulting from this function. The I-V curve has the shape of an “inverted S”.

Fitting this model to the measured data with the barrier height ϕ and the cross sectional area A as free parameters leads to information about the magnitude of the barrier within the ion channel but not of the origin of the barrier. Attraction forces from the charged amino acids lining the pore wall and image forces are possible explanations for the energy barrier. To calculate the influence of the former, the above model can be extended by the Poisson function. The PNP (Poisson Nernst Planck) model considers the continuous charge density of ions passing a channel with fixed charges (Chen and Eisenberg, 1993). However, in this case anions and cations show a different reaction. The result would be an inverted S-shaped curve for each ion flux. The total ion flux is an addition of these two inverted S-shaped curves, which results in an S-shaped curve.

6.2 Voltage dependency

In the 1950s Hodgkin and Huxley (1952) already described voltage dependent gating of conductances in the axonal membrane of the squid. In the meantime such gating processes have been described for many ion channels (Gordon and

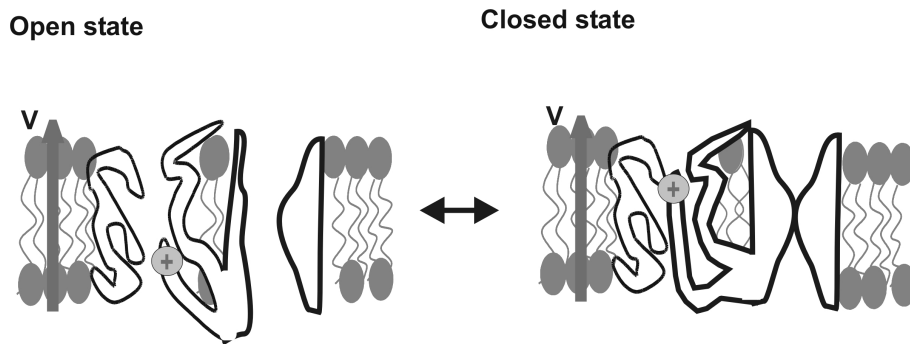


Figure 6.3: Schematic drawing of an ion channel with a sensor located in a membrane

Many ion channels display characteristic voltage dependent gating transitions between open and closed states. For this, a sensor with the charge q is located in the membrane and senses a change in the membrane potential V . Here, the positively charged amino acid acts as a sensor. With a negative membrane potential the sensor is moved within the membrane. This acts indirectly on a channel gate and the channel is closed.

Haydon, 1972; Latorre and Alvarez, 1981; Neher and Sakmann, 1976). Ion channels are defined as pores that can switch between an open and a closed state. In many cases the transition between these two states is voltage dependent. In the following, a function to describe the voltage dependent probability that a channel is in its open state is derived according to Jackson (2006).

For voltage dependent gating, ion channels possess a sensor that is located within the membrane where it senses changes in the electrical potential across the membrane. In Fig.6.3 the sensor is indicated as a positive charge. This reacts to a change in the membrane potential. Upon a negative membrane potential it is moved within the membrane. The free energy (ΔG_{vd}) that accompanies this transitional change is dependent on the membrane potential V :

$$\Delta G_{vd} = \sum_{i=1}^m q_i \delta_i V = \alpha V \quad (6.9)$$

Where, m is the total amount of particles that are located on the sensor with the charge q_i , and δ_i is the distance by which the charges are moved within the membrane. The parameter α is the voltage sensitivity.

The total free energy of the translocation of the membrane includes this voltage dependent term (G_{vd}) and an additional voltage independent term (ΔG_{vi}):

$$\Delta G^0 = \Delta G_{vi} + \alpha V \quad (6.10)$$

The free energy change (ΔG) for the conversion between the two states is determined as the difference of the molar free energy of the closed state G_c and that of the open state G_o . At equilibrium this equals 0:

$$\Delta G = G_c - G_o \quad (6.11)$$

with

$$G_o = G_o^0 + RT \ln [o] \quad (6.12)$$

and

$$G_c = G_c^0 + RT \ln [c] \quad (6.13)$$

where R is the gas constant, T the temperature, G_o^0 and G_c^0 are the molar free energies of the standard state and $[o]$ and $[c]$ are the concentrations of the open and closed state, respectively. Substituting equation 6.13 and 6.12 in equation 6.11, leads to:

$$\Delta G = G_c^0 - G_o^0 + RT \ln \frac{[c]}{[o]} \quad (6.14)$$

and at equilibrium

$$G_c^0 - G_o^0 + RT \ln \frac{[c]}{[o]} = 0 \quad (6.15)$$

or

$$\Delta G^0 = -RT \ln \frac{[c]_{eq}}{[o]_{eq}} \quad (6.16)$$

where ΔG^0 is $G_c^0 - G_o^0$. The exponential of the equation gives:

$$\frac{[c]_{eq}}{[o]_{eq}} = e^{-\Delta G^0 / RT} \quad (6.17)$$

This is equivalent to a Boltzmann distribution. It gives the ratio of the relative probabilities of the closed and open state as an exponential function of the difference of the respective energies. Substituting equation 6.10 for ΔG^0 gives:

$$\frac{[c]_{eq}}{[o]_{eq}} = e^{-(\Delta G_{vi}^o + \alpha V)/RT} \quad (6.18)$$

The open probability of an ion channel is defined as:

$$p_o = \frac{[o]}{[o] + [c]}; \quad (6.19)$$

and yields:

$$p_o = \frac{1}{1 + e^{-A(V-V_0)}} \quad (6.20)$$

where $A = RT/\alpha$ and $-V_0/V_s = \Delta G^0/RT$

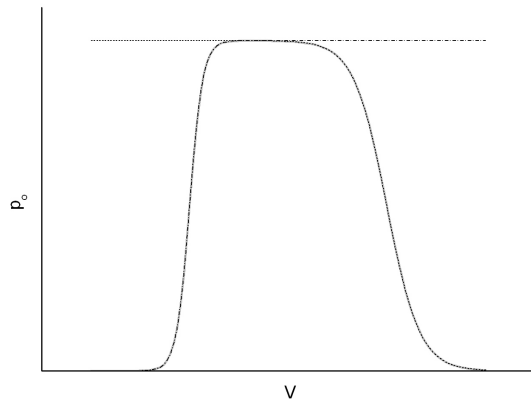


Figure 6.4: Schematic diagram of open probability curves

Two single curves were generated with equation 6.20 to simulate the open probability of a channel with a sensor sensitive for negative voltages and of a channel sensitive to positive voltages. The superposition of both these curves is in agreement with the generated curve with equation 6.21 to simulate a channel with two voltage sensors.

An ion channel with two different voltage sensors arranged in opposite direction or of opposite polarity may display a bell-shaped open probability curve. Such a curve is then given by the double open probability function (Fig.6.4):

$$p_o = \frac{1}{(1 + e^{-A(V-V_0)})(1 + e^{-A'(V-V'_0)})} \quad (6.21)$$

V_0 is the voltage at which the probability that the channel is open is 1:2. A describes the voltage sensibility and is indicated as the slope in the point of inflection.

6.3 Characteristics of a double-barreled pores

Channels that form double-barreled pores are characterized by frequent transitions between three different states. An open state, a closed state, and a half open state. Such a channel has been described for the CLC-O channel (Miller, 1982). Double-barreled pores possess two types of gates. On the one hand, independent transitions for each of the pores between a closed and an open conformation can be observed. On the other hand, a common gating mechanism exists that causes a simultaneous opening or closing of both pores.

These properties can be examined with different methods of data analysis of electrophysiological measurements. The existence of three conductance levels can be confirmed, with current all-point histograms for example.

In Fig.6.5A a current trace of a double-barreled pore is indicated. The channel can occupy the closed state (1), the open state (2), and the half-open state (3). These were visualized with current level all-point histograms. For double-barreled channels the spacing between the three resulting peaks would have to be equidistant.

For visualization of the two different types of transitions observed in double-barreled channels, variance-mean plots can be created according to Patlak (1988, 1993). For this, a “sliding window” consisting of N data points is passed over the recorded current trace of a stationary measurement, and from each set of N points the mean current $\langle I \rangle$ and the sample variance $\text{var}(I)$ are calculated and plotted versus each other. If the channel is closed, then $\langle I \rangle$ and $\text{var}(I)$ are both zero. If the channel is open, then $\langle I \rangle$ corresponds to the single channel current, and the signal variance $\text{var}(I)$ is zero. When the channel is in a sub-conductance level (Fig.6.5A, level 3), the mean current $\langle I \rangle$ is reduced, and the signal variance $\text{var}(I)$ is zero. During a transition between two states values between the two current levels are assigned to $\langle I \rangle$, and $\text{var}(I)$ is greater than zero. This transition is displayed as parabolic arch (inverted parabola) between nodes at the current levels since $\text{var}(I)$ is defined as:

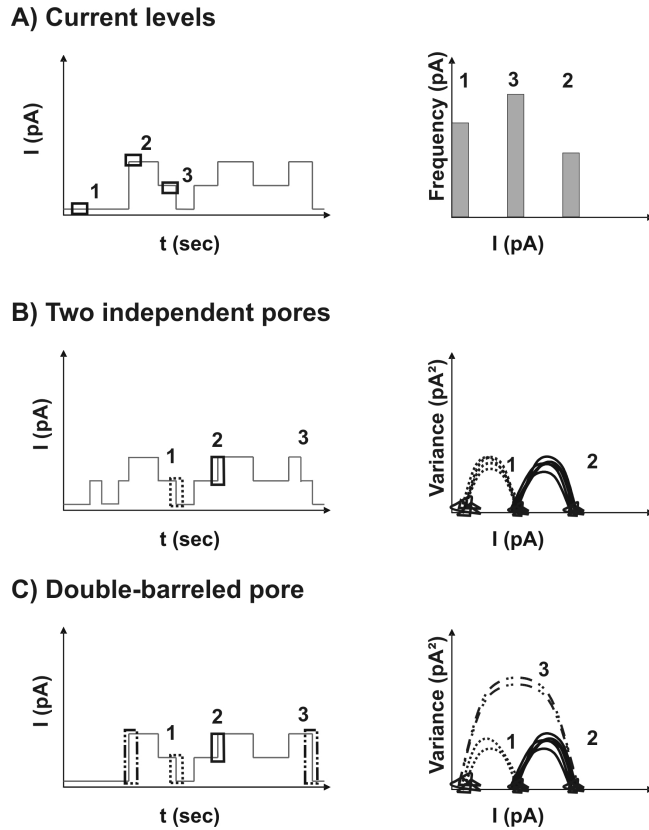


Figure 6.5: Schematic drawing of the analysis of the properties of double-barreled channels

A) Current trace displaying three current levels found in double-barreled pores; 1, closed state; 2, open state; 3, half-open state (left). These current levels are represented as peaks in the corresponding current level all-point histogram (right). The spacing between the three peaks is equidistant.

B) Current trace and variance-mean plot of two independent pores. No direct transitions between the open and closed state are observed. The gating of the individual pores is visualized as a double arch in the variance-mean plot.

C) Current trace and variance-mean plot of a double-barreled pore. Transitions 1 and 2, correspond to the closing/opening of the single subunits. Transition 3 emerges as a result of the common gate and connects two non-adjacent nodes. The transitions between the various current levels are visualized as arches in the variance-mean plot (right).

$$\text{var}(I) = \langle \langle I \rangle - I \rangle^2 \quad (6.22)$$

In Fig.6.5B and C schematic current traces and variance-mean plots are displayed from two independent pores and from a double-barreled pore. The three conductance levels (closed, half-open, open) are represented as three nodes in the variance-mean plot. The indicated transitions 1 and 2 correspond to closing and opening of the single subunits. Transition 3 indicates a transition within the channel resulting in a closure or opening of both pores simultaneously. For two independent pores this transition is rarely observed. In the double-barreled pore, however, a common gate exists, and this transition is visualized as a parabolic arch in the variance-mean plot connecting the two non-adjacent nodes that correspond to the closed and open state.

7 Discussion

Many pathways and components that participate in the process of protein translocation into mitochondria have been described. The participation of the TOM complex as the entry site for virtually all nuclear encoded proteins destined for the mitochondria has been well established (Neupert and Herrmann, 2007; Rehling et al., 2004; Stojanovski et al., 2006). However, the exact mechanism of this translocation is still poorly understood at the biophysical level. Little is known about the conformational changes required for the TOM machinery to enable the translocation of the various precursors across the membrane. With this study, I was able to shed some light onto this problem. By analyzing the single channel properties of TOM protein isolated from the filamentous fungus *Neurospora crassa*, I gained information on the conformational dynamics of the pore. Furthermore, I have elucidated the role of different subunits in this process.

The basis of the electrophysiological measurements, however, was the biochemical isolation and characterization of the proteins involved in the translocation process. In the following chapter I discuss the results from the biochemical, biophysical, and electrophysiological characterization of (i) TOM core complex, (ii) TOM core complex lacking one of the small Tom proteins, and (iii) Tom40. Thereafter, I propose two models that describe the observed dynamics of the TOM machinery and discuss the potential role of Tom22 as a modulator of the gating behavior of the TOM core complex.

7.1 TOM core complex

In the following, I discuss the isolation of TOM core complex consisting of the major pore-forming unit Tom40, the receptor protein Tom22, and the three small Tom proteins Tom5, Tom6, and Tom7.

7.1.1 Biochemical and biophysical characterization of TOM core complex

Since the first isolation protocol of native TOM core complex from the mitochondria of *N. crassa* was developed (Ahting et al., 1999), many adaptations have been made to the original protocol. For example, by increasing the pH from 7.2 to 8.5 during the initial solubilization, degradation of Tom22 was decreased (Schmitt, 2005).

For the experiments conducted in this study, it was very important to obtain high amounts of pure protein samples. For the structural studies such as 3-D and 2-D crystallization high amounts of protein are required. For the former, at least 10 mg protein is required with a protein concentration of about 10 mg/ml (Hunte et al., 2003, chapter 7). Trials with the latter method can be performed with less material (1-2 mg) at protein concentrations ranging from 0.5 - 2 mg/ml (Hunte et al., 2003; Kühlbrandt, 1992). For the other biophysical experiments performed in this study – FCS measurements and electrophysiological bilayer measurements – relative low amounts of protein are required. However, the purity of the samples is extremely important in these experiments. As fluctuations of the average fluorescent counts are measured and analyzed with FCS measurements contamination with other proteins leads to a decrease of the signal to noise ratio (Culbertson et al., 2000). In electrophysiological single channel measurements contaminants can also incorporate into the membrane. In bilayer measurements it is, therefore, very important to measure a large amount of single channels and to statistically exclude measurements of such contaminations. The purification of membrane proteins, however, in such quantities and of such quality is still a challenge (Lacapère et al., 2007). Using a detergent to isolate the protein from the membrane by shielding the hydrophobic patches, and keeping the protein in a soluble but functional form is still difficult.

Improvement of the isolation procedure for TOM core complex

An adaptation to the isolation protocol for TOM core complex was made in this study by exchanging the quantity of Ni-NTA material from 20 ml to 1 ml (formerly purchased from Qiagen, now from GE Healthcare). This did not only cut the cost of the protein isolation, but also the time required for the isolation.

As a further optional purification step, I have demonstrated that TOM core

complex can be eluted from blue native polyacrylamide gels without loss of function. For this, the TOM core complex containing band was excised from a native gel and incubated in buffer containing detergent. After two days the components of the TOM core complex could be detected on a silver stained SDS gel, and the functionality of the isolated complex was confirmed with electrophysiological measurements. The elution of TOM core complex from a blue native gel is of advantage to either increase the degree in purity or to test the influence of various detergents and reducing agents on the TOM core complex.

In the past, native Tom protein was isolated in large amounts from a genetically engineered mutant with a hexahistidinyll-tagged form of Tom22 (GR107; Ahting et al., 1999; Künkele et al., 1998a). During this study I have established an isolation protocol for native TOM core complex from wild-type *N. crassa* and mutants lacking such a hexahistidinyll-tag. Wild-type TOM protein isolated in this manner showed identical biochemical and electrophysiological characteristics as the protein from the GR107 mutant. The electrophysiological measurements indicated that the additional six histidines on Tom22 did not influence the channel behavior of TOM core complex. Due to the higher amounts of protein (approximately 4 times more) that can be obtained with the GR107 mutant, protein isolated from this mutant was used for further characterization of TOM core complex.

Reconstitution of TOM core complex into lipid membranes

Due to the detergent required during the isolation of membrane proteins as well as the limited hydrophilic surfaces within membrane proteins it is difficult to obtain three dimensional crystals thereof. This problem is reflected by the ratio of solved structures of membrane proteins to soluble proteins which is less than 1:100 (updated: 12/04/07; www.rcsb.org/pdb; cited:12/10/07). The 2-D crystallization is an alternative method for the characterization of membrane proteins. As the proteins are incorporated into artificial lipid membranes, they are in a more natural environment without the presence of detergent micelles as in the 3-D crystallization approach (Levy et al., 2001; Walz et al., 1994). Furthermore, the requirements of the purified samples are not as high as for 3-D crystallization (Hunte et al., 2003, chapter 15). A protein concentration of 0.5 - 2 mg/ml has been sufficient in the most cases for 2-D crystallization (Kühlbrandt, 1992). For 3-D crystallization, however, 10 mg of protein with a concentration of at least 10 mg /ml is required (Hunte et al., 2003, chapter 7). Furthermore, protein sam-

ples with contaminations have been shown to crystallize with the 2-D crystallization approach in the past. For example, bacteriorhodopsin even forms 2-D crystals in native membrane and, therefore, in the presence of other membrane proteins (Henderson and Unwin, 1975). Other proteins, such as the SecYEG complex from *E.coli*, have also shown to crystallize in an equilibrium of different oligomeric states (Collinson et al., 2001).

For 2-D crystallization trials of the TOM machinery, TOM core complex was reconstituted into lipid membranes. The detergent DDM was successfully removed with the application of bio-beads, and the isolated protein incorporated into the membrane. The best conditions were a low lipid to protein ratio (L:P (w/w) of 0.3). Using the unsaturated lipid DMPC was an important step for vesicle formation. Adding cardiolipin to the samples resulted in larger protein containing vesicles. It appears to have a stabilizing effect on the TOM core complex.

The obtained vesicles were 0.2 - 0.4 μm in size and the incorporated proteins were not ordered. Vesicles and membrane sheets of 5 - 10 μm in size and with ordered protein can be used for structure determination with electron diffraction (Walz and Grigorieff, 1998). Future optimized 2-D crystallization trials will show if TOM core complex can form large enough ordered patches to determine the structure by electron diffraction.

7.1.2 Electrophysiological properties of TOM core complex

The pore forming properties of the TOM machinery have been described previously (Ahting et al., 1999, 2001; Becker et al., 2005; Grigoriev et al., 2004; Henry et al., 1996; Hill et al., 1998; Künkele et al., 1998b; Meisinger et al., 2001; Muro et al., 2003). However no comprehensive examination of the exact number of sub-conductance levels, their occupancy probability, and the transitions between these states has been available to date. I have, therefore, elucidated the dynamics and gating properties of the TOM core complex in more detail. I have described the number of conductance states, the voltage dependent occupancy probability of the channel in these states, as well as the transitions between these states, and I offer a preliminary kinetic model describing these transitions. Additionally, I have reevaluated the hypothesis that TOM core complex forms a double-barreled channel similar to the CIC-O channels (Babini and Pusch, 2004; Miller, 1982).

Characterization of the channel properties of TOM core complex

The most abundant protein in the mitochondrial outer membrane that forms pores with similar magnitude of TOM core complex is VDAC (Freitag et al., 1982). I have, therefore, purified and measured VDAC to compare it with TOM core complex channels. The VDAC measurements revealed conductance levels of 4 nS and a sub-conductance state of 2 nS in 1M KCl. This is consistent with the literature (Benz, 1994; Engelhardt et al., 2007). The former is a factor two larger than the main conductance state of TOM core complex. Recently, a new complex has been identified in the outer membrane, the SAM complex, which is involved in the translocation of β -barreled proteins in the mitochondrial outer membrane (Paschen et al., 2003; Wiedemann et al., 2003). Isolated SAM spontaneously incorporated into lipid bilayers and formed channels with an average conductance of 3.7 nS in 1 M KCl. At voltages higher than 70 mV the channels partially closed (Paschen et al., 2003). As these properties are not identical with the properties presented in this study for TOM core complex, I conclude that neither VDAC nor SAM contributed to the measurements reported here.

The results presented here showed six electrically distinct conductance states (S0-S5) with voltage dependent occupancies between these states. In earlier studies the existence of additional conductance levels besides the main conductance state had been described (Henry et al., 1996; Hill et al., 1998; Künkele et al., 1998b; Meisinger et al., 2001). However, no further characterization of these sub-conductance states has been published so far.

For a better comparison of my data with published data concerning the conductance levels, I have measured the salt dependency of the TOM core complex. The dynamic properties of the channels formed by TOM core complex at lower salt concentration (125 mM KCl, 250 mM KCl) were comparable with the properties at 1000 mM KCl. Analyzing the influence of the salt concentration on the conductivity of the different states revealed a Michaelis-Menten relationship with apparent affinity constants (k_D) between 2 and 4 M.

Two types of I-V characteristics are found for the conductance levels of TOM core complex

Applying voltage ramps to single channel measurements enabled the generation of I-V surface maps (Eckert, 1993; Sansom and Mellor, 1990). These revealed an in-

interesting I-V behavior as two different types of characteristics could be observed. The S5 state revealed an ohmic characteristic as expected for a channel with a large pore (see section 6.1). The S3, S2, and S1 states, however, revealed a non-linear I-V characteristic. It had the shape of an “inverted S”. Since the occupancy probability of the S4 state is very low, S4 was not detected with this method. For a more quantitative description of the non-linear I-V characteristics, I generated I-V curves from longer stationary measurements. The S5 and S4 state revealed a linear I-V characteristic. This is consistent with a simple electrical pore model where the channel acts like a cylindrical pore (Hille, 1992). The I-V curves could be fitted with a Nernst-Planck barrier model (Cooper et al., 1985; Hall et al., 1973). For this, a symmetrical triangular barrier was assumed. A fixed width of 70 Å was considered, which corresponds to the length of the TOM core complex pore as determined with electron tomography (Ahting et al., 1999). The fit allowed an estimation of the barrier height and the effective radius of the channel. The barrier heights were approximately 3.6, 2.2, and 0.7 k_bT for the S1, S2, and S3 state, respectively. The magnitude of these barriers is in agreement with barriers determined for the nicotinic acetylcholine receptor and glycine receptor channels (Adcock et al., 1998). To my knowledge, however, no ion channel with such large pores ($r_{S1} = 5$ Å, $r_{S2} = 5$ Å, $r_{S3} = 6$ Å, $r_{S4} = 7$ Å, $r_{S5} = 9$ Å) has been described to contain an energy barrier that results in an inverted s-shaped I-V curve. The pore radius determined for the S5 ($r_{S5} = 9$ Å) state is in good agreement with the value estimated by electron microscopy ($r = 10$ Å; Ahting et al., 1999).

An explanation for the presence of these two different classes of pores found in one channel could be a switching from a fully open state (S5, S4) to a tight state (S1-S3), in which the ions sense a repelling electrostatic force. This force could originate from surface charges of the residues lining the pore wall and from image forces within the pore. Since the TOM channel allows the permeation of both cation and anions the latter is more likely. However, to fully understand the existence of these two types of pores, and to elucidate if only the fully open state accommodates the threading of a polypeptide across the membrane further studies are required. In section 7.4, two models are presented that address this question in more detail.

Kinetic analysis of the TOM core complex

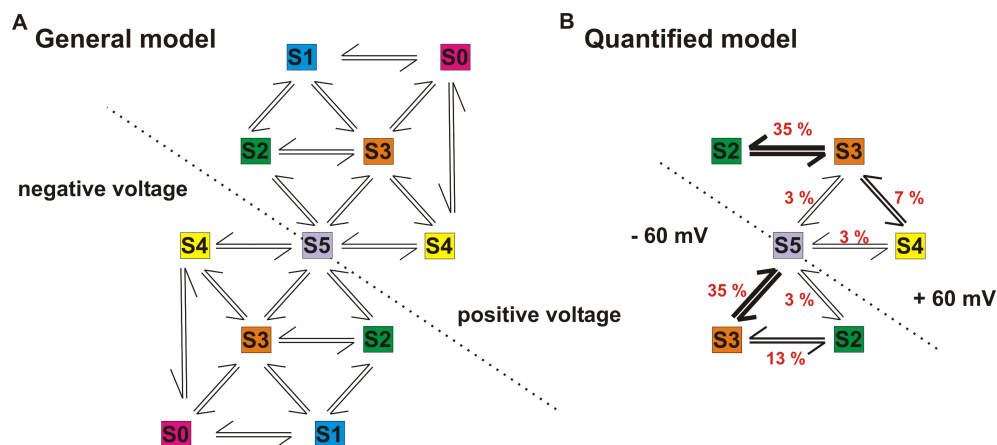


Figure 7.1: Proposed kinetic model for TOM core complex channels

A) General scheme: overview of all observed transitions between the sub-states. Transitions between the various conductance levels were made visible by generating variance-mean plots. The analysis of more than 20 independent measurements revealed that transitions between all conductance levels were possible.

B) Quantitative model: relative transition frequencies calculated at a holding potential of ± 60 mV. The recorded data from nine independent single channel measurements ($t=10$ sec) were analyzed and the relative transition frequencies between the different conductance states were determined and are displayed in the diagram. The dashed line indicates the different transition frequencies observed for the respective polarity of the membrane potential.

With the data collected in this study a preliminary kinetic model (Fig.7.1) was established. It considers the number of sub-conductance states, the transitions between these, and the asymmetric gating behavior displayed by TOM core complex.

The first model represents all transitions that were observed in variance-mean plots. However, as described earlier, the transition between the various conductance states are voltage dependent. It is interesting to note that all sub-states S1-S4 could be reached by switching the membrane potential to negative and positive voltages. For each voltage the model can be refined to the respective transition frequencies estimated for that voltage as demonstrated in the second model for ± 60 mV (Fig.7.1B). For this, event lists were generated from nine independent single channel measurements to determine the relative frequencies for the transitions between the individual conductance states (Colquhoun and Sigworth, 1983).

These frequencies are presented in the model. The asymmetry of the gating behavior is demonstrated by the reflection of the model about the dotted line.

Additionally, it must be remembered that the sub-states presented here are only conductance states. Within each conductance state a number of kinetic states may be hidden. This could be expected for TOM core complex, as I have frequently observed a “mode switching” (see Fig.5.22). “Mode switching” is the phenomenon that different gating modes exist with a channel, and low frequency switching between these modes occurs e.g. changes from a phase with slow gating to a phase with fast flickering as seen in Fig.5.22 (McManus and Magleby, 1988).

Is TOM core complex a double-barreled pore?

Previous studies have suggested that the TOM core complex acts as a double-barreled pore (Ahting et al., 1999, 2001; Becker et al., 2005; Henry et al., 1996; Hill et al., 1998; Künkele et al., 1998b; Meisinger et al., 2001; Muro et al., 2003). In electrophysiological measurements they have demonstrated that the TOM core complex occupies a main open state and a half open state. These measurements were in agreement with the structure of the TOM core complex (Ahting et al., 1999, 2001). It was, therefore, speculated that the TOM core complex forms a double-barreled pore similar to the CLC-O chloride channels (Babini and Pusch, 2004; Miller, 1982).

I have addressed this question with various electrophysiological approaches. These were (i) determination of the conductance levels, (ii) analysis of the transitions between the various conductance states, (iii) analysis of the occupancy probability of the various states.

(i) Conductance levels:

For a double-barreled channel one would expect the presence of two equidistant open states. Current level all-point histograms generated from single channel measurements of such channels can be normally fitted with three Gaussian functions. The current means determined with these functions correspond to the closed state, the half-open state, and the open state. The spacing between these is equidistant.

In my measurements (see Fig.5.22), however, no equal spacing of the determined conductance levels was observed, except when higher voltages were

applied. At these voltages the S1, S2, S3 state showed a non-linear I-V characteristic and, therefore, current traces did not represent the general channel properties.

(ii) Variance-mean analysis:

Double-barreled channels are characterized by two different types of transitions between the observed conductance levels. On the one hand, two independent gates influence the transition between the open and closed state of each pore. On the other hand, a common gate leads to the simultaneous closing or opening of *both* pores. The transitions between conductance levels resulting from the two independent gates are visible as a double-arch in variance-mean plots (see section 6.3). The transition resulting from the common gate is represented as a parabolic arch connecting the non-adjacent nodal points. This can be distinguished from two separate channels by the absence of the large arches as concurrent transitions in two independent channels are rare.

In the variance-mean plots generated from single TOM core complex channels, the latter transitions between non-adjacent nodal points were sometimes observed but no parabolic arches between equidistant nodal points were observed (see Fig.5.29).

(iii) Occupancy probability:

If a complex contains identical and independently gating channels the probability that k channels of a total of n are open should follow a binomial distribution (Ding and Sachs, 2002):

$$P_k(V) = \binom{n}{k} p(V)^k (1 - p(V))^{n-k} \quad (7.1)$$

$p(V)$ was determined by using the binomial formula and assuming that $P_5(V)$ corresponded to the open probability of the S5 state of TOM core complex. With this the $P_k(V)$ values of the other sub states were estimated. The calculated curves were compared with the occupancy probability plots determined from single channel measurements. For each conductance state, a significant difference between the two different curves was observed (see Fig.7.2).

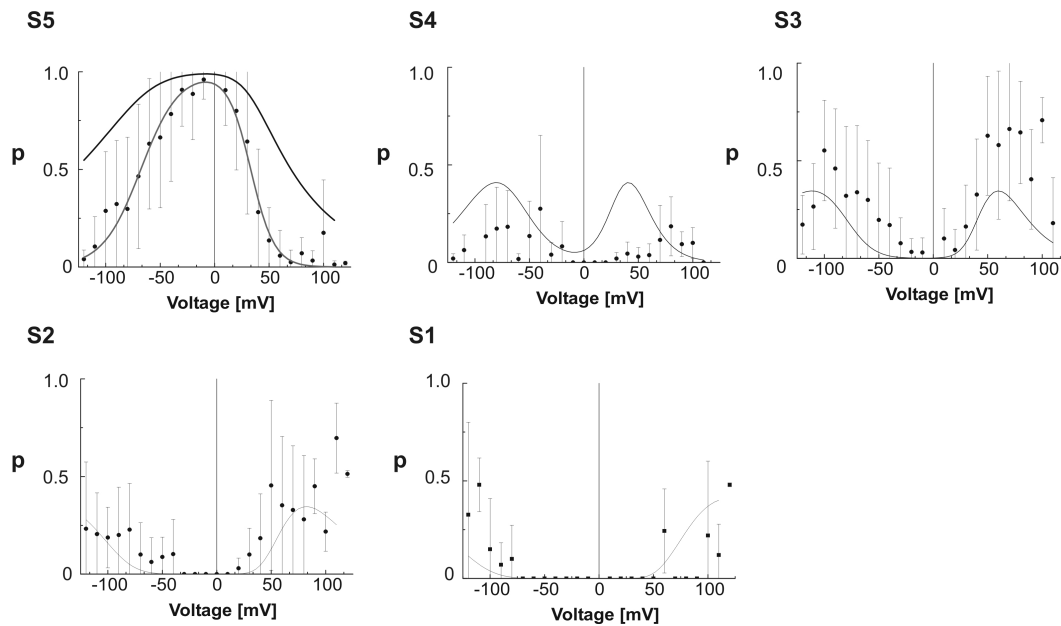


Figure 7.2: Binomial distribution

Binomial distribution of the probability that five independent pathways exist in the TOM core complex. These were overlaid in the voltage dependent occupancy probability plots generated from single channel stationary measurements. These were not in agreement.

Taken together, this electrophysiological study did not support a simple twin-pore model like that for CLC-O. Whereas some sections of the measurements, especially data recorded at high voltages ($|V| > 100$ mV), appeared to confirm the double-barreled pore hypothesis, the complete data set offered no evidence for this hypothesis. However, the data do not completely rule out a more complex arrangement. In section 7.4 I will further discuss the possibility of a multipore model consisting of non-identical pores.

7.2 TOM core complex lacking one of the small Tom proteins

To analyze the different influence of the various subunits on the dynamics of the TOM core complex from *N. crassa*, knock-out mutants lacking one of the small Tom proteins were analyzed. These mutants were: Δ Tom5, Δ Tom6, and Δ Tom7. Previously, only TOM core complex from the Δ Tom5 mutant has been purified

and analyzed in vitro (Schmitt et al., 2005).

7.2.1 Biochemical characterization of TOM core complex lacking one of the small Tom proteins

During cultivation of the Δ Tom5, Δ Tom6, and Δ Tom7 knock-out mutants no obvious differences in growth compared to wild-type and the GR107 mutant were observed. Simply the orange color of the culture was fainter than those of the wild-type and GR107 strain. Thus, no adaptations were required for the isolation of mitochondria, for the subsequent isolation of the OMVs, and for the isolation of TOM core complex.

The isolated complexes contained the other four components of the TOM core complex and formed channels in the bilayer setup with the same functional characteristics as described for the entire core complex. The molecular mass determined by size exclusion chromatography was identical to the molecular mass of wild-type complex (approximately 400 kD). However, samples separated with BNGE showed minor differences. The samples were less homogeneous in size: TOM core complex lacking Tom6 showed a higher population of monomeric Tom40 as well as some Tom40 protein in a 120 kD complex. Furthermore, fewer amounts of Tom5 and Tom7 were detected in purified TOM core complex from this mutant. In the sample lacking Tom7, Tom40 was found to form increased amounts of a highly oligomeric structure. This is in agreement with previous studies that assessed the functions of these small proteins (Hönlinger et al., 1996; Sherman et al., 2005). It was suggested that Tom6 and Tom7 play opposite roles concerning the channel stability. Tom6 seemed to stabilize the complex by binding Tom22 to Tom40, whereas Tom7 destabilized the complex (Hönlinger et al., 1996).

7.2.2 Electrophysiological properties of TOM core complex lacking one of the small Tom proteins

The previous studies in which the functions of TOM core complex lacking one of the small Tom proteins have been analyzed, focused on import of proteins, assembly of the TOM machinery, and stability of the complex (Dekker et al., 1998; Dietmeier et al., 1997; Hönlinger et al., 1996; Johnston et al., 2002; Schmitt et al.,

2005; Sherman et al., 2005). In this study, I have focused on the pore forming function of the TOM machinery. Chord conductance, subconductance levels, and voltage-dependent gating behavior of the channels formed by TOM core complex lacking one of the small TOM proteins were found to be comparable to the properties of wild-type channels. Therefore, Tom5, Tom6, and Tom7 alone may play only a minor role in the TOM channel activity. It will be interesting to see if the lack of these proteins has any influence on the binding of precursor protein. This question can now be addressed with electrophysiological methods.

7.3 Tom40

It has been shown, that the main component of the TOM core complex, Tom40, forms a conductive pore in the mitochondrial outer membrane (Ahting et al., 2001; Becker et al., 2005; Hill et al., 1998). To compare pores formed by Tom40 alone with channels formed by the complete TOM core complex, I developed a protocol for the isolation of native Tom40 from *N. crassa*.

7.3.1 Biochemical characterization of Tom40

In this study, I have established a one-step purification procedure for the purification of Tom40 protein from isolated mitochondria from the GR107 *N. crassa* mutant. 1 - 2 mg Tom40 can be purified from 2 g mitochondria with this protocol. The other components of the TOM core complex were not detectable with antibody decoration. Analysis of the isolated material by size exclusion chromatography indicated that Tom40 was in its monomeric state, as recombinant yeast Tom40 isolated from inclusion bodies (Hill et al., 1998). Why a previous study in which native Tom40 was isolated from *N. crassa* demonstrated that Tom40 formed a homooligomeric structure of about 380 kD, is not yet clear (Ahting et al., 2001). A possible explanation for this is that Tom40 purified from isolated TOM core complex (instead of directly from mitochondria) contained non-dissociated complex of 380 kD. In line with this, the analysis of the sample with electron microscope had indicated an inhomogeneous sample. Furthermore, they stated that their sample was not stable in octylglucoside. This was not the case with my preparation.

The large amounts of purified Tom40 protein allowed me to conduct 3-D crys-

tallization trials. First 3-D crystals of purified TOM core complex had been obtained in our laboratory by Dr. Simone Schmitt (Schmitt, 2005). The X-ray diffraction patterns of these crystals, however, only indicated a resolution up to 8 Å. This suggested that the protein crystal was disordered. Explanations for this could have been: inhomogeneity of the sample, presence of degradation products, and unstructured domains inside the complex, as well as a flexible stoichiometry of the subunits.

Monomeric Tom40 may, therefore, be a more promising candidate for 3-D crystallization, as opposed to the whole complex. From one of the crystals obtained in this study a diffraction pattern with a resolution of 0.8 Å was obtained. The diffraction pattern is currently being analyzed by our collaborators, Dr. Reinhard Albrecht and Dr. Kornelius Zeth (Max-Planck Institut für Entwicklungsbiologie, Tübingen, Germany). The high resolution of the diffraction pattern, however, questioned if the protein inside the crystal really was Tom40, or a degradation product thereof. The preparation of the sample used for that crystal had contained an unusually high amount of Tom6. Reproduction of the determined conditions and optimization thereof should bring clarity to this problem. Nevertheless, the new isolation protocol for Tom40 is a good basis for the crystallization of this protein, as the protein can now be isolated in large amounts and is free of other contaminating protein besides Tom6.

7.3.2 Electrophysiological properties of Tom40

For comparison with TOM core complex, a detailed electrophysiological characterization of the pore forming properties of purified Tom40 was conducted.

Four different conductance levels were observed with Tom40 channels, which were similar to four of the five conductance levels of TOM core complex (S2-S5). The K:Cl permeability ratio of the Tom40 channels was determined to be 1:1.8 indicating similar cation selectivity as that previously described for TOM core complex (1:3; Künkele et al., 1998a).

When applying low voltages a significant decrease in the transitions between the different conductance states was observed compared to TOM core complex channels. A similar reduction of the transition frequencies was also observed by Hill et al. for recombinant yeast Tom40 channels (Hill et al., 1998). Channels measured with TOM core complex that was treated with trypsin showed a similar

reduction of transitions (Ahting, 2002). The hydrophobic domain of Tom22 and the small Tom proteins were removed with trypsin treatment. However, my measurements of channels formed with purified Tom40 revealed an interesting gating behavior after the application of higher voltages. The transitions between conductance states were observed again. The determined open probability function of such channels was comparable with the open probability for TOM core complex channels confirming the notion that Tom40 is required and sufficient to carry out the pore function.

From this observation, the question arose: which subunit of the TOM core complex was responsible for this change in gating behavior? For this, I have analyzed the electrophysiological characteristics of TOM core complex from mutants lacking one of the small Tom proteins. As Tom22 is essential in *N. crassa*, no Tom22-knock-out studies could be performed (Baker et al., 1990; Hönlinger et al., 1995; Nargang et al., 1995). TOM complex lacking one of the small Tom proteins showed similar electrophysiological properties as wild-type TOM machinery. Thus, the small Tom proteins do not influence the gating behavior of TOM core complex, or they substitute for each other and can “help out” when one of them is missing. In the former case, Tom22 would then be responsible for the observed difference in the transition frequencies between Tom40 and TOM core complex.

In a previous study it has been suggested that Tom22, acts as the central organizer of the complex and converts a simple channel into a complex and dynamic machinery (van Wilpe et al., 1999). It was suggested that Tom22 represents a component of the machinery that controls the gate of the channel. However, a mechanism explaining how Tom22 influences the gate was not proposed. With the present analysis of Tom40 channels I have demonstrated that the voltage dependent sensor and the gate were both located on Tom40. Tom22 or the small Tom proteins modulated the gate. The voltage dependent gating could be reversibly switched on and off for Tom40 channels once the voltage applied to the membrane passed a certain threshold. This threshold was reduced in the presence of Tom22 or the small Tom proteins. The magnitude of this energy reduction was determined by comparing the open probability of TOM core complex channels with that of Tom40 channels when only lower voltages were applied ($|V| > 70$ mV; Fig.7.3). The resulting ΔV_0 was proportional to the reduction of activation energy required for the transition between two conformational states. For Tom40 channels, a transition energy of $9 k_b T$ was estimated and for TOM core complex

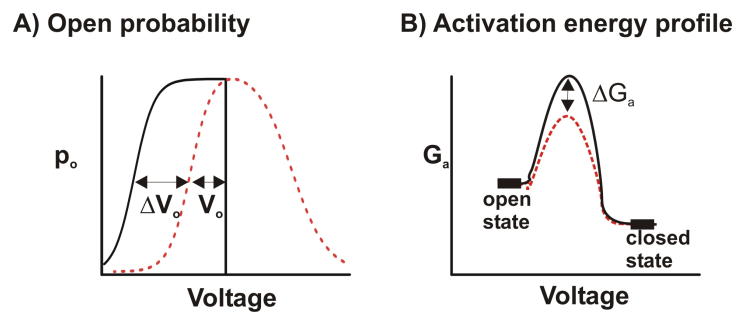


Figure 7.3: Reduction of the activation energy between Tom40 channels and TOM core complex

A) The open probability of Tom40 channels (with lower voltages applied; continuous line) and of TOM core complex channels (dashed line) were described with Boltzmann fit functions. The observed difference in the point of inflection for negative voltages is indicated (ΔV_o).

B) Schematic plot of the energy activation profile for the transition between the open state and a closed state for Tom40 channels (with lower voltages applied, continuous line) and TOM core complex channels (dashed line). The reduction in activation energy is indicated (ΔG_a). This was proportional to ΔV_o .

channels a transition energy of $3.3 k_b T$. Thus, the presence of Tom22 or the small Tom proteins reduced the transition energy by ca. $6 k_b T$ (ΔG_a).

Other studies support the hypothesis that Tom22 modulates the TOM core complex by reducing the energy needed to switch between the various conformational states. A study examining the sensitivity to proteolytic attack showed that the assembly of Tom40 is influenced by Tom22 (Rapaport et al., 1998). Distinct structural alterations of Tom40 were observed that indicated that a cross talk between preprotein receptor and translocation pore exists. Similar alterations have been reported for the translocation of ATPase SecA, a peripheral component of the bacterial plasma membrane (Duong et al., 1997). Furthermore, Tom22 and Tom40 are tightly connected in mammal, as shown for rat (Suzuki et al., 2004) and in Vero cells (Saeki et al., 2000). Tom22 from the latter complemented defects of growth in Δ Tom22 yeast cells.

Recently, a similar “gate- modulator” has been described for the TIM23 translocase of the inner membrane (Meinecke et al., 2006). They propose a model for the closing of the Tim23 channel in which the hydrophilic cis domain of Tim50 maintains the permeability barrier of mitochondria by closing the translocation pore in a peptide-regulated manner.

7.4 Conclusions

Two unexpected discoveries were made with the electrophysiological study:

- (i) Single channel measurements of Tom40 channels revealed a significant decrease in transition frequencies compared to those of TOM core complex. This was only altered after applying higher voltages to the membrane.
- (ii) Two different classes of conductance levels were described for the TOM core complex. Class 1 (S4 and S5 state) behaved like a cylindrical pore allowing ions to pass without being influenced by image forces and surface charges of the pore wall. The second class (states S1-S3) comprised conductance states in which the ions were influenced by such image forces inside the channel. The ions were only able to pass the pore after surmounting an energy barrier.

In the following, I propose two alternative models that account for these properties(Fig.7.4).

In both models a conformational change between an open and a sub-state is induced by the application of high voltages or by Tom22, which induces an additional flexibility. In the Iris Model (upper panel), this conversion is achieved via an iris-like conformational change of the channel. This conformational change within the large pore leads to a narrowing of the pore. This results in more interactions of the permeating ions with the pore wall, which results in the presented energy barrier (indicated with dashed line). Blocking the open state with a polypeptide leads to a complete closure of the pore, as the ions cannot pass the pore.

In the Two Pore Model (lower panel), the two different conductance classes arise from two non-identical pores. The larger pore corresponds to a conductance state in which the ions pass without any interference. Ion translocation through the smaller pore, however, is influenced by the interaction with the channel wall (indicated with dashed line). Transition between the open state and the sub-state is accompanied by conformational changes leading to a blockage of the large pore. The ions can still pass through the small pore. It may be speculated that the small conductance pathway through the TOM core complex is only permeable for ions but not for unfolded polypeptides.

In the following I compare the two different models and discuss various observations that would be made in different situations.

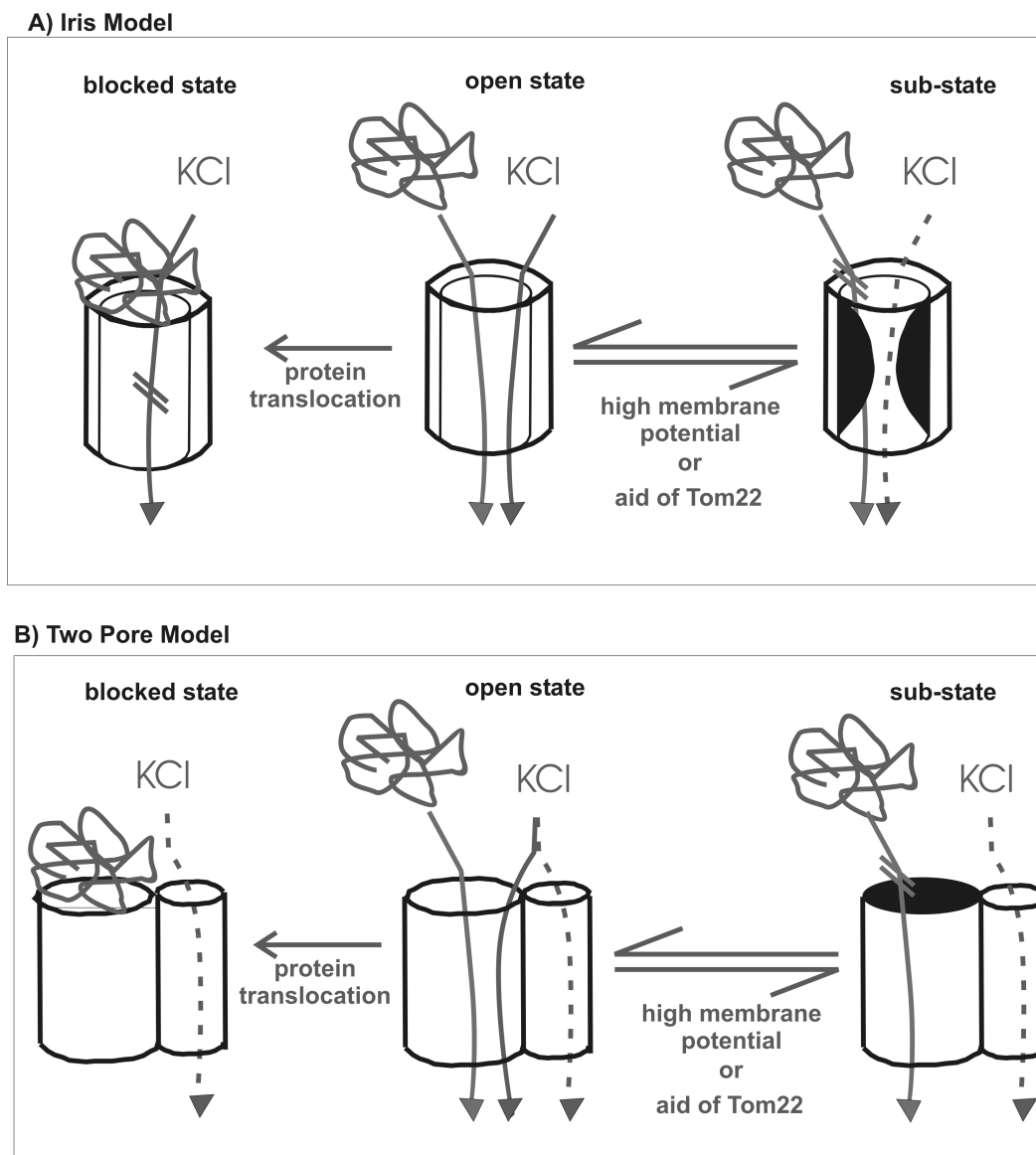


Figure 7.4: Possible mechanisms for translocation of polypeptides through the TOM machinery

In the Iris Model a transition between an open state and a sub-state occurs through an iris-like conformational change within the pore leading to a reduced pore radius. The polypeptide can no longer pass the pore, and the salt ions are influenced by the macroscopic forces of the channel wall (indicated with a dashed line). During protein translocation the channel is in a blocked state. No current is measured as the ions can not pass the channel.

In the Two Pore Model the two different classes of conductance states are demonstrated as two non-identical pores. Transition between the open and sub-state is accompanied by closure of the large pore. The polypeptide can no longer pass the pore and the salt ions pass the second narrow pore while sensing the macroscopic forces of the pore wall (indicated with a dashed line). During protein translocation the channel is in the blocked state. Ions can, however, pass through the small pore.

What effect would a binding of a polypeptide have?

After addition of a polypeptide to the electrophysiological measurement setup, a reduction of the conductance level is expected as the channel is blocked by the polypeptide. In the case of the Iris Model, a complete closure of the channel would occur and no current would be detected.

With the Two Pore Model, only the main conductance level is blocked, and ions can still pass the second smaller pore.

How can these models be extended to account for the six different conductance levels that the TOM core complex can occupy?

With both models three different conductance levels are described: an open state, a partially open state, and a closed state. In the Iris Model, additional sub-conductance levels could emerge from different conformational changes of the pore resulting in at least five different diameters of the pore.

In the Two Pore Model, additional pores could be added to the model. However, it must be considered, that these pores might also gate individually. For example, it is possible that the small pore in the Two Pore Model could also occupy an open and a closed state. Thus, four different conductance levels would be observed: an open state, a partially open state with ions passing the large pore and not the small pore, a second partially open state with ions passing the small pore and not the large pore, and a closed state. The addition of further individual gating pores would therefore lead to a high increase in possible conductance states. In a third model the two presented models could perhaps be combined to a model with two different pores with iris-like conformational changes leading to immense possibilities in conductance levels.

In which conductance states can a blockage of the channel be observed?

TOM core complex switched between different conductance levels in the absence of polypeptides. In the Iris Model, a blockage of the channel with a polypeptide can only occur when the channel is occupying the main conductance state. In the sub-conductance state the channel pore would be too small for the polypeptide to enter.

In the Two Pore Model, a blockage of the polypeptide would not be possible if

only the small pore were open. However, if the channel is in a sub-conductance state evolving from a closure of only the small pore, a blockage of the channel could occur.

7.5 Future prospects

Recent high resolution electrophysiological studies have revealed first insights into the translocation of polymers through aqueous pores, e.g. the translocation of oligonucleotides through the model pore hemolysin (Akeson et al., 1999; Kasianowicz et al., 1996; Meller et al., 2000). The translocation of polysugars (Bezrukov et al., 1994) and peptides (Movileanu et al., 2005) have been analyzed as well with electrophysiological approaches. However, until now it was difficult to apply such an approach to the TOM machinery. With its highly dynamic gating behavior, differentiating between a translocation event and a normal transition between two states was not yet possible. In this study, I have contributed to a more detailed description of the gating behavior of the TOM complex in the absence of substrate. Additional events caused by binding or translocation of a peptide should, therefore, be distinguishable. Electrophysiological observation of binding of peptide and the analysis of the resulting current blockage event should enable us to distinguish between the two models described in Fig.7.4.

8 Abbreviations

Adh	alcohol dehydrogenase
AP	alkaline phosphatase
Apo	apoferritin
APS	ammonium peroxodisulfate
ATP	adenosine 5'-triphosphate
ATPase	adenosine triphosphatase
β -ME	β -mercaptoethanol
BCIP	5-Brom-4-chloro-3-indolyl-phosphat
BLM	black lipid membrane
BNGE	blue native polyacrylamide gel electrophoresis
BSA	bovine serum albumine
C-terminus	carboxy terminus
Da	Dalton
DDM	n-dodecyl- β -maltopyranosid
$\Delta\Psi$	difference in the trans membrane potential
DHFR	dihydrofolate reductase
DiphPC	Diphytanoyl-phosphatidylcholine
DMPC	Dimyristoyl phosphatidyl choline
DMPE	dimyristoyl-phosphatidyl-ethanolamine
DMPG	dimyristoyl phosphatidyl glycerol
DMSO	dimethylsulfoxid
DNA	deoxyribonucleic acid
DOPC	dioleylphosphatidyl choline
DTT	Dithiothreitol
EPC	egg phosphatidyl choline
ER	endoplasmatic reticulumn
FCS	fluorescence correlation spectroscopy
FCCS	fluorescence cross correlation spectroscopy
FRET	fluorescence resonance energy transfer
GFP	green fluorescent protein
GIP	general import pore
GTP	guanosine triphosphate
HEPES	N-2 hydroxyl piperazine-N'-2-ethane sulphonic acid

Hsp	heat shock protein
IMS	intermembrane space
IPTG	isopropil- β ,D-tiogalactopyranoside
kD	kilo Dalton
L:P	lipid to protein ratios
MOPS	N-morpholinopropane sulphonic acid
NBT	Nitro blue tetrazolium chloride
n.d.	not determined
Ni-NTA	nickel-nitrilo triacetic acid
NMR	nuclear magnetic resonance
N-terminus	amino terminus
OD _x	optical density at x nm
OMV	outer membrane vesicle
Ova	ovalbumin
PAGE	polyacrylamide gel electrophoresis
PEG	Polyethylenglykol
PMSF	phenylmethylsulfonylfluoride
PSC	peptide-sensitive channel
PVDF	Polyvinyliden-difluorid
rpm	rounds per minute
SANS	small angle neutron scattering
SCAM	substituted cysteine accessibility method
SDS	sodiumdodecylsulfat
SDS-PAGE	sodium dodecyl sulfate-poly-. acrylamide gel electrophoresis
Su9	subunit 9 of the F1Fo-ATP synthase
TEMED	N,N,N',N'-tetramethylene diamine
TBS	Tris buffered saline
TCA	trichloroacetic acid
TCEP	tris-(2-carboxyethyl)phosphine
Thy	thyroglobulin
TIC	translocase of the chloroplastic inner envelope
TOC	translocase of the chloroplastic outer envelope
Tris	tris-(hydroxymethyl)-aminomethane
UV	ultra violet
VDAC	voltage dependent anion channel
v/v	volume per volume
w/v	weight per volume

Bibliography

- Y. Abe, T. Shodai, T. Muto, K. Mihara, H. Torii, S. Nishikawa, T. Endo, and D. Kohda. Structural basis of presequence recognition by the mitochondrial protein import receptor Tom20. *Cell*, 100(5):551–560, Mar 2000.
- C. Adcock, G. R. Smith, and M. S. Sansom. Electrostatics and the ion selectivity of ligand-gated channels. *Biophys J*, 75(3):1211–1222, Sep 1998.
- U. Ahting, C. Thun, R. Hegerl, D. Typke, F.E. Nargang, W. Neupert, and S. Nussberger. The TOM core complex: the general protein import pore of the outer membrane of mitochondria. *J Cell Biol*, 147(5):959–968, Nov 1999.
- U. Ahting, M. Thieffry, H. Engelhardt, R. Hegerl, W. Neupert, and S. Nussberger. Tom40, the pore-forming component of the protein-conducting TOM channel in the outer membrane of mitochondria. *J Cell Biol*, 153(6):1151–1160, Jun 2001.
- U. Ahting, T. Waizenegger, W. Neupert, and D. Rapaport. Signal-anchored proteins follow a unique insertion pathway into the outer membrane of mitochondria. *J Biol Chem*, 280(1):48–53, Jan 2005.
- Uwe Ahting. *Der TOM-Core-Komplex und die kanalbildende Komponente Tom40 der Proteintranslokase der äußeren Mitochondrienmembran von Neurospora crassa*. Ph.D. thesis, LMU, München, 2002.
- M. Akeson, D. Branton, J.J. Kasianowicz, E. Brandin, and D.W. Deamer. Microsecond time-scale discrimination among polycytidylic acid, polyadenylic acid, and polyuridylic acid as homopolymers or as segments within single RNA molecules. *Biophys J*, 77(6):3227–3233, Dec 1999.
- R. Albrecht, P. Rehling, A. Chacinska, J. Brix, S.A. Cadamuro, R. Volkmer, B. Guiard, N. Pfanner, and K. Zeth. The Tim21 binding domain connects the preprotein translocases of both mitochondrial membranes. *EMBO Rep*, 7(12):1233–1238, Dec 2006.
- E. Babini and M. Pusch. A two-holed story: structural secrets about CIC proteins become unraveled? *Physiology (Bethesda)*, 19:293–299, Oct 2004.

- K. P. Baker, A. Schaniel, D. Vestweber, and G. Schatz. A yeast mitochondrial outer membrane protein essential for protein import and cell viability. *Nature*, 348 (6302):605–609, Dec 1990.
- M. F. Bauer, C. Sirrenberg, W. Neupert, and M. Brunner. Role of Tim23 as voltage sensor and presequence receptor in protein import into mitochondria. *Cell*, 87 (1):33–41, Oct 1996.
- L. Becker, M. Bannwarth, C. Meisinger, K. Hill, K. Model, T. Krimmer, R. Casadio, K.N. Truscott, G.E. Schulz, N. Pfanner, and R. Wagner. Preprotein translocase of the outer mitochondrial membrane: reconstituted Tom40 forms a characteristic TOM pore. *J Mol Biol*, 353(5):1011–1020, Nov 2005.
- J. Beers, D. M. Glerum, and A. Tzagoloff. Purification, characterization, and localization of yeast Cox17p, a mitochondrial copper shuttle. *J Biol Chem*, 272(52):33191–33196, Dec 1997.
- R. Benz. Permeation of hydrophilic solutes through mitochondrial outer membranes: review on mitochondrial porins. *Biochim Biophys Acta*, 1197(2):167–196, Jun 1994.
- J. Bereiter-Hahn and M. Vöth. Dynamics of mitochondria in living cells: shape changes, dislocations, fusion, and fission of mitochondria. *Microsc Res Tech*, 27 (3):198–219, Feb 1994.
- P. Bessonneau, V. Besson, I. Collinson, and F. Duong. The SecYEG preprotein translocation channel is a conformationally dynamic and dimeric structure. *EMBO J*, 21(5):995–1003, Mar 2002.
- S. M. Bezrukov, I. Vodyanoy, and V. A. Parsegian. Counting polymers moving through a single ion channel. *Nature*, 370(6487):279–281, Jul 1994.
- L. Bolliger, T. Junne, G. Schatz, and T. Lithgow. Acidic receptor domains on both sides of the outer membrane mediate translocation of precursor proteins into yeast mitochondria. *EMBO J*, 14(24):6318–6326, Dec 1995.
- M. M. Bradford. A rapid and sensitive method for the quantitation of microgram quantities of protein utilizing the principle of protein-dye binding. *Anal Biochem*, 72:248–254, May 1976.
- J. Brix, K. Dietmeier, and N. Pfanner. Differential recognition of preproteins by the purified cytosolic domains of the mitochondrial import receptors Tom20, Tom22, and Tom70. *J Biol Chem*, 272(33):20730–20735, Aug 1997.
- A. Chacinska, S. Pfannschmidt, N. Wiedemann, V. Kozjak, L.A. Sanjuán Szklarz, A. Schulze-Specking, K.N. Truscott, B. Guiard, C. Meisinger, and N. Pfanner. Essential role of Mia40 in import and assembly of mitochondrial intermembrane space proteins. *EMBO J*, 23(19):3735–3746, Oct 2004.

- A Chacinska, M. Lind, A.E. Frazier, J. Dudek, C. Meisinger, A. Geissler, A. Sickmann, H.E. Meyer, K.N. Truscott, B. Guiard, Pfanner; N., and P. Rehling. Mitochondrial presequence translocase: switching between TOM tethering and motor recruitment involves Tim21 and Tim17. *Cell*, 120(6):817–829, Mar 2005.
- D. Chen and R. Eisenberg. Charges, currents, and potentials in ionic channels of one conformation. *Biophys J*, 64(5):1405–1421, May 1993.
- I. Collinson, C. Breyton, F. Duong, C. Tziatzios, D. Schubert, E. Or, T. Rapoport, and W. Kühlbrandt. Projection structure and oligomeric properties of a bacterial core protein translocase. *EMBO J*, 20(10):2462–2471, May 2001.
- M. Colombini. A candidate for the permeability pathway of the outer mitochondrial membrane. *Nature*, 279(5714):643–645, Jun 1979.
- D. Colquhoun and F. Sigworth. *Fitting and statistical analysis of single-channel records*. In: B. Sakmann and Neher (eds):*Single Channel Recording*. Plenum Press, 1983.
- K. Cooper, E. Jakobsson, and P. Wolynes. The theory of ion transport through membrane channels. *Prog Biophys Mol Biol*, 46(1):51–96, 1985.
- C. T. Culbertson, S. C. Jacobson, and J. M. Ramsey. Microchip devices for high-efficiency separations. *Anal Chem*, 72(23):5814–5819, Dec 2000.
- H. Davson and J. F. Danielli. Studies on the permeability of erythrocytes: Factors in cation permeability. *Biochem J*, 32(6):991–1001, Jun 1938.
- J. de Keyzer, C. van der Does, and A. J M Driessen. The bacterial translocase: a dynamic protein channel complex. *Cell Mol Life Sci*, 60(10):2034–2052, Oct 2003.
- P. J. Dekker, M. T. Ryan, J. Brix, H. Müller, A. Hönlinger, and N. Pfanner. Pre-protein translocase of the outer mitochondrial membrane: molecular dissection and assembly of the general import pore complex. *Mol Cell Biol*, 18(11):6515–6524, Nov 1998.
- K. Dietmeier, A. Hönlinger, U. Bömer, P. J. Dekker, C. Eckerskorn, F. Lottspeich, M. Kübrich, and N. Pfanner. Tom5 functionally links mitochondrial preprotein receptors to the general import pore. *Nature*, 388(6638):195–200, Jul 1997.
- S. DiMauro and E.A. Schon. Mitochondrial respiratory-chain diseases. *N Engl J Med*, 348(26):2656–2668, Jun 2003.
- S. Ding and F. Sachs. Evidence for non-independent gating of P2X2 receptors expressed in *Xenopus* oocytes. *BMC Neurosci*, 3:17, Nov 2002.
- P. Dolezal, V. Likic, J. Tachezy, and T. Lithgow. Evolution of the molecular machines for protein import into mitochondria. *Science*, 313(5785):314–318, Jul 2006.

- F. Duong, J. Eichler, A. Price, M. R. Leonard, and W. Wickner. Biogenesis of the gram-negative bacterial envelope. *Cell*, 91(5):567–573, Nov 1997.
- S.D. Dyall, M.T. Brown, and P.J. Johnson. Ancient invasions: from endosymbionts to organelles. *Science*, 304(5668):253–257, Apr 2004.
- R. Eckert. *Biophysikalische Charakterisierung von Gap-junction-Kanälen in Säugerzellkulturen*. Ph.D. thesis, Universität Stuttgart, Stuttgart, 1993.
- T. Endo, H. Yamamoto, and M. Esaki. Functional cooperation and separation of translocators in protein import into mitochondria, the double-membrane bounded organelles. *J Cell Sci*, 116(Pt 16):3259–3267, Aug 2003.
- H. Engelhardt, T. Meins, M. Poynor, V. Adams, S. Nussberger, W. Welte, and K. Zeth. High-level expression, refolding and probing the natural fold of the human voltage-dependent anion channel isoforms I and II. *J Membr Biol*, 216(2-3):93–105, Apr 2007.
- M. Esaki, T. Kanamori, S. Nishikawa, I. Shin, P.G. Schultz, and T. Endo. Tom40 protein import channel binds to non-native proteins and prevents their aggregation. *Nat Struct Biol*, 10(12):988–994, Dec 2003.
- M. Esaki, H. Shimizu, T. Ono, H. Yamamoto, T. Kanamori, S. Nishikawa, and T. Endo. Mitochondrial protein import. Requirement of presequence elements and Tom components for precursor binding to the TOM complex. *J Biol Chem*, 279(44):45701–45707, Oct 2004.
- H. Freitag, W. Neupert, and R. Benz. Purification and characterisation of a pore protein of the outer mitochondrial membrane from *Neurospora crassa*. *Eur J Biochem*, 123(3):629–636, Apr 1982.
- F. Fèvre, J. P. Henry, and M. Thieffry. Solubilization and reconstitution of the mitochondrial peptide-sensitive channel. *J Bioenerg Biomembr*, 25(1):55–60, Feb 1993.
- A. Geissler, J. Rassow, N. Pfanner, and W. Voos. Mitochondrial import driving forces: enhanced trapping by matrix Hsp70 stimulates translocation and reduces the membrane potential dependence of loosely folded preproteins. *Mol Cell Biol*, 21(20):7097–7104, Oct 2001.
- I. Gentle, K. Gabriel, P. Beech, R. Waller, and T. Lithgow. The Omp85 family of proteins is essential for outer membrane biogenesis in mitochondria and bacteria. *J Cell Biol*, 164(1):19–24, Jan 2004.
- S. M. Glaser, B. R. Miller, and M. G. Cumsky. Removal of a hydrophobic domain within the mature portion of a mitochondrial inner membrane protein causes its mislocalization to the matrix. *Mol Cell Biol*, 10(5):1873–1881, May 1990.

- A. Goffeau, B. G. Barrell, H. Bussey, R. W. Davis, B. Dujon, H. Feldmann, F. Galibert, J. D. Hoheisel, C. Jacq, M. Johnston, E. J. Louis, H. W. Mewes, Y. Murakami, P. Philippsen, H. Tettelin, and S. G. Oliver. Life with 6000 genes. *Science*, 274 (5287):546, 563–546, 567, Oct 1996.
- L. G. Gordon and D. A. Haydon. The unit conductance channel of alamethicin. *Biochim Biophys Acta*, 255(3):1014–1018, Mar 1972.
- M. W. Gray. Evolution of organellar genomes. *Curr Opin Genet Dev*, 9(6):678–687, Dec 1999.
- S.M. Grigoriev, C. Muro, L.M. Dejean, M.L. Campo, S. Martinez-Caballero, and K.W. Kinnally. Electrophysiological approaches to the study of protein translocation in mitochondria. *Int Rev Cytol*, 238:227–274, 2004.
- J. E. Hall. Access resistance of a small circular pore. *J Gen Physiol*, 66(4):531–532, Oct 1975.
- J E Hall, C A Mead, and G Szabo. A barrier model for current flow in lipid bilayer membranes. *J. Membrane Biol.*, 11:75– 97, 1973.
- W Hanke and W.-R. Schlue. *Plana Lipid Bilayers – Methods and Applications*. Academic Press, 1993.
- E. Haustein and P. Schwille. Ultrasensitive investigations of biological systems by fluorescence correlation spectroscopy. *Methods*, 29(2):153–166, Feb 2003.
- E. Haustein and P. Schwille. Fluorescence correlation spectroscopy: novel variations of an established technique. *Annu Rev Biophys Biomol Struct*, 36:151–169, 2007.
- K. Hell, W. Neupert, and R. A. Stuart. Oxa1p acts as a general membrane insertion machinery for proteins encoded by mitochondrial DNA. *EMBO J*, 20(6):1281–1288, Mar 2001.
- R. Henderson and P. N. Unwin. Three-dimensional model of purple membrane obtained by electron microscopy. *Nature*, 257(5521):28–32, Sep 1975.
- J. P. Henry, P. Juin, F. Vallette, and M. Thieffry. Characterization and function of the mitochondrial outer membrane peptide-sensitive channel. *J Bioenerg Biomembr*, 28(2):101–108, Apr 1996.
- K. Hill, K. Model, M. T. Ryan, K. Dietmeier, F. Martin, R. Wagner, and N. Pfanner. Tom40 forms the hydrophilic channel of the mitochondrial import pore for preproteins. *Nature*, 395(6701):516–521, Oct 1998.
- B. Hille. *Ionic Channels of Excitable Membranes*. Sinauer Associates, 1992.

- A. Hönlinger, M. Kübrich, M. Moczko, F. Gärtner, L. Mallet, F. Bussereau, C. Eckerskorn, F. Lottspeich, K. Dietmeier, and M. Jacquet. The mitochondrial receptor complex: Mom22 is essential for cell viability and directly interacts with preproteins. *Mol Cell Biol*, 15(6):3382–3389, Jun 1995.
- A. Hönlinger, U. Bömer, A. Alconada, C. Eckerskorn, F. Lottspeich, K. Dietmeier, and N. Pfanner. Tom7 modulates the dynamics of the mitochondrial outer membrane translocase and plays a pathway-related role in protein import. *EMBO J*, 15(9):2125–2137, May 1996.
- A. L. Hodgkin and A. F. Huxley. A quantitative description of membrane current and its application to conduction and excitation in nerve. *J Physiol*, 117(4):500–544, Aug 1952.
- N. Hoogenraad, L.A. Ward, and M.T. Ryan. Import and assembly of proteins into mitochondria of mammalian cells. *Biochim Biophys Acta*, 1592(1):97–105, Sep 2002.
- C Hunte, G Jagow, and H Schägger. *Membrane protein purification and crystallization. 2nd edition. A practical guide.* Academic Press, 2nd edition, 2003.
- M. B. Jackson. *Molecular and Cellular Biophysics.* Cambridge University Press, 2006.
- J.Gumbart and K. Schulten. Molecular dynamics studies of the archaeal translocon. *Biophys J*, 90(7):2356–2367, Apr 2006.
- A. E. Johnson and M. A. van Waes. The translocon: a dynamic gateway at the ER membrane. *Annu Rev Cell Dev Biol*, 15:799–842, 1999.
- A.J. Johnston, J. Hoogenraad, D.A. Dougan, K.N. Truscott, M. Yano, M. Mori, N.J. Hoogenraad, and M.R. Ryan. Insertion and assembly of human Tom7 into the preprotein translocase complex of the outer mitochondrial membrane. *J Biol Chem*, 277(44):42197–42204, Nov 2002.
- P. Juin, M. Pelleschi, C. Sagné, J. P. Henry, M. Thieffry, and F. M. Vallette. Involvement of the peptide sensitive channel in the translocation of basic peptides into mitochondria. *Biochem Biophys Res Commun*, 211(1):92–99, Jun 1995. doi: 10.1006/bbrc.1995.1782. URL <http://dx.doi.org/10.1006/bbrc.1995.1782>.
- P. Juin, M. Thieffry, J. P. Henry, and F. M. Vallette. Relationship between the peptide-sensitive channel and the mitochondrial outer membrane protein translocation machinery. *J Biol Chem*, 272(9):6044–6050, Feb 1997.
- J. J. Kasianowicz, E. Brandin, D. Branton, and D. W. Deamer. Characterization of individual polynucleotide molecules using a membrane channel. *Proc Natl Acad Sci U S A*, 93(24):13770–13773, Nov 1996.
- W. Kühlbrandt. Two-dimensional crystallization of membrane proteins. *Q Rev Biophys*, 25(1):1–49, Feb 1992.

- M. Kiebler, P. Keil, H. Schneider, I. J. van der Klei, N. Pfanner, and W. Neupert. The mitochondrial receptor complex: a central role of MOM22 in mediating preprotein transfer from receptors to the general insertion pore. *Cell*, 74(3):483–492, Aug 1993.
- K. P. Künkele, S. Heins, M. Dembowski, F. E. Nargang, R. Benz, M. Thieffry, J. Walz, R. Lill, S. Nussberger, and W. Neupert. The preprotein translocation channel of the outer membrane of mitochondria. *Cell*, 93(6):1009–1019, Jun 1998a.
- K. P. Künkele, P. Juin, C. Pompa, F. E. Nargang, J. P. Henry, W. Neupert, R. Lill, and M. Thieffry. The isolated complex of the translocase of the outer membrane of mitochondria. characterization of the cation-selective and voltage-gated preprotein-conducting pore. *J Biol Chem*, 273(47):31032–31039, Nov 1998b.
- T. Komiya, S. Rospert, C. Koehler, R. Looser, G. Schatz, and K. Mihara. Interaction of mitochondrial targeting signals with acidic receptor domains along the protein import pathway: evidence for the ‘acid chain’ hypothesis. *EMBO J*, 17(14):3886–3898, Jul 1998.
- A. Kuhn, R. Stuart, R. Henry, and R. E. Dalbey. The Alb3/Oxa1/YidC protein family: membrane-localized chaperones facilitating membrane protein insertion? *Trends Cell Biol*, 13(10):510–516, Oct 2003.
- T. Kuwana and D. D. Newmeyer. Bcl-2-family proteins and the role of mitochondria in apoptosis. *Curr Opin Cell Biol*, 15(6):691–699, Dec 2003.
- J. Kyhse-Andersen. Electrophoretic transfer of multiple gels: a simple apparatus without buffer tank for rapid transfer of proteins from polyacrylamide to nitrocellulose. *J Biochem Biophys Methods*, 10(3-4):203–209, Dec 1984.
- J. Lacapère, E. Pebay-Peyroula, J. Neumann, and . Etchebest. Determining membrane protein structures: still a challenge! *Trends Biochem Sci*, 32(6):259–270, Jun 2007.
- U. K. Laemmli. Cleavage of structural proteins during the assembly of the head of bacteriophage T4. *Nature*, 227(5259):680–685, Aug 1970.
- R. Latorre and O. Alvarez. Voltage-dependent channels in planar lipid bilayer membranes. *Physiol Rev*, 61(1):77–150, Jan 1981.
- D. Levy, M. Chami, and J. L. Rigaud. Two-dimensional crystallization of membrane proteins: the lipid layer strategy. *FEBS Lett*, 504(3):187–193, Aug 2001.
- D.R. Lide. *CRC Handbook of Chemistry and Physics*. CRC Press Inc, 2003.
- R. Lill and G. Kispal. Maturation of cellular Fe-S proteins: an essential function of mitochondria. *Trends Biochem Sci*, 25(8):352–356, Aug 2000.

- Q. Liu, P. D'Silva, W. Walter, J. Marszalek, and E. A. Craig. Regulated cycling of mitochondrial Hsp70 at the protein import channel. *Science*, 300(5616):139–141, Apr 2003.
- D. Macasev, J. Whelan, E. Newbigin, M. C. Silva-Filho, T. D. Mulhern, and T. Lithgow. Tom22', an 8-kDa trans-site receptor in plants and protozoans, is a conserved feature of the TOM complex that appeared early in the evolution of eukaryotes. *Mol Biol Evol*, 21(8):1557–1564, Aug 2004.
- C. A. Mannella. Structure and dynamics of the mitochondrial inner membrane cristae. *Biochim Biophys Acta*, 1763(5-6):542–548, 2006.
- C. A. Mannella, A. F. Neuwald, and C. E. Lawrence. Detection of likely transmembrane beta strand regions in sequences of mitochondrial pore proteins using the gibbs sampler. *J Bioenerg Biomembr*, 28(2):163–169, Apr 1996.
- A. Mayer, F. E. Nargang, W. Neupert, and R. Lill. MOM22 is a receptor for mitochondrial targeting sequences and cooperates with MOM19. *EMBO J*, 14(17):4204–4211, Sep 1995a.
- A. Mayer, W. Neupert, and R. Lill. Mitochondrial protein import: reversible binding of the presequence at the trans side of the outer membrane drives partial translocation and unfolding. *Cell*, 80(1):127–137, Jan 1995b.
- O. B. McManus and K. L. Magleby. Kinetic states and modes of single large-conductance calcium-activated potassium channels in cultured rat skeletal muscle. *J Physiol*, 402:79–120, Aug 1988.
- M. Meinecke, R. Wagner, P. Kovermann, B. Guiard, D. U. Mick, D. P. Hutu, W. Voos, K. N. Truscott, A. Chacinska, N. Pfanner, and P. Rehling. Tim50 maintains the permeability barrier of the mitochondrial inner membrane. *Science*, 312(5779):1523–1526, Jun 2006.
- C. Meisinger, M. T. Ryan, K. Hill, K. Model, J. H. Lim, A. Sickmann, H. Müller, H. E. Meyer, R. Wagner, and N. Pfanner. Protein import channel of the outer mitochondrial membrane: a highly stable Tom40-Tom22 core structure differentially interacts with preproteins, small tom proteins, and import receptors. *Mol Cell Biol*, 21(7):2337–2348, Apr 2001.
- A. Meller, L. Nivon, E. Brandin, J. Golovchenko, and D. Branton. Rapid nanopore discrimination between single polynucleotide molecules. *Proc Natl Acad Sci U S A*, 97(3):1079–1084, Feb 2000.
- N. Mesecke, N. Terziyska, C. Kozany, F. Baumann, W. Neupert, K. Hell, and J. M. Herrmann. A disulfide relay system in the intermembrane space of mitochondria that mediates protein import. *Cell*, 121(7):1059–1069, Jul 2005.

- D. Milenkovic, J. Müller, D. Stojanovski, N. Pfanner, and A. Chacinska. Diverse mechanisms and machineries for import of mitochondrial proteins. *Biol Chem*, 388(9):891–897, Sep 2007.
- C. Miller. Open-state substructure of single chloride channels from torpedo electropax. *Philos Trans R Soc Lond B Biol Sci*, 299(1097):401–411, Dec 1982.
- D. Mokranjac, S. A. Paschen, C. Kozany, H. Prokisch, S. C Hoppins, F. E. Nargang, W. Neupert, and K. Hell. Tim50, a novel component of the TIM23 preprotein translocase of mitochondria. *EMBO J*, 22(4):816–825, Feb 2003.
- L. Movileanu, J. P. Schmittschmitt, J. M. Scholtz, and H. Bayley. Interactions of peptides with a protein pore. *Biophys J*, 89(2):1030–1045, Aug 2005.
- P. Mueller, D. O. Rudin, H. T. Tien, and W. C. Wescott. Reconstitution of cell membrane structure in vitro and its transformation into an excitable system. *Nature*, 194:979–980, Jun 1962.
- Concepción Muro, Serguei M Grigoriev, Dawn Pietkiewicz, Kathleen W Kinnally, and María Luisa Campo. Comparison of the TIM and TOM channel activities of the mitochondrial protein import complexes. *Biophys J*, 84(5):2981–2989, May 2003.
- F. E. Nargang, K. P. Künkele, A. Mayer, R. G. Ritzel, W. Neupert, and R. Lill. ‘sheltered disruption’ of *Neurospora crassa* MOM22, an essential component of the mitochondrial protein import complex. *EMBO J*, 14(6):1099–1108, Mar 1995.
- E. Neher and B. Sakmann. Single-channel currents recorded from membrane of denervated frog muscle fibres. *Nature*, 260(5554):799–802, Apr 1976.
- B. Neumcke and P. Läuger. Nonlinear electrical effects in lipid bilayer membranes. ii. integration of the generalized nernst-planck equations. *Biophys J*, 9(9):1160–1170, Sep 1969.
- W. Neupert and J. M. Herrmann. Translocation of proteins into mitochondria. *Annu Rev Biochem*, 76:723–749, 2007.
- M. Orth and A. H. Schapira. Mitochondria and degenerative disorders. *Am J Med Genet*, 106(1):27–36, 2001.
- G. E. Palade. The fine structure of mitochondria. *Anat Rec*, 114(3):427–451, Nov 1952.
- N. Panchuk-Voloshina, R. P. Haugland, J. Bishop-Stewart, M. K. Bhalgat, P. J. Millard, F. Mao, W. Y. Leung, and R. P. Haugland. Alexa dyes, a series of new fluorescent dyes that yield exceptionally bright, photostable conjugates. *J Histochem Cytochem*, 47(9):1179–1188, Sep 1999.

- S. A. Paschen, T. Waizenegger, T. Stan, M. Preuss, M. Cyrklaff, K. Hell, D. Rapaport, and W. Neupert. Evolutionary conservation of biogenesis of beta-barrel membrane proteins. *Nature*, 426(6968):862–866, Dec 2003.
- J. B. Patlak. Sodium channel subconductance levels measured with a new variance-mean analysis. *J Gen Physiol*, 92(4):413–430, Oct 1988.
- J. B. Patlak. Measuring kinetics of complex single ion channel data using mean-variance histograms. *Biophys J*, 65(1):29–42, Jul 1993.
- M. Preuss, M. Ott, S. Funes, J. Luirink, and J. M. Herrmann. Evolution of mitochondrial oxa proteins from bacterial YidC. Inherited and acquired functions of a conserved protein insertion machinery. *J Biol Chem*, 280(13):13004–13011, Apr 2005.
- D. Rapaport, A. Mayer, W. Neupert, and R Lill. Cis and trans sites of the TOM complex of mitochondria in unfolding and initial translocation of preproteins. *J Biol Chem*, 273(15):8806–8813, Apr 1998.
- P. Rehling, K. Brandner, and N. Pfanner. Mitochondrial import and the twin-pore translocase. *Nat Rev Mol Cell Biol*, 5(7):519–530, Jul 2004.
- J. L. Rigaud, G. Mosser, J. J. Lacapere, A. Olofsson, D. Levy, and J. L. Ranck. Bio-beads: an efficient strategy for two-dimensional crystallization of membrane proteins. *J Struct Biol*, 118(3):226–235, Apr 1997.
- M. Rissler, N. Wiedemann, S. Pfannschmidt, K. Gabriel, B. Guiard, N. Pfanner, and A. Chacinska. The essential mitochondrial protein Erv1 cooperates with Mia40 in biogenesis of intermembrane space proteins. *J Mol Biol*, 353(3):485–492, Oct 2005.
- D. Roise and G. Schatz. Mitochondrial presequences. *J Biol Chem*, 263(10):4509–4511, Apr 1988.
- F. Sachs. *Automated analysis of single-channel records*. In: B. Sakmann and Neher (eds): *Single Channel Recording*. Plenum Press, 1983.
- K. Saeki, H. Suzuki, M. Tsuneoka, M. Maeda, R. Iwamoto, H. Hasuwa, S. Shida, T. Takahashi, M. Sakaguchi, T. Endo, Y. Miura, E. Mekada, and K. Mihara. Identification of mammalian TOM22 as a subunit of the preprotein translocase of the mitochondrial outer membrane. *J Biol Chem*, 275(41):31996–32002, Oct 2000.
- T. Saitoh, M. Igura, T. Obita, T. Ose, R. Kojima, K. Maenaka, T. Endo, and D. Kohda. Tom20 recognizes mitochondrial presequences through dynamic equilibrium among multiple bound states. *EMBO J*, 26(22):4777–4787, Nov 2007.
- J. Sambrook, E.F. Fritsch, and T. Maniatis. *Molecular cloning*. CSH Laboratory Press, Cold Spring Harbor., 1989.

- M.S.P. Sansom and I. R. Mellor. Analysis of the gating of single ion channels using current-voltage surfaces. *J.theor Biol.*, 144:213–223, 1990.
- H. Schägger and G. von Jagow. Blue native electrophoresis for isolation of membrane protein complexes in enzymatically active form. *Anal Biochem*, 199(2): 223–231, Dec 1991.
- S. Schmitt. *Strukturelle und funktionelle Untersuchung der Proteintranslokase der mitochondrialen Außenmembran*. Ph.D. thesis, LMU, München, 2005.
- S. Schmitt, U. Ahting, L. Eichacker, B. Granvogl, N. E. Go, F. E. Nargang, W. Neupert, and S. Nussberger. Role of Tom5 in maintaining the structural stability of the TOM complex of mitochondria. *J Biol Chem*, 280(15):14499–14506, Apr 2005.
- H. C. Schneider, J. Berthold, M. F. Bauer, K. Dietmeier, B. Guiard, M. Brunner, and W. Neupert. Mitochondrial Hsp70/MIM44 complex facilitates protein import. *Nature*, 371(6500):768–774, Oct 1994.
- W. Sebald, W. Neupert, and H. Weiss. Preparation of neurospora crassa mitochondria. *Methods Enzymol*, 55:144–148, 1979.
- E. Laura Sherman, Nancy E Go, and Frank E Nargang. Functions of the small proteins in the TOM complex of Neurospora crassa. *Mol Biol Cell*, 16(9):4172–4182, Sep 2005.
- O. Shimomura, F. H. Johnson, and Y. Saiga. Extraction, purification and properties of aequorin, a bioluminescent protein from the luminous hydromedusan, aequorea. *J Cell Comp Physiol*, 59:223–239, Jun 1962.
- H. Stahlberg, T. Braun, B. de Groot, A. Philippsen, M. J. Borgnia, P. Agre, W. Kühlbrandt, and A. Engel. The 6.9-Å structure of GlpF: a basis for homology modeling of the glycerol channel from Escherichia coli. *J Struct Biol*, 132(2): 133–141, Nov 2000.
- D. Stojanovski, M. Rissler, N. Pfanner, and C. Meisinger. Mitochondrial morphology and protein import—a tight connection? *Biochim Biophys Acta*, 1763(5-6): 414–421, 2006.
- R. Stuart. Insertion of proteins into the inner membrane of mitochondria: the role of the Oxa1 complex. *Biochim Biophys Acta*, 1592(1):79–87, Sep 2002.
- L. A. Sturtz, K. Diekert, L. T. Jensen, R. Lill, and V. C. Culotta. A fraction of yeast Cu,Zn-superoxide dismutase and its metallochaperone, CCS, localize to the intermembrane space of mitochondria. A physiological role for SOD1 in guarding against mitochondrial oxidative damage. *J Biol Chem*, 276(41):38084–38089, Oct 2001.

- H. Suzuki, Y. Okazawa, T. Komiya, K. Saeki, E. Mekada, S. Kitada, A. Ito, and K. Mihara. Characterization of rat TOM40, a central component of the preprotein translocase of the mitochondrial outer membrane. *J Biol Chem*, 275(48):37930–37936, Dec 2000.
- H. Suzuki, T. Kadowaki, M. Maeda, H. Sasaki, J. Nabekura, M. Sakaguchi, and K. Mihara. Membrane-embedded C-terminal segment of rat mitochondrial TOM40 constitutes protein-conducting pore with enriched beta-structure. *J Biol Chem*, 279(48):50619–50629, Nov 2004.
- M. Swain and N. W. Ross. A silver stain protocol for proteins yielding high resolution and transparent background in sodium dodecyl sulfate-polyacrylamide gels. *Electrophoresis*, 16(6):948–951, Jun 1995.
- A. B. Taylor, B. S. Smith, S. Kitada, K. Kojima, H. Miyaura, Z. Otwinowski, A. Ito, and J. Deisenhofer. Crystal structures of mitochondrial processing peptidase reveal the mode for specific cleavage of import signal sequences. *Structure*, 9(7):615–625, Jul 2001.
- N. Terziyska, T. Lutz, C. Kozany, D. Mokranjac, N. Mesecke, W. Neupert, J. M. Herrmann, and K. Hell. Mia40, a novel factor for protein import into the intermembrane space of mitochondria is able to bind metal ions. *FEBS Lett*, 579(1):179–184, Jan 2005.
- H. Towbin, T. Staehelin, and J. Gordon. Electrophoretic transfer of proteins from polyacrylamide gels to nitrocellulose sheets: procedure and some applications. *Proc Natl Acad Sci U S A*, 76(9):4350–4354, Sep 1979.
- K. N. Truscott, P. Kovermann, A. Geissler, A. Merlin, M. Meijer, A. J. Driessen, J. Rassow, N. Pfanner, and R. Wagner. A presequence- and voltage-sensitive channel of the mitochondrial preprotein translocase formed by Tim23. *Nat Struct Biol*, 8(12):1074–1082, Dec 2001.
- B. Van den Berg, W.M. Clemons, I. Collinson, Y. Modis, E. Hartmann, S.C. Harrison, and T.A. Rapoport. X-ray structure of a protein-conducting channel. *Nature*, 427(6969):36–44, Jan 2004.
- A. P. van Loon, A. W. Brändli, and G. Schatz. The presequences of two imported mitochondrial proteins contain information for intracellular and intramitochondrial sorting. *Cell*, 44(5):801–812, Mar 1986.
- S. van Wilpe, M. T. Ryan, K. Hill, A. C. Maarse, C. Meisinger, J. Brix, P. J. Dekker, M. Moczko, R. Wagner, M. Meijer, B. Guiard, A. Hönlinger, and N. Pfanner. Tom22 is a multifunctional organizer of the mitochondrial preprotein translocase. *Nature*, 401(6752):485–489, Sep 1999.
- M. Vergnolle, C. Baud, A. Golovanov, F. Alcock, P. Luciano, L. Lian, and K. Tokatlidis. Distinct domains of small Tims involved in subunit interaction and substrate recognition. *J Mol Biol*, 351(4):839–849, Aug 2005.

- S. Vial, H. Lu, S. Allen, P. Savory, D. Thornton, J. Sheehan, and K. Tokatlidis. Assembly of Tim9 and Tim10 into a functional chaperone. *J Biol Chem*, 277(39):36100–36108, Sep 2002.
- R. Voulhoux, M. P. Bos, J. Geurtsen, M. Mols, and J. Tommassen. Role of a highly conserved bacterial protein in outer membrane protein assembly. *Science*, 299(5604):262–265, Jan 2003.
- Walz and Grigorieff. Electron crystallography of two-dimensional crystals of membrane proteins. *J Struct Biol*, 121(2):142–161, 1998.
- T. Walz, B. L. Smith, M. L. Zeidel, A. Engel, and P. Agre. Biologically active two-dimensional crystals of aquaporin chip. *J Biol Chem*, 269(3):1583–1586, Jan 1994.
- C. T Webb, M. A. Gorman, M. Lazarou, M. T. Ryan, and J. M. Gulbis. Crystal structure of the mitochondrial chaperone TIM9-10 reveals a six-bladed alpha-propeller. *Mol Cell*, 21(1):123–133, Jan 2006.
- K. Weisshart, V. Jüngel, and S. J. Briddon. The LSM 510 META - ConfoCor 2 system: an integrated imaging and spectroscopic platform for single-molecule detection. *Curr Pharm Biotechnol*, 5(2):135–154, Apr 2004.
- D. Wessel and U. I. Flügge. A method for the quantitative recovery of protein in dilute solution in the presence of detergents and lipids. *Anal Biochem*, 138(1):141–143, Apr 1984.
- N. Wiedemann, V. Kozjak, A. Chacinska, B. Schönfish, S. Rospert, M. T Ryan, N. Pfanner, and C. Meisinger. Machinery for protein sorting and assembly in the mitochondrial outer membrane. *Nature*, 424(6948):565–571, Jul 2003.
- N. Wiedemann, A. E. Frazier, and N. Pfanner. The protein import machinery of mitochondria. *J Biol Chem*, 279(15):14473–14476, Apr 2004.
- Y. Wu and B. Sha. Crystal structure of yeast mitochondrial outer membrane translocon member Tom70p. *Nat Struct Mol Biol*, 13(7):589–593, Jul 2006.
- M. Yano, K. Terada, and M. Mori. Mitochondrial import receptors Tom20 and Tom22 have chaperone-like activity. *J Biol Chem*, 279(11):10808–10813, Mar 2004.
- J. C Young, N. J Hoogenraad, and F. U. Hartl. Molecular chaperones Hsp90 and Hsp70 deliver preproteins to the mitochondrial import receptor Tom70. *Cell*, 112(1):41–50, Jan 2003.

9 Curriculum Vitae

Personal Details

Name	Melissa Ann Poynor
Date and place of birth	16.11.1977, Emmeloord, The Netherlands
Nationality	US-American

Education

Stuttgart, as of April 2004	Continuation of my PhD at the Biologische Institut (Universität Stuttgart)
Munich, Nov. 2002 – Mar. 2004	Commencement of my PhD work at the Ludwig-Maximilians-Universität München
Heidelberg, Jan. – Aug. 2002	Diploma thesis at the Institut für Molekulare Genetik
Heidelberg, Oct. 1997 – Dec. 2001	Studies in Biology at Ruprecht-Karls-Universität Heidelberg
Mosbach, Sep. 1988 – June 1997	Nicolaus- Kistner- Gymnasium

Publications

Dynamics of the preprotein translocation channel of the outer membrane of mitochondria

M. Poynor, R. Eckert, and S. Nussberger (in preparation)

High level expression, refolding and probing the natural fold of the human voltage-dependent anion channel isoforms I and II

H. Engelhardt, T. Meins, *M. Poynor*, V. Adams, S. Nussberger, W. Welte, and K. Zeth (Journal of Membrane Biology, 216(2-3):93-105, Apr 2007)

Gene duplication of the eight-stranded beta-barrel OmpX produces a functional pore: a scenario for the evolution of transmembrane beta-barrels.

T. Arnold, *M. Poynor*, S. Nussberger, A. Lupas, D. Linke (Journal of Molecular Biology, 366(4):1174-84, Mar 2007)

10 Acknowledgements

This thesis would not have been possible without the help and support of many people.

First, I would like to thank, my supervisor, Professor Stephan Nußberger for providing the possibility for me to conduct this work and for all the help and advice during my Ph.D. studies.

Special thanks goes to Dr. Reiner Eckert for teaching me much about ion channels and scientific writing and for the always “up-to-date version” of SANALYSIS.

I thank Beate for her technical assistance with the *Neurospora crassa* cultures. And all the other colleagues of the Biologische Institut, but especially: Simon, Mercé, Marianne, Alice, Margarida, Martina, Silvia, Dagmar, Julia, and all the students that helped out in the lab for shorter and longer periods.

I would like to thank all the collaborators that worked with me on the various projects: the lab of Prof. Dr. Rigaud in Paris with the 2-D crystallization trials, Dr. Reinhard Albrecht from Tübingen with the 3-D crystallization experiments, and Dr. Elke Haustein and the other members of Prof. Schwille’s group with the FCS measurements in Dresden. I would also like to thank Prof. Walter Neupert and all of his group members for helping me in the beginning of my thesis and for the fun time in Munich.

I would like to thank Kerstin, Martin, Karen, Vanessa, Sonja, Annina, and all my other friends for the wonderful moments outside of the lab and Hans for all his patience, love, and elephant jokes, and for not being jealous at TOM.

Finally, I would like to thank my parents and my sisters for loving and believing in me.